ABSTRACT

Title of dissertation: EXPLORATION OF EARTH'S INTERIOR THROUGH TUNGSTEN ISOTOPE GEOCHEMISTRY OF THE HAWAIIAN MANTLE PLUME

Lori Willhite, Doctor of Philosophy, 2025

Dissertation directed by: Distinguished University Professor, Richard J. Walker, Department of Geology

The advancement of analytical techniques has enabled the discovery of $\mu^{182}W$ (the parts-per-million deviation of $^{182}W/^{184}W$ relative to the presumed composition of the bulk silicate Earth) isotopic differences among Earth materials. Variations in $\mu^{182}W$ are particularly useful for probing early Earth events because radiogenic ^{182}W was only produced during the initial ~60 million years of the Solar System, requiring anomalous $\mu^{182}W$ in the modern mantle to have formed and been preserved for over 4.5 billion years. Characterization of $\mu^{182}W$ in modern ocean island basalts (OIB) has revealed that some mantle plumes contain $\mu^{182}W$ deficits in one or more of their source components. Investigation of the well characterized Hawaiian mantle plume, from a single volcano scale to the archipelago scale, provides new insights into the materials and processes that affect the expression of $\mu^{182}W$ in erupted OIB. In Chapter 2, a systematic study of the Mauna Kea volcano indicates that the anomalous $\mu^{182}W$ is present in small volumes, such that it is not always sampled by melting events, even when present in the mantle source of a volcano. Through a two-step acid leaching procedure on ~5 Ma powders from Kauai, Chapter 3 confirms that the $\mu^{182}W$ measured in minimally altered, subaerial OIB is a reliable tracer of the mantle source composition.

Throughout fourteen volcanic centers in the archipelago, Chapter 4 concludes there are gaps in the plume, where no anomalous $\mu^{182}W$ component is present, which could reflect inconsistent entrainment of the anomalous mantle source. The chemical characteristics of Hawaiian lavas with $\mu^{182}W$ deficits, both within and among volcanic centers, suggest that the anomalous component in the Hawaiian plume is relatively refractory, is associated with relatively radiogenic $^{208}Pb/^{204}Pb$, and is enriched in Ti and Nb, relative to similarly incompatible elements. The probability of a Hawaiian volcano expressing negative $\mu^{182}W$ is related to the thermal and physical structure of the plume, such that higher mantle potential temperature and magmatic flux are more likely to produce lavas with anomalous $\mu^{182}W$.

EXPLORATION OF EARTH'S INTERIOR THROUGH TUNGSTEN ISOTOPE GEOCHEMISTRY OF THE HAWAIIAN MANTLE PLUME

by

Lori Nicole Willhite

Dissertation submitted to the Faculty of the Graduate School of the
University of Maryland, College Park, in partial fulfillment
of the requirements for the degree of
Doctor of Philosophy
2025

Advisory committee:
Distinguished Professor Richard J. Walker, Chair
Assistant Research Scientist Valerie Finlayson
Distinguished Professor Theodore Jacobson (Dean’s Representative)
Professor Vedran Lekic
Assistant Professor Megan Newcombe
Research Scientist Igor Puchtel

Preface

Portions of this dissertation have been previously published in peer-reviewed journals. Chapter 2 is published in Earth and Planetary Science Letters. Chapters 3 and 4 are in preparation for submission for peer review and publication. The contributions of each author are detailed here.

Chapter 2

Lori N Willhite, Valerie A Finlayson, Richard J Walker (2024) Evolution of tungsten isotope systematics in the Mauna Kea volcano provides new constraints on anomalous $\mu^{182}W$ and high $^{3}He/^{4}He$ in the mantle. *Earth and Planetary Science Letters*. **640**, 118795.

In this study I conducted all chemical analyses for W and Os isotopic compositions, and highly siderophile element and W concentration measurements. I interpreted these data and wrote the first draft of the manuscript. Valerie Finlayson and Richard Walker provided edits and suggestions.

Chapter 3

Lori Willhite, Michelle Jordan, Nicole Williamson, Igor Puchtel, Valerie Finlayson, Dominique Weis, Richard Walker (*In prep*) Acid leaching effects on the tungsten-182 of Hawaiian lavas

I collected W isotope data and performed the leaching experiments in the laboratory. Michelle Jordan and I collected elemental abundance data for the leachate solutions. Nicole Williamson and Dominique Weis provided expertise on sample selection and geologic context, as well as

photomicrographs of sample thin sections. Igor Puchtel and Valerie Finlayson gave advice on the leaching protocol and data interpretation. I wrote the first draft of the manuscript and received edits and improvements from all authors.

Chapter 4

Lori Willhite, Nicole Williamson, Valerie Finlayson, Dominique Weis, Richard J Walker (*In prep*) Pulsing plume or mantle mixing?: dynamics of the Hawaiian plume through the lens of $\mu^{182}W$.

I conducted all W and Os isotopic analyses, as well as W and siderophile element abundance measurements. Nicole Williamson and Dominique Weis collected and provided the samples, in addition to their geologic context, major and trace element data, as well as Sr, Nd, Hf, Pb isotopic data for a subset of the samples. Valerie Finlayson provided a subset of samples, including those from West Kaʻena Ridge and the Kamaʻehuakanaloa seamount. I interpreted the data and wrote the first draft of the manuscript. All authors provided edits and improvements to the text.

Table of Contents

List of Tables

List of Figures

Chapter 1: Introduction

1.1 Mantle geochemistry: ocean island basalts

Earth's mantle comprises approximately 67% of the total mass of the planet, and over 80% of the volume, making it the largest chemical reservoir on the planet. Determination of the mantle composition at present, and throughout Earth's history, is critical to understanding how the Earth formed and evolved into a habitable planet. For example, mantle outgassing has been invoked as a mechanism for the formation of the oceans and atmosphere (*e.g.*, Javoy, 1998; Hirschmann, 2012). Continuous mantle depletion to form the continents and establish plate tectonics may make Earth uniquely habitable among the terrestrial planets in our Solar System (*e.g.*, Foley, 2015). Whether the deep mantle contains a large reservoir of carbon, water, and other volatiles is debated (Hirschmann, 2006; Dasgupta and Hirschmann, 2010; Ohtani, 2015). Finally, how the mantle interacts with other major chemical reservoirs, for example, the metal core, rocky crust, liquid ocean, and the gaseous atmosphere, is an important and on-going area of research. This work explores potential evidence for core-mantle interaction and/or the storage of geochemical signatures in physically distinct, deep mantle reservoirs for nearly all of Earth's history.

Direct access to mantle rocks is limited to ophiolites (sections of oceanic crust and mantle that have been tectonically thrust onto the surface), mantle xenoliths (solid mantle rocks that are plucked by magma and brought to the surface during an eruption), and possibly through deep ocean floor drilling (*e.g.*, Lin et al., 2024). A majority of Earth's surface area is covered by basalt, the igneous rock that is formed by partial melting of the mantle. These rocks provide a way to investigate mantle compositions, although indirectly, with much wider global coverage than ophiolites, xenoliths, or via technologically difficult and expensive drilling programs. Mid-ocean

ridges, or spreading centers, erupt basalt formed by adiabatic decompression melting of the mantle. This style of eruption makes up more than half of Earth's magma flux. The result is a surficial layer of the oceanic crust called MORB (mid-ocean ridge basalt). MORB compositions indicate that the upper mantle is made of peridotite and is largely depleted in incompatible elements (*i.e.,* elements that are preferentially extracted from the solid mantle during melting) (*e.g.*, Hofmann, 1997). The history of mantle depletion is recorded by radiogenic isotope systems, such as the $^{87}Rb \rightarrow {}^{87}Sr$ and $^{147}Sm \rightarrow {}^{143}Nd$ systems. The elements that make up the parent nuclides, Rb and Sm, are fractionated from the daughter elements, Sr and Nd, during melting. Rubidium is more incompatible (preferentially partitions into the melt) than Sr, and Sm is less incompatible than Nd. During mantle melting, the melt will evolve with a higher Rb/Sr and lower Sm/Nd than the residual mantle. MORB has unradiogenic $^{87}Sr/^{86}Sr$ and radiogenic $^{143}Nd/^{144}Nd$ compared to best estimates of the bulk silicate Earth, which is consistent with long-term depletion of the MORB mantle sources (White and Hofmann, 1982; Hofmann et al., 1986; Hofmann, 1997).

In addition to spreading centers, partial mantle melts are found at seamounts and ocean islands. At these locations, the rocks formed are generalized into a category called ocean island basalts (OIB). These are the rocks formed in mantle plume settings, although not all seamounts and islands are necessarily formed by a mantle plume. The concept of mantle plumes was introduced by Morgan (1971), as convective upwellings that dredge up "relatively primordial" material from a thermal boundary layer in the deep mantle. The idea that plumes access "relatively primordial" material was intuited by Morgan before there was geochemical evidence for this. In the classical model, a large head and thin tail (<200 km) compose plumes that are primarily thermal features initiated at a thermal boundary layer (Campbell and Griffiths, 1990). Using seismic tomography, large (>500 km thick) conduits have been observed beneath plume localities such as

Hawaii, Galapagos, and Samoa, confirming the presence of physically and/or chemically distinct plumes in the mantle (French and Romanowicz, 2015). Many of these features traverse the mantle extending to seismically distinct, low velocity structures near the core-mantle boundary, termed ultra-low velocity zones (ULVZ) (Williams and Garnero, 1996; McNamara et al., 2010; French and Romanowicz, 2015). Plume localities on the surface have also been linked to larger mantle structures, termed large low shear wave velocity provinces (LLSVP), indicating plumes may comprise, or at least sample, mantle domains that are more dense and potentially chemically heterogeneous compared to ambient mantle (Thorne et al., 2004).

Prior to Morgan's work, it had been recognized that OIB were chemically distinct from MORB (Gast et al., 1964; Engel et al., 1965; Gast, 1968). Islands and seamounts, where OIB are found, have higher frequencies of alkaline basalts—*i.e.*, rocks enriched in K, Rb, Ba, Rb, Sr, and other incompatible elements—compared to MORB (Engel et al., 1968; Gast, 1968). Gast (1964; 1968) showed that the chemical differences between OIB and MORB were not simply the result of varying degrees of fractional crystallization, but instead imply that OIBs sample chemically distinct mantle reservoirs with different long-term depletion and enrichment histories. In addition to fundamental chemical distinctions between MORB and OIB, lithophile radiogenic isotope systems indicate that plumes access mantle sources with a greater range of compositions (*e.g.,* Zindler and Hart, 1986). A simplified interpretation would be that the chemical and isotopic heterogeneities in the upper mantle have been attenuated by convective stirring and continual depletion via melting, and the lower mantle is more heterogenous and has not been depleted to the same degree, and/or has been replenished by recycling of crustal and mantle lithologies.

Two fundamental works, both titled *Chemical Geodynamics* established mantle endmembers that describe the extreme compositions observed at plume localities compared to

mid-ocean ridges (Allègre, 1982; Zindler and Hart, 1986). These works established "mantle zoology" (*i.e.,* the study of geochemically and physically distinct mantle components). Traditionally, five major components have been included in the "mantle zoo": the depleted MORB mantle (DMM), two geochemically enriched mantle sources (EM1 and EM2), a high-μ (where μ = $^{238}U/^{204}Pb$) mantle source that evolved to very radiogenic Pb isotopic compositions (HIMU), and a ubiquitous component (*e.g.*, the FOcal Zone or FOZO) that has elevated $^{3}He/^{4}He$ (>30 R_A, where R_A denotes relative to Earth's atmosphere) compared to the accessible upper mantle sampled by MORB (9 ± 1 Ra) and seems to be the central composition that others trend toward (Zindler and Hart, 1986; Hart et al., 1992; Graham, 2002). Other components conceptually similar to FOZO have been discussed, such as the central component (Component C; Hanan and Graham, 1996), the prevalent mantle (PREMA; Zindler and Hart, 1986), and primitive helium mantle (PHEM; Farley et al., 1992). The conceptual models for each continue to evolve with additional geochemical and geodynamic observations. Whether these endmembers reflect physical regions of the mantle or conceptual entities that manifest from similar processes, is an on-going area of research (*e.g.,* Stracke, 2021; Stracke et al., 2022).

The mantle components comprising the "zoo" are largely defined by radiogenic isotope compositions of Sr-Nd-Hf-Pb. Thus, these endmembers are likely the result of variable ages and extents of silicate differentiation, recycling of crustal lithologies, and other geochemical processes like metasomatism and chemical alteration. In this regard, mantle endmembers provide a useful framework to understand the effects of these processes and materials on the composition of Earth's mantle over time. For example, investigation of EM2 lavas revealed that surface materials, such as continental-derived sediments, are mixed back into the mantle and can be entrained in mantle plumes (Jackson et al., 2007). HIMU lavas, which have radiogenic Pb isotopic compositions

compared to other oceanic lavas, may result from recycling of oceanic crust that experienced Pb loss prior to or during subduction via hydrothermal alteration (Hofmann and White, 1982; Palacz and Saunder, 1986; Chauvel et al., 1992). HIMU lavas also tend to have depletions in other fluid mobile elements in addition to Pb, including Ba, K, Sr, etc., indicating fluid-mediated loss of large ion lithophile elements from oceanic crust during subduction (Palacz and Saunder, 1986; Hanyu et al., 2014). These lavas demonstrate that chemical modification near the surface can impart significant chemical and isotopic changes in the mantle over time.

The significance of high $^{3}He/^{4}He$ as a defining characteristic of FOZO is that elevated $^{3}He/^{4}He$ in erupted basalts (up to ~60 R_A; Willhite et al., 2019; Horton et al., 2023) has been interpreted to reflect long-term storage of noble gases somewhere in the deep mantle (Lupton and Craig, 1975; Kurz et al., 1983; Farley et al., 1992). The implication is that there is a physically distinct and stable region in the mantle that has retained primordial noble gas nuclides to a greater extent than the convecting mantle for the duration of Earth's history. If true, this mantle region may have other compositional signatures associated with early Earth processes, and deep, buoyant mantle plumes may transport those signatures to the surface to be expressed in some OIB.

Short-lived radiogenic isotopic systems provide further, complementary insight into chemical differentiation events and the geodynamics of the Earth. The $^{146}Sm \rightarrow {}^{142}Nd$ system ($t_{1/2}$ = 103 Myr), is comprised of lithophile elements for both the parent and daughter nuclides, and is useful for tracking silicate differentiation events within the first ~500 Myr of Earth's history (given that a parent nuclide is extant for approximately 5-6 times the half-life). One question that has been probed using the $^{146}Sm \rightarrow {}^{142}Nd$ system is whether the high $^{3}He/^{4}He$ mantle domain was formed by silicate differentiation during the first ~500 Myr. Ocean island basalts from Samoa and Hawaii with a large range of $^{3}He/^{4}He$, from 4.5 to 32.2 R_A, have indistinguishable $\mu^{142}Nd$ (*i.e.*, the part-

per-million deviation of $^{142}Nd/^{144}Nd$ from the terrestrial standard composition) (Horan et al., 2018). If the high $^{3}He/^{4}He$ mantle domain was formed by an early Earth silicate differentiation event while ^{146}Sm was extant, such as magma ocean crystallization, then the $\mu^{142}Nd$ composition has likely been overprinted by subsequent mantle mixing.

The $^{182}Hf \rightarrow {}^{182}W$ system ($t_{1/2}$ = 8.9 Myr) is suited to record events that are synchronous with or occurred shortly after core formation (within the first ~60 Myr of Solar System history). This makes $\mu^{182}W$ (the part-per-million $^{182}W/^{184}W$ difference from the W standard) a fingerprint for geological events that occurred during the early Hadean Eon. Due to the lithophile nature of Hf and moderately siderophile nature of W, this system can be used to probe both silicate-silicate and metal-silicate differentiation events. During accretion, the Earth likely inherited a broadly chondritic $\mu^{182}W$ composition, which evolved to approximately -200, as is observed in chondrites and other primitive meteorites (Kleine et al., 2002, 2004a; Hellmann et al., 2024). As a consequence of the siderophile nature of W, the core sequestered more than 90% of Earth's W (McDonough, 2003). Mass balance estimates predict that the core has a $\mu^{182}W$ of -220 (Kleine and Walker, 2017). The silicate portion of the Earth inherited a suprachondritic Hf/W ratio as a consequence of formation, and evolved to a much higher $\mu^{182}W$ compared to its building blocks.

The $\mu^{182}W$ of the bulk silicate Earth (BSE) immediately following core formation and the extinction of ^{182}Hf is debated. Most Eoarchean rocks that have been measured for W isotopes have an average $\mu^{182}W$ approximately 13-15 ppm greater than the average modern mantle composition of ~0 ± 3.5 (Willbold et al., 2011; Touboul et al., 2012, 2014; Willbold et al., 2015; Puchtel et al., 2018; Reimink et al., 2018; Rizo et al., 2019). These compositions have led to the postulation that the Eoarchean mantle had a $\mu^{182}W$ of approximately +13. A corollary hypothesis is that the average BSE $\mu^{182}W$ has decreased to ~0 over time due to continual mixing of long lived mantle

heterogeneities formed prior to or during late accretion (Willbold et al., 2015; Puchtel et al., 2018) or core-mantle exchange (Touboul et al., 2012; Rizo et al., 2019; Peters et al., 2024). Late accretion likely delivered materials with negative $\mu^{182}W$, near chondritic values (~-200) (Willbold et al., 2011). Grainy late accretion, in which isolated mantle reservoirs may have experienced variable degrees of late accretion, could have produced $\mu^{182}W$ variability among mantle regions. As the mantle experienced a greater degree of homogenization over time, the $\mu^{182}W$ may have decreased from approximately +13–as observed in some Eoarchean rocks, to ~0, which is observed in the modern MORB mantle (Rizo et al., 2016; Mundl et al., 2017; Peters et al., 2024). Alternatively, but not mutually exclusive to late accretion, core-mantle exchange could also have contributed negative $\mu^{182}W$ relative to the Archean (and modern) mantle (*e.g.*, Scherstén et al., 2004; Brandon and Walker, 2005).

The Schapenberg komatiites from South Africa represent some of the oldest (3.55 Ga) komatiites accessible today, and are rare among Archean localities in their *negative* $\mu^{182}W$ (average of -8.4 ± 1.6) (Puchtel et al., 2016). Negative $\mu^{182}W$ in the mantle source of the Schapenberg komatiites illustrates that the Archean mantle was not uniformly positive with respect to $\mu^{182}W$. It is unlikely that direct mass transfer from the core is responsible for a decrease in $\mu^{182}W$ in the Schapenberg mantle source, as additional expected consequences of core entrainment have not been observed. For example, the highly siderophile element concentrations of the core are significantly higher than the silicate mantle. The Pt concentration of the core is estimated to be ~5700 ppb (McDonough, 2003) and the estimate for the BSE is 7.7 ppb Pt (Becker et al., 2006). To explain a $\mu^{182}W$ value of -8, assuming the Archean mantle had a $\mu^{182}W$ of +20 and W concentration of 13 ppb, 0.4% core material ($\mu^{182}W$ = -220, W concentration = 470 ppb) would need to be added to the mantle source. The resultant Pt concentration would be ~30 ppb, which is

unlikely to represent the mantle source of the Schapenberg komatiites that have Pt concentrations ranging from ~2.5 to 4 ppb Pt, because Pt is not significantly fractionated during mantle partial melting and crystal-liquid fractionation (Pitcher et al., 2009; Puchtel et al., 2016).

In the case of the Schapenberg komatiites, $\mu^{182}W$ and $\mu^{142}Nd$ are both negative relative to the terrestrial standard. Silicate differentiation, such as crystal-liquid fractionation in an early magma ocean, might produce an incompatible-element-enriched liquid with low Hf/W and low Sm/Nd (Brown et al., 2014; Puchtel et al., 2016). The liquid would then evolve to negative $\mu^{182}W$ and $\mu^{142}Nd$ as long as the crystal-liquid fractionation event occurred within ~60 Myr of Earth history. The Schapenberg mantle source may host signatures from an ancient, geochemically enriched domain that has not been mixed away despite billions of years of mantle convection.

In modern mantle-derived rocks (*i.e.*, <15 Ma), $\mu^{182}W$ values range from +3 to -25 (*e.g.*, Mundl et al., 2017; Rizo et al., 2019; Mundl-Petermeier et al., 2020; Jackson et al., 2020; Peters et al., 2021, 2024; Archer et al., 2023; Chapter 2 of this dissertation). Tungsten isotopic compositions observed in MORB have a limited range (average = -1.2 ± 4.4; n = 9; Rizo et al., 2016; Mundl et al., 2017; Peters et al., 2024) compared to OIB. Mantle plume settings have erupted basalts with both "normal" (i.e., BSE-like $\mu^{182}W$ ~0) and resolvable $\mu^{182}W$ deficits, implying there are regions of the mantle that have either stored $\mu^{182}W$ variability since <60 Myr following the start of the Solar System, or there has been isotopic exchange between the core and mantle at some point in Earth's history. Some individual volcanoes and plume localities, for example Hawaii, Iceland, Galapagos, and Samoa, exhibit statistically significant correlations between $\mu^{182}W$ and $^{3}He/^{4}He$ (Chapter 2 of this dissertation; Mundl et al., 2017; Mundl-Petermeier et al., 2020; Jackson et al., 2020). This observation links the storage of primordial noble gas nuclides to the isotopic composition of the refractory, moderately siderophile element, W.

There are three primary hypotheses in the literature that endeavor to explain the relationship between $\mu^{182}W$ and $^{3}He/^{4}He$. The first is isotopic equilibration and diffusion at the core-mantle boundary (Rizo et al., 2019; Mundl-Petermeier et al., 2020; Ferrick and Korenaga, 2023; Chapter 2 of this dissertation). In this scenario, the extreme negative $\mu^{182}W$ of the core allows for some ^{182}W to exchange with the mantle without net transfer of W to the mantle. Helium may also undergo isotopic equilibration and/or diffusion from the core, which can plausibly store elevated $^{3}He/^{4}He$ if sufficient He was trapped in the core during core formation (Porcelli and Halliday, 2001; Bouhifd et al., 2013). These processes can occur at any point during Earth's history. The exact mechanism of isotopic equilibration is little understood.

The second hypothesis is that an early formed silicate reservoir has maintained negative $\mu^{182}W$ and high $^{3}He/^{4}He$ signatures since >4.5 Ga (Touboul et al., 2012; Chapter 2 of this dissertation). In this scenario, crystallization of bridgmanite and/or Ca-perovskite in the lower mantle would produce a residual magma ocean with low Hf/W. If the crystal-liquid fractionation occurred during the lifetime of ^{182}Hf, the liquid would evolve negative $\mu^{182}W$. The liquid that was in equilibrium with bridgmanite and/or Ca-perovskite may have been stored at the core-mantle boundary (*e.g.*, a basal magma ocean or later crystallized product of the residual liquid) without complete homogenization via mantle mixing and degassing; it may still have negative $\mu^{182}W$ and high $^{3}He/^{4}He$. This reservoir is likely highly viscous and dense in order to have survived the Moon-forming impact and billions of years of mantle convective mixing, etc.

The third hypothesis includes the storage of nonuniformly distributed late accreted isotopic signatures in the mantle (Puchtel et al., 2016; Nakanishi et al., 2021; Archer et al., 2023). As mentioned previously, late accretion would have added materials with low $\mu^{182}W$ (and high $^{3}He/^{4}He$) compared to the BSE. Grainy late accretion, in which isolated reservoirs of the mantle

experience or store an unequal proportion of late accreted signatures, would generate portions of Earth's interior with broadly chondritic signatures such as negative $\mu^{182}W$. This hypothesis presents the challenge of physically transporting (*e.g.*, convective mixing) late accreted signatures to the lower mantle (where storage over billions of years is more plausible), and entrainment of these signatures in mantle plumes, without subsequent convective mixing to erase the anomalous compositions. Strong evidence for grainy late accretion would be the observation of negative $\mu^{182}W$ paired with nucleosynthetic anomalies, which are associated with primitive Solar System materials, such as components of meteorites and bulk chondrites and iron meteorites (Warren, 2011; Burkhardt et al., 2012; Bermingham et al., 2018; Worsham et al., 2019; Tornabene et al., 2020; Archer et al., 2023; Hellmann et al., 2024). For OIB, data are limited such that a conclusive statement cannot yet be made about the possible presence of nucleosynthetic anomalies in mantle reservoirs.

The mode of origin of $\mu^{182}W$ deficits observed in some OIB is unresolved. In OIB, there are no identified correlations between $\mu^{182}W$ and short- or long-lived lithophile radiogenic isotopic systems to reveal a silicate differentiation history of the mantle source(s) with negative $\mu^{182}W$ (Horan et al., 2018; Jackson et al., 2020). Similarly, siderophile isotopic systems, such as $^{186}Os/^{188}Os$ and $^{187}Os/^{188}Os$, show no clear sign of metal-silicate interaction and indicate the origin of $\mu^{182}W$ deficits in OIB is unrelated to the Pt-Os and Re-Os history of the mantle source (Chapter 2 of this dissertation; Mundl et al., 2017). At present, the global OIB $\mu^{182}W$ dataset comprises 15 localities, which each have complex mantle componentry, and their melts experience different petrogenetic environments. This makes relating $\mu^{182}W$ to chemical and isotopic characteristics difficult in the global array. A detailed study of a single, well-characterized mantle plume over time and space may provide new insights into: (1) the chemical and physical properties of the

mantle source(s) with $\mu^{182}W$ deficits; (2) the shallow mantle processes that may affect the expression of $\mu^{182}W$ in erupted material; and (3), potentially the origin of $\mu^{182}W$ deficits in the mantle.

1.2 The Hawaiian mantle plume: application of $\mu^{182}W$ to a single plume system

The Hawaiian mantle plume is the best sampled plume localities. The Hawaiian Islands of Kauai, Oahu, Lānaʻi, Maui, and Hawaii, as well the submarine West Keana Ridge and Kamaʻehuakanaloa Seamount (formerly Lōʻihi), represent >500 km and ~5.5 Myr of volcanic products from the plume. Furthermore, tomographic evidence suggests that the Hawaiian plume is rooted in a ULVZ at the core mantle boundary and near the edge of a LLSVP, and therefore may plumb heterogeneous mantle reservoirs, including regions that may have been rheologically stable over billions of years (Cottaar and Romanowicz, 2012; Zhao et al., 2015; Kim et al., 2020).

It has been established that volcanoes along the archipelago comprise two parallel geographic and geochemical trends, the so-called Loa and Kea trends (Abouchami et al., 2005; Weis et al., 2011). In fact, geologist J.D. Dana, working for the United States Navy, first mapped the geographic distribution of two parallel chains of volcanoes as part of the *US Navy Exploring Expedition* from September 1840 to April 1841 (Dana, 1849). Considerable debate has been centered on the origin of Loa and Kea trends, and their distribution in the Hawaiian mantle plume (*e.g.,* DePaolo et al., 2001; Blichert-Toft et al., 2003; Eisele et al., 2003; Abouchami et al., 2005; Bryce et al., 2005; Farnetani and Hofmann, 2010; Weis et al., 2011, 2020; Harrison et al., 2017). The Loa trend is typically geochemically enriched compared to Kea, and if the apparent bilateral zonation of Loa and Kea lavas at the surface reflects deep mantle structure, Loa signatures may

result from incorporation of primitive and recycled materials housed in the LLSVP that is not sampled by the Kea side of the plume (Weis et al., 2011, 2020; Harrison et al., 2017). The Kea trend is generally geochemically depleted and less heterogeneous than Loa, but is distinct from the isotopic composition of regional Pacific mid-ocean ridge basalts (MORB), leading to the hypothesis that Kea reflects the deep Pacific mantle (Weis et al., 2011, 2020; Harrison et al., 2017). The $\mu^{182}W$ systematics of the Loa and Kea trends will be explored in Chapter 4.

Several prior studies have reported that Hawaiian volcanics have a range of $\mu^{182}W$, from compositions similar to the BSE (~0), to the most extreme negative $\mu^{182}W$ observed in OIB, -25.6 (Mundl et al., 2017; Mundl-Petermeier et al., 2020). Given that Hawaiian lavas span the entire range of $\mu^{182}W$ observed in modern oceanic lavas, Hawaiian volcanic centers present the opportunity to investigate potential relationships among petrologic, He-Sr-Nd-Hf-Pb-Os isotopic characteristics, and $\mu^{182}W$. Whether $\mu^{182}W$ varies in a systematic way over time in a single volcano may reveal petrogenetic (*e.g.*, temperature, melt degree, crystal-liquid fractionation) factors that influence $\mu^{182}W$, as well as plume structural insights (*e.g.*, predictable zoning or gradation of anomalous $\mu^{182}W$ in the plume). Study of a single volcano also limits the complexity of the global dataset, which may uncover previously masked correlations among trace element ratios, Sr-Nd-Hf-Pb-Os isotopic compositions, and $\mu^{182}W$. In Chapter 2, the $\mu^{182}W$ and $^{3}He/^{4}He$ systematics in a ~3 km (~600 kyr) stratigraphic section of the Mauna Kea volcano will be explored.

Among Hawaiian volcanic centers, $\mu^{182}W$ systematics may provide new insights into the interaction of recycled materials and anomalous $\mu^{182}W$ component(s). For example, whether sufficient W is recycled to attenuate a primitive, negative $\mu^{182}W$ composition entrained by the Hawaiian plume is unknown. Different types of recycled lithologies are speculated to account for the distinct Sr-Nd-Hf-Pb-Os isotopic ratios among Hawaiian volcanic centers. If these signatures,

and therefore, potentially the associated recycled materials, systematically affect $\mu^{182}W$ along the Hawaiian archipelago, constraints can then be placed on the relative contributions, distribution, and physical nature of the distinct $\mu^{182}W$ component(s). The long-term (~5 Myr) spatio-temporal pattern of $\mu^{182}W$ along the archipelago can also provide information about deep mantle structure. Furthermore, whether anomalous $\mu^{182}W$ material is constantly present, comes in pulses, or is stochastically sampled by the plume is unknown but can provide critical information about the entrainment and ascension of deep mantle heterogeneity. In Chapter 4 of this dissertation, variations in $\mu^{182}W$ are characterized in the context of the Kea and Loa trends, as well as each of six subgroups that have been defined within the larger trends (Weis et al., 2020), to test what portions of the plume are likeliest to carry an anomalous $\mu^{182}W$ signature, and what subsequent processes and materials effect the expression of the $\mu^{182}W$ in erupted lavas.

Chapter 2: Evolution of tungsten isotope systematics in the Mauna Kea volcano provides new constraints on anomalous $\mu^{182}W$ and high $^{3}He/^{4}He$ in the mantle

This chapter has previously been published in *Earth and Planetary Science Letters, Volume 640*.

Lori N Willhite, Valerie A Finlayson, Richard J Walker (2024) Evolution of tungsten isotope systematics in the Mauna Kea volcano provides new constraints on anomalous $\mu^{182}W$ and high $^{3}He/^{4}He$ in the mantle. *Earth and Planetary Science Letters*. **640**, 118795.

2.1 Abstract

Highly siderophile element abundances and $^{182}W/^{184}W$ and $^{187}Os/^{188}Os$ were determined for a suite of Mauna Kea lavas from the Hawaiian Scientific Drilling Project phase 2 drill core. The new analyses, combined with previous measurements, compose the largest database for $\mu^{182}W$ (the parts-per-million deviation of $^{182}W/^{184}W$ from a terrestrial standard) for a single volcano (n = 16). Although most lavas analyzed are characterized by negative $\mu^{182}W$ values, lavas with values similar to the modern bulk silicate Earth are found throughout the entire stratigraphic column. This suggests that components with normal $\mu^{182}W$ are collocated with components that host $\mu^{182}W$ deficits in the plume. Negative $\mu^{182}W$ values are associated with elevated $^{3}He/^{4}He$, as well as elevated Ti and Nb. These correlations may link $\mu^{182}W$ anomalies to ancient deep mantle crystal-liquid fractionation processes. Consistent with previously measured $^{3}He/^{4}He$ (R/R_A) in the drill core, the magnitude of negative $\mu^{182}W$ values was greatest when Mauna Kea was close to the plume axis then generally decreased over the ~400 kyr captured by the stratigraphic section. The

component with anomalous $\mu^{182}W$ was either concentrated near the plume axis, or was more effectively sampled by melting near the plume axis where the temperature excess was greatest, suggesting it was less fusible than the dominant plume components. The process leading to the generation of a mantle component with a negative $\mu^{182}W$ anomaly could either be related to some form of core-mantle isotopic equilibration, or early-Earth fractionation within the silicate Earth. At present each possibility remains viable.

2.2 Introduction

With a half-life of 8.9 Ma (Vockenhuber et al., 2004), the $^{182}Hf \rightarrow ^{182}W$ radiogenic isotope system was extant for only the first ~ 60 Ma of solar system history. Despite the short lifetime of the system, both ancient and modern terrestrial rocks have been found to exhibit isotopic variability in $^{182}W/^{184}W$ ratios, reflecting variable ingrowth of ^{182}W from ^{182}Hf (Willbold et al., 2011; Mundl et al., 2017). Deficits in $\mu^{182}W$ (the parts-per-million deviation of $^{182}W/^{184}W$ from terrestrial standards believed to be representative of the bulk silicate Earth; BSE) observed in a subset of modern ocean island basalts (OIB) have been interpreted to either reflect some form of core-mantle interaction, or the preservation of isotopic signatures of processes that occurred in the early silicate Earth, such as magma ocean differentiation or grainy late accretion (Rizo et al., 2019; Mundl-Petermeier et al., 2020; Archer et al., 2023; Peters et al., 2024). The observation that, in some OIB systems, increasingly negative $\mu^{182}W$ anomalies correlate with increasing $^{3}He/^{4}He$ provides further evidence for long-term storage of primitive geochemical signals in Earth's interior (Mundl et al., 2017; Rizo et al., 2019; Mundl-Petermeier et al., 2020). The magnitude of $\mu^{182}W$ at a given $^{3}He/^{4}He$ (*i.e.*, the slope in W-He isotopic space) varies by plume locality. In global OIB systems, this has been explained as a result of mixing of at least three components, including ambient mantle, an early-formed mantle reservoir with high $^{3}He/^{4}He$ and normal $\mu^{182}W$, and a core-

equilibrated mantle reservoir that has inherited negative $\mu^{182}W$ through isotopic equilibration with the metal core (Mundl-Petermeier et al., 2020).

In the global dataset for recent plume-derived systems, $\mu^{182}W$ does not appear to correlate with lithophile or other siderophile radiogenic isotope compositions (Jackson et al., 2020; Walker et al., 2023), making it difficult to link anomalous $\mu^{182}W$ in the mantle to processes such as silicate differentiation or metal-silicate interaction. The magnitude of $\mu^{182}W$ anomalies in plume sources has likely been attenuated by variable mixing among the anomalous component(s), ambient mantle, and W-rich recycled lithosphere (Jackson et al., 2020). Deconvolving the origin and evolution of anomalous $\mu^{182}W$ in the mantle using global OIB, therefore, is challenging due to the complexity of recycled componentry and diverse petrogenesis of volcanic rocks among different plume-derived systems.

Here, we focus on the $\mu^{182}W$ and $^{3}He/^{4}He$ systematics of a single volcano over time, the Mauna Kea volcano, as sampled by the Hawaiian Scientific Drilling Project phase 2 core (HSDP-2). Detailed study of a single volcano limits the complexity of mantle source componentry, and permits addressing questions that include: (1) Are $\mu^{182}W$ and $^{3}He/^{4}He$ systematics consistent with two component mixing within a single volcano? (2) Do other petrologic and/or geochemical parameters correlate with $\mu^{182}W$ or predict W-He behavior? (3) Do stratigraphic variations in $\mu^{182}W$ and $^{3}He/^{4}He$ inform plume structure and dynamics?

The HSDP-2 yielded a ~3500 meter long core representing a ~ 680 kyr record of volcanism (Sharp and Renne, 2005). The majority of the stratigraphic section comprises lavas from the Mauna Kea volcano, although ~250 meters of Mauna Loa lavas were also sampled in the upper section of the drill core. We report new $\mu^{182}W$ data for twelve Mauna Kea lavas. These same lavas have been previously characterized for, and represent a range of, $^{3}He/^{4}He$ and petrologic type (Kurz et al.,

2004; Rhodes and Vollinger, 2004). The new $\mu^{182}W$ values are combined with four previous $\mu^{182}W$ analyses from HSDP-2 (Mundl et al., 2017; Mundl-Petermeier et al., 2020). These data allow investigation of the W-He systematics of the volcano over a well-defined period of time (**Table 1**). Although the focus of this study is Mauna Kea, we also report three new $\mu^{182}W$ data from the Mauna Loa section at the top of the drill core for comparison with Mauna Kea. Mauna Kea and Mauna Loa volcanoes represent the archetypal volcanoes of the respective geographic and geochemical "Kea" and "Loa" trends that have been identified in Hawaii (Abouchami et al., 2005). The two trends have been interpreted to reflect sampling of distinct deep mantle sources (Weis et al., 2011) and have implications for the structure and dynamics of the Hawaiian mantle plume. Therefore, whether there are distinct $\mu^{182}W$ and $^{3}He/^{4}He$ systematics of the two trends warrants investigation.

Table 2.1. New (bold) and previously published $\mu^{182}W$, $^{187}Os/^{188}Os$, and W concentration data, as well as previously published $^{3}He/^{4}He$ and MgO wt. % for lavas from the Hawaiian Scientific Drilling Project 2.

Sample	Volcano	MgO wt. %	Depth (mbsl)	Model age (ka)	$\mu^{182}W$ (6/3)	2SE	W ppb	$^{3}He/^{4}He$ (R/R_A)	(1σ)	$^{187}Os/^{188}Os$
SR0008-4.2	ML	7.64	-9.5		**1.9**	**2.4**	**109**	8.0	0.1	**0.1360**
SR0113-6.1	ML	18.72	-222.5		**-3.7**	**3.7**	**45**	14.6	0.2	**0.1332**
SR0117-3.8	ML	19.42	-234.6		**-6.5**	**4.0**	**130**	17.6	0.2	**0.1335**
SR0167-5.7	MK	8.94	-378.4	312.8	**-2.6**	**2.2**	**96**	7.3	0.6	**0.1293**
SR0267-6.3	MK	23.16	-615.8	353.7	**-2.9**	**3.0**	**131**	8.2	0.3	**0.1282**
SR0372-3.2	MK	8.17	-871.2	381.8	**-4.3**	**3.6**	**119**	11.5	0.1	**0.1295**
SR0455-6.8	MK	26.01	-1098.2	406.8	**-4.0**	**3.1**	**54**	12.3	0.1	**0.1291**
SR0548-8.0	MK	19.5	-1404.1	440.5	**-8.6**	**3.4**	**96**	10.3	0.04	**0.1289**
SR0683-5.75	MK	19.55	-1763.3	480.0	-1.8	4.7	**70**	10.7	1.5	**0.1297**
SR0750-12.45	MK	17.23	-2032.8	512.9	-11.5	5.2	114	23.2	0.1	**0.1296**
SR0756-14.3	MK	18.91	-2098.6	516.8	**-6.3**	**3.2**	**103**	17.4	0.1	0.1295
SR0762-4.6	MK	17.93	-2123.8	519.6	-8.7	3.5	**64**	19.8	0.8	**0.1301**
SR0860-6.5	MK	7.77	-2615	573.7	**-5.8**	**3.5**	**160**	16.5	0.2	**0.1293**
SR0891-15.10	MK	22.04	-2730.4	586.3	-10	3.7	90	14.0	0.1	0.1299
SR0913-2.3	MK	12.47	-2825.8	596.8	**-3.2**	**2.3**	**98**	14.9	0.1	**0.1303**
SR0940-7.7	MK	13.59	-2967.8	612.5	**-16.6**	**3.8**	**110**	21.0	0.1	**0.1291**
SR0954-7.4	MK	18.03	-3009.2	617.0	**-12.0**	**3.6**	**99**	13.9	0.1	**0.1276**
SR0956-9.3	MK	7.01	-3019	618.1	**-12.1**	**3.7**	**156**	12.8	0.2	**0.1300**
SR0967-2.8	MK	15.39	-3068	623.6	**-3.8**	**3.3**	**114**	11.9	0.1	**0.1295**

$\mu^{182}W$ is the deviation of $^{182}W/^{184}W$ of a sample from that of the average of repeated measurements of an Alfa Aesar tungsten standard (2SD = 2.9; *n* = 21). New data are presented in bold. The 2SE represents the internal standard error of a single analysis. All $\mu^{182}W$ values are normalized to $^{186}W/^{183}W$; other normalizations are given in Supplementary Table S2. ML = Mauna Loa. MK = Mauna Kea. MgO wt. % is from Rhodes and Vollinger (2004). Depth, age, and $^{3}He/^{4}He$ are from Kurz et al. (2004). Previous $\mu^{182}W$ and W concentration data are from Mundl et al. (2017) and Mundl-Petermeier et al. (2020). Previous $^{187}Os/^{188}Os$ data are from Ireland et al. (2009b).

2.3 Methods

2.3.1 Tungsten isotopic analyses

Tungsten isotopic compositions were analyzed via negative-ion thermal ionization mass spectrometry (N-TIMS) on a *Thermo Scientific Triton*™ multicollector thermal ionization mass spectrometer in the Isotope Geochemistry Laboratory at the University of Maryland, College Park. Details on sample preparation, including chemical separation methods for isotopic analysis, are provided in the supplementary materials. Laboratory total procedural blanks for W chemistry averaged 380 pg and were always well below 1% of the total W. Following chemical separation, approximately 1000 ng of W was loaded onto Re filaments in 1 µL of 0.5M HCl + 0.5M HF and dried down. After letting the loaded W sit on the Re filament overnight, 1 µL of La (9 ng/µL) and Gd (3 ng/µL) activator was added to improve ionization of W. Mass spectrometric measurements followed the Faraday cup and amplifier configuration and per-integration oxide correction from (Archer et al., 2017). Typical beam intensities were ~1 V on mass $^{184}WO_3$ using 10^{11} Ω resistor amplifiers and analysis time was 12 hours and 15 minutes per sample, including 45 minutes of baseline measurements.

Isotopic ratios were corrected for mass fractionation assuming an exponential law and normalizing to $^{186}WO_3/^{184}WO_3$ of 1.9859 (additional normalization schemes are presented in Supplementary Tables S1 and S2 for standards and samples, respectively). $^{181}TaO_3$ was monitored for $^{180}TaO_3$ isobaric interference on $^{180}WO_3$. Tungsten oxide isotopologues including ^{18}O (*e.g.*, $^{186}W^{16}O_2{}^{18}O$) were measured using 10^{12} Ω resistor amplifiers to improve signal to noise of low abundance oxides and correct for O isotope variability (Archer et al., 2017). The *Alfa Aesar* W standard (Lot No.: 211576G) was analyzed repeatedly throughout the analytical sessions (n = 21)

with an average $^{182}W/^{184}W$ (normalized to $^{186}W/^{183}W = 1.9859$) of 0.864861 and an external reproducibility of 2.9 ppm (2SD) and 0.6 ppm (2SE; Supplementary Table S1).

2.3.2 Determination of W concentration

Tungsten concentrations were determined using the isotope dilution method with ~100 mg fractions of the same sample powders generated for W isotopic analysis. Following addition of a ^{182}W spike, dissolution and chemical separation (described in the supplementary material), the W fraction was measured by multi-collector inductively-coupled-plasma mass spectrometry (MC-ICP-MS) using a *Thermo Scientific Neptune Plus* instrument in the Plasma Laboratory at the University of Maryland, College Park. The total procedural blanks for W isotope dilution measurements ranged from 14 to 50 pg, which is less than 0.5% of the W mass from the sample.

2.3.3 Highly-siderophile element concentrations and Os isotopic composition

Separation of highly siderophile elements (HSE) utilized Carius tube digestion followed by solvent extraction and microdistillation to purify Os, and anion exchange column chemistry for Re, Ru, Pd, Ir, and Pt (see supplementary material). The Os fraction was analyzed by N-TIMS for Os concentration and $^{187}Os/^{188}Os$ using the *Thermo Scientific Triton* in the Isotope Geochemistry Laboratory at the University of Maryland, College Park. Analytical precision (internal 2SE) for all samples was less than 0.15 %. Total procedural blanks for Os averaged 1.9 pg. Following chemical separation, Re, Ru, Pt, Ir, and Pd were analyzed using a *Thermo Scientific Neptune Plus* MC-ICPMS instrument in the Plasma Laboratory at the University of Maryland, College Park. Average total procedural blanks for Re, Ru, Pt, Ir, and Pd were 2.4, 34, 13, 1.1, and 18 pg.

2.4 Results

2.4.1 Tungsten concentration and isotopic composition of HSDP-2 lavas

Tungsten concentrations of Mauna Kea lavas from HSDP-2 range from 45 to 160 ppb. The W/Th of the samples range from 0.08 to 0.24, all of which are within the range cited for the canonical value (*e.g.*, 0.19 ± 0.15) for the BSE estimated from global mantle-derived lavas (Arevalo and McDonough, 2008). Tungsten concentration varies as an approximately sigmoidal function of MgO wt. % (**Figure 2.1.**). The $\mu^{182}W$ values of Mauna Kea lavas measured in this study range from -1.8 to -16.6, while Mauna Loa lavas analyzed in this study have $\mu^{182}W$ that ranges from +1.9 to -6.5. The typical analytical uncertainty for $\mu^{182}W$ of the samples was 3.3 ppm (internal 2SE). There is no correlation evident between $\mu^{182}W$ and W concentration in this dataset (Supplementary Figure A.2.1). Given the 2.9 ppm (2SD) and 0.6 ppm (2SE) reproducibility of the *Alfa Aesar* W standard, eight out of the nineteen HSDP-2 samples have $\mu^{182}W$ values that are resolvable from the two standard deviation of the terrestrial standard and thirteen are resolvable from the two standard error of the standard (**Table 2.1, Figure 2.2.**). As a measure of data quality, the $\mu^{183}W$ (*i.e.*, $^{183}W/^{184}W$ normalized to $^{186}W/^{184}W$) of the samples was monitored (Supplementary Table S2). The average $\mu^{183}W$ of all HSDP-2 samples was +1.5 ± 4.6 (2SD) and there is no correlation between $\mu^{182}W$ and $\mu^{183}W$ regardless of which isotopic ratio $\mu^{182}W$ is normalized to (Supplementary Figure A.2.2). Previously observed correlations between $\mu^{182}W$ and $\mu^{183}W$, as well as between $\mu^{182}W$ and mass of W processed through chemistry, have been attributed to an analytical origin (Archer et al., 2023); neither correlation is observed in the dataset presented here.

Resolvable $\mu^{182}W$ deficits are more prevalent in the lower portion of the 3000-meter-long stratigraphic column, where the greatest magnitude anomalies and the greatest variation of $\mu^{182}W$ values are also observed. Mauna Kea HSDP-2 lavas exhibit a correlation between $\mu^{182}W$ and $^{3}He/^{4}He$ (*i.e.*, Pearson's correlation coefficient $R^2 = 0.4$; p-value = 0.009, where a significant p-value is <0.05). Normal W isotopic compositions (*i.e.*, $\mu^{182}W = 0 \pm 3.3$) appear throughout the entire stratigraphic section. There is a rebound to larger magnitude $\mu^{182}W$ and $^{3}He/^{4}He$ observed at the transition from Mauna Kea to Mauna Loa volcanics in the HSDP-2 drill core.

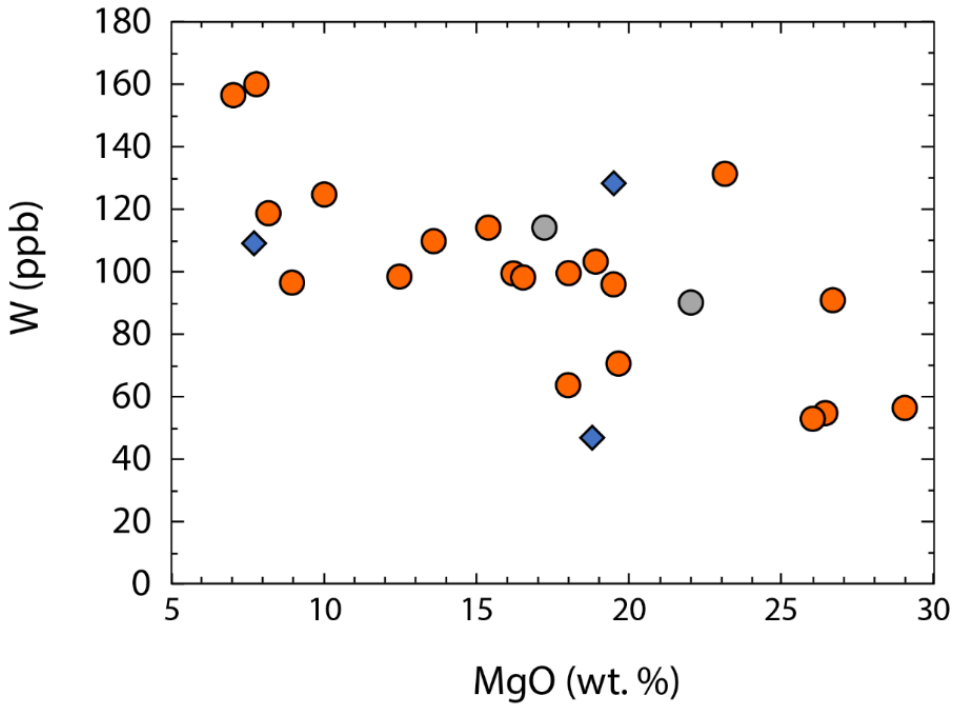

Figure 2.1. Tungsten concentration (ppb) versus MgO (wt. %) of HSDP-2 lavas. Orange circles represent new W concentration measurements for Mauna Kea. Grey circles represent W concentrations of Mauna Kea from previous studies (Mundl et al., 2017). Blue diamonds represent new Mauna Loa data. Uncertainties for MgO and W concentrations are smaller than the symbols. For all samples, MgO wt. % is from Rhodes and Vollinger (2004).

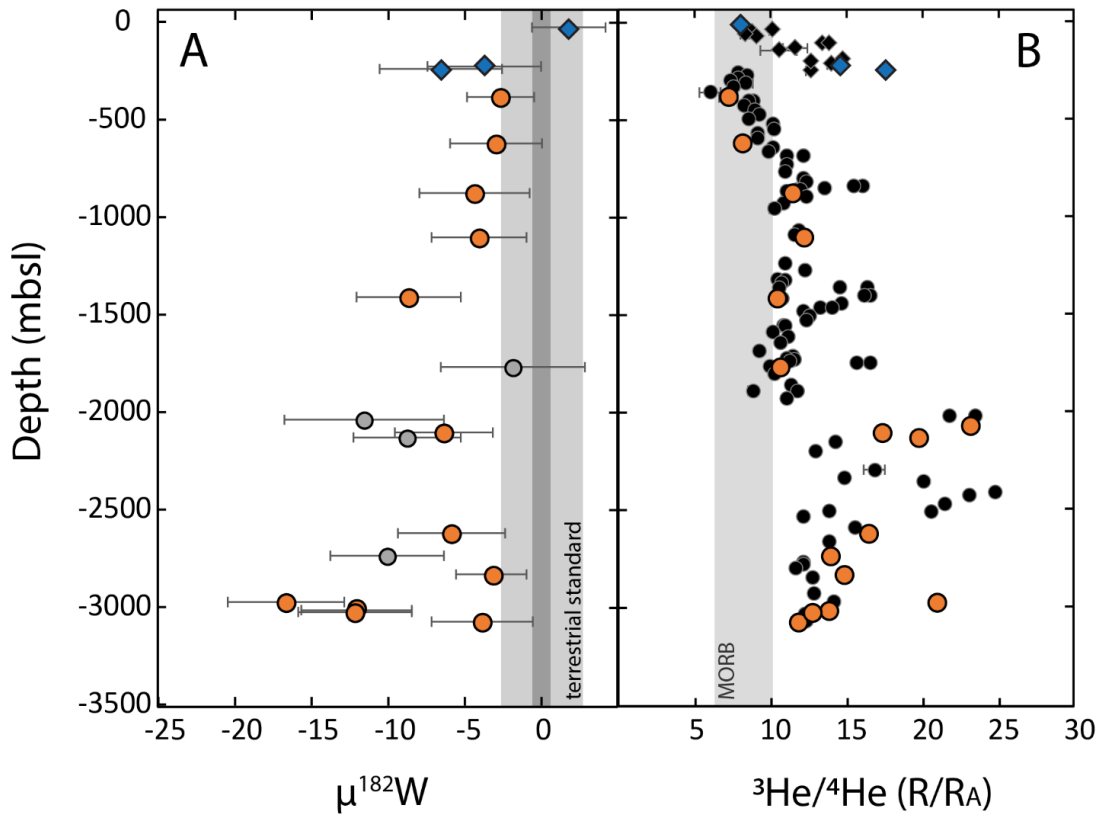

Figure 2.2. Tungsten and helium isotopic compositions as a function of stratigraphic depth (meters below sea level). **(A)** The orange circles are new $\mu^{182}W$ measurements for Mauna Kea volcanics from HSDP-2. Blue diamonds are new $\mu^{182}W$ measurements for Mauna Loa volcanics from HSDP-2. Grey symbols represent previously published $\mu^{182}W$ data (Mundl et al., 2017; Mundl-Petermeier et al., 2020). Vertical grey bands reflect the 2SD (light grey) and 2SE (dark grey) external reproducibility of the *Alfa Aesar* W standard. **(B)** Orange circles represent Mauna Kea samples that have been characterized for both $^3He/^4He$ and $\mu^{182}W$. Blue diamond symbols represent Mauna Loa samples that have been characterized for both $^3He/^4He$ and $\mu^{182}W$. Black circles and diamonds represent $^3He/^4He$ measurements that do not have paired $\mu^{182}W$ analyses. All He data are from Kurz et al. (2004). The vertical grey band reflects the typical range of $^3He/^4He$ (8 ± 2 R/R_A) observed in global MORB distal from mantle plumes (Graham, 2002).

2.4.2 Highly siderophile element concentrations and Os isotopic compositions

Highly siderophile element abundances and $^{187}Os/^{188}Os$ are summarized in Supplementary Table S3**.** Osmium, Ir, and Ru are positively correlated with MgO wt. % (Supplementary Figure A.2.3). Rhenium concentrations are inversely proportional to MgO wt. % (Supplementary Figure A.2.3). Platinum and Pd abundances are not correlated with MgO content, and Pt abundances exhibit the least variance among HSDP-2 lavas (Supplementary Figure A.2.3). There is no correlation between Pt abundance (or any HSE abundance) and $\mu^{182}W$ in HSDP-2 lavas (Supplementary Figure A.2.4).

The new Mauna Kea data are characterized by $^{187}Os/^{188}Os$ that range from 0.1276 to 0.1306 (**Table 1**). Consistent with previous studies, the three Mauna Loa samples examined in this study are more radiogenic than the Mauna Kea lavas, with $^{187}Os/^{188}Os$ ranging from 0.1332 to 0.1396 (Brandon et al., 1999; Bryce et al., 2005; Ireland et al., 2009b). There is no correlation between $^{187}Os/^{188}Os$ and Pt concentration (Supplementary Figure A.2.5).

2.5. Discussion

2.5.1 Highly siderophile element abundance and Os isotopic characteristics of HSDP-2 lavas

Mauna Kea samples from HSDP-2 are depleted in Os, Ru, Ir, Pt, and Pd relative to the BSE (**Figure 2.3.**). Rhenium abundances are typically similar to or enriched compared to BSE. Mauna Loa samples have similar absolute and relative HSE abundances to Mauna Kea in HSDP-2 (**Figure 2.3.**). Platinum does not vary with whole rock MgO, as the incompatible (Re) and compatible (Os, Ir, Ru) HSE vary negatively and positively with MgO wt. %, respectively (Supplementary Figure A.2.3). During igneous differentiation, Pt is not strongly compatible in olivine, chromite, or sulfide (Pitcher et al., 2009). Therefore, Pt is not highly fractionated from the source composition. Since

there is no covariation of Pt abundance with $\mu^{182}W$, it is concluded that the anomalous $\mu^{182}W$ component is not associated with strongly elevated HSE abundances in Mauna Kea's mantle source.

Mauna Kea lavas have relatively un-radiogenic $^{187}Os/^{188}Os$ compared to other Hawaiian volcanic centers (Lassiter and Hauri, 1998; Ireland et al., 2009b). This may indicate a lesser proportion of recycled oceanic crust and sediments contributing to melts generated in the Mauna Kea source region compared to the sources of other Hawaiian volcanic centers (Lassiter and Hauri, 1998). In HSDP-2 Mauna Kea lavas, there is no correlation between Pt abundance and $^{187}Os/^{188}Os$ indicating that the HSE abundance of the mantle source is not related to variation in $^{187}Os/^{188}Os$ observed in the lavas. Additionally, there is no evidence for a relationship between $^{187}Os/^{188}Os$ and $\mu^{182}W$ in Mauna Kea to suggest coupling of $\mu^{182}W$ with siderophile, radiogenic isotope systematics (Supplementary Figure A.2.6).

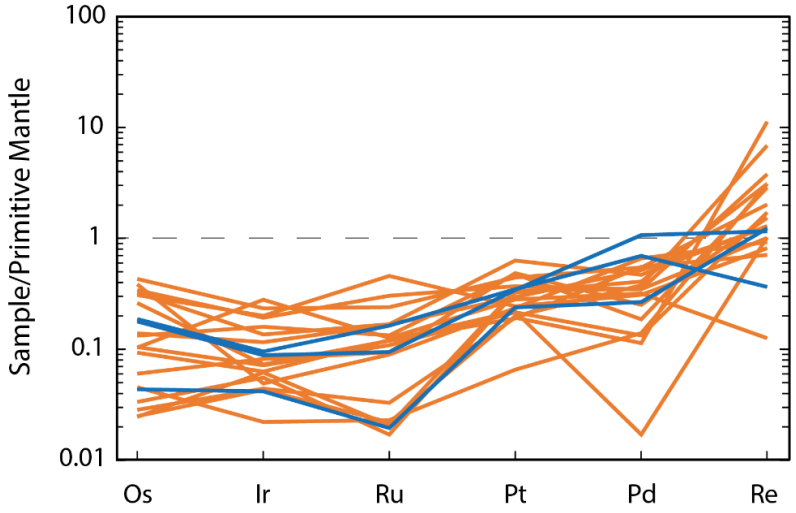

Figure 2.3. Primitive mantle (Becker et al., 2006) normalized highly siderophile element abundances of Mauna Kea (orange) and Mauna Loa (blue) samples from HSDP-2.

2.5.2 Tungsten composition and isotope systematics of the Mauna Kea volcano

Ireland et al. (2009a) estimated that the W concentration of the Mauna Kea source was 8 ± 7 ppb W. This concentration overlaps with estimates of both the BSE, 13 ± 10 ppb W, and the depleted MORB mantle (DMM), 3.0 ± 2.3 ppb W (Arevalo and McDonough, 2008). The canonical W/Th ratios of Mauna Kea lavas reported here support the contention that the Mauna Kea source is not strongly enriched in W relative to other OIB or the DMM. Nevertheless, the estimated W abundance for the Mauna Kea mantle source is permissive of, but does not require entrained recycled material, a less geochemically depleted mantle source, or core material. Additionally, there is no relationship between W concentration and isotopic composition within the HSDP-2 Mauna Kea lavas to indicate that anomalous $\mu^{182}W$ is hosted by a W-rich component or phase in the plume, or that W-rich recycled components have attenuated negative $\mu^{182}W$ values to produce the normal, BSE-like $\mu^{182}W$ of a subset of the HSDP-2 lavas (Supplementary Figure A.2.1).

The new HSDP-2 $\mu^{182}W$ data, combined with corresponding published $^{3}He/^{4}He$ data from the same lava flows, are broadly consistent with the previously reported Hawaiian W-He trend defined by lavas from Mauna Kea, Mauna Loa, Kohala, Kīlauea, and Kamaʻehuakanaloa volcanic centers (**Figure 2.4.**). Variation in the Hawaiian suite cannot be accounted for by a simple two-component mixing model. Thus, as with the global OIB database, a minimum of three component mixing may be required to explain the variance among Hawaiian volcanic centers, although some shallow plume processes may decouple $\mu^{182}W$ from $^{3}He/^{4}He$, leading to data that diverge from two-component mixing models (see Supplementary Material S.4).

For Mauna Kea lavas, the scatter in $\mu^{182}W$ and $^{3}He/^{4}He$ space is less than for the entire Hawaiian suite. This may, in part, reflect the fact that Mauna Kea lavas do not capture the extreme

W and He isotopic compositions observed in other volcanic centers in Hawaii, particularly Kama‘ehuakanaloa. In Mauna Kea, the correlation between $\mu^{182}W$ and $^{3}He/^{4}He$ is statistically robust ($R^2 = 0.4$; p-value = 0.009).

In order to assess whether simple two component mixing can account for the W-He variations present in the Mauna Kea suite, multiple mixing models were considered. It is found that certain two-component mixing models can account for nearly all Mauna Kea samples within the analytical uncertainties (**Figure 2.4.; Supplementary Material S.4**). For example, in the solid-solid mixing model presented in **Figure 2.4.**, the isotopic composition of the ambient mantle is defined by a He isotopic composition of 7 R/R_A, within the range of typical MORB (Graham, 2002), a ^{4}He concentration estimated for primitive mantle of approximately 1×10^{-5} cm^3 STP/g (Gonnermann and Mukhopadhyay, 2007), and $\mu^{182}W$ of 0. The isotopic composition of the anomalous endmember is defined by a possible core isotopic composition of $\mu^{182}W = -220$ (Kleine and Walker, 2017) and $^{3}He/^{4}He$ of 120 R/R_A (Mahaffy et al., 1998). The W concentration for both endmembers is assumed to be the same as the BSE, ~13 ppb (Arevalo and McDonough, 2008) and the He concentration of the anomalous component is defined as having a ^{4}He concentration of 2×10^{-5} cm^3 STP/g (Mahaffy et al., 1998; Ballentine et al., 2002; Gonnermann and Mukhopadhyay, 2007). The W-He composition of the anomalous component may be characteristic of mantle source at the core-mantle boundary if there was isotopic equilibration between the core and the mantle component (*e.g.*, Ferrick and Korenaga, 2023), and is considered further below. By contrast, a solid-solid mixing model in which the ambient mantle endmember is defined by $\mu^{182}W$ of 0, but a substantially lower W concentration of 3 ppb, representative of the DMM (Arevalo and McDonough, 2008), fails to capture the majority of the Mauna Kea data (Supplementary Figure

A.2.7A). Further details and additional mixing scenarios (Supplementary Figures S2.7A-C) are described in Supplementary Material S.4 and parameters are reported in Supplementary Table S4.

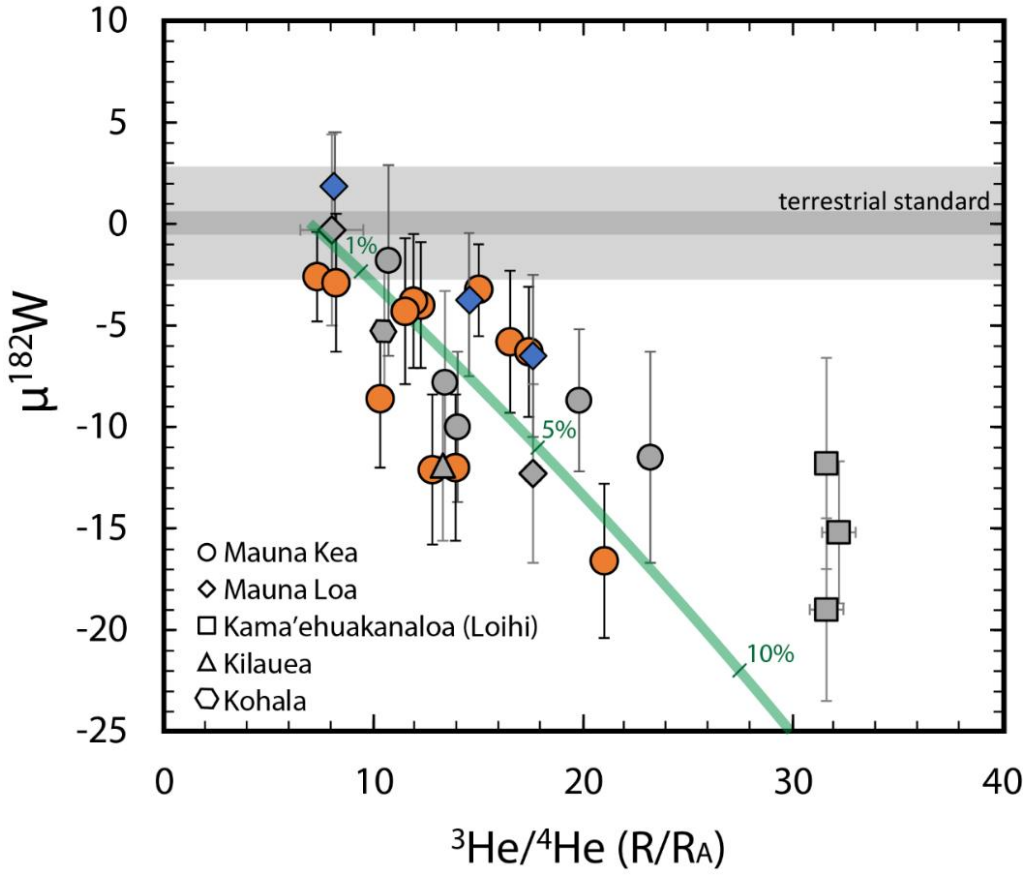

Figure 2.4. Tungsten isotopic composition versus $^{3}He/^{4}He$ (Kurz et al., 2004) for all Hawaiian lavas characterized thus far. The orange circles are new $\mu^{182}W$ measurements for Mauna Kea volcanics from HSDP-2. Blue diamonds are new $\mu^{182}W$ measurements for Mauna Loa volcanics from HSDP-2. Grey symbols represent previously published data (Mundl et al., 2017; Mundl-Petermeier et al., 2020). The green band is a mixing curve between ambient and an anomalous component (details in the text). Tick marks show the compositions with 1, 5, and 10% contributions of the low $\mu^{182}W$, high $^{3}He/^{4}He$ component.

2.5.3 Tungsten-He correlations with other geochemical parameters?

Although mixing involving hypothetical mantle that isotopically equilibrated with the core can satisfy model requirements for the anomalous component of the Mauna Kea source, the true origin of the anomalous $\mu^{182}W$ and elevated $^{3}He/^{4}He$ remains unknown. The $\mu^{182}W$ deficits and the correlation between $\mu^{182}W$ and $^{3}He/^{4}He$ in OIB have previously been interpreted to have resulted from early silicate differentiation, or uneven mixing of late accreted materials into the mantle, termed *grainy late accretion*, in addition to isotopic equilibration with the metallic core (Rizo et al., 2019; Mundl-Petermeier et al., 2020; Archer et al., 2023; Ferrick and Korenaga, 2023). Identification of correlations between $\mu^{182}W$-$^{3}He/^{4}He$ and other geochemical parameters could narrow the possible options for the generation of the anomalies.

Tungsten isotopic compositions in Mauna Kea do not correlate with $^{87}Sr/^{86}Sr$, $^{176}Hf/^{177}Hf$, or $^{187}Os/^{188}Os$ (Supplementary Figure A.2.8). Thus, the mantle componentry recorded by these isotopic systems does not appear related to the expression of $\mu^{182}W$ in the erupted basalts. Moreover, although data are limited, Hawaiian lavas do not appear to exhibit a correlation between $\mu^{182}W$ and the $^{146}Sm \rightarrow ^{142}Nd$ ($t_{1/2}$ = 103 Myr) system, that could provide corroborative evidence for early silicate differentiation as the origin of $\mu^{182}W$ variation (Horan et al., 2018). Given the absence of significant correlations between $\mu^{182}W$ and other long- and short-lived isotopic systems in Hawaiian lavas characterized thus far, if silicate differentiation while ^{182}Hf was extant produced $\mu^{182}W$ variability in the Hawaiian plume source, supporting isotopic evidence for the ancient Hf/W fractionation event may have since been overprinted by subsequent differentiation or mixing events.

Certain types of core-mantle interactions or the effects of grainy late accretion might be expected to lead to correlations between $\mu^{182}W$ and HSE source abundances, given the high HSE

abundances in the metallic core and bulk chondrites (Touboul et al., 2012; Puchtel et al., 2016; Peters et al., 2023; Walker et al., 2023). Correlation between $\mu^{182}W$ and Ru/Ir has been previously observed within a group of Hawaiian lavas from Mauna Kea, Mauna Loa, Kama‘ehuakanaloa, Kīlauea, and Kohala, and was inferred to reflect low-pressure, metal-silicate equilibration that occurred early in Earth's history (Peters et al., 2023). Neither $\mu^{182}W$ nor $^{3}He/^{4}He$, however, correlate with Ru/Ir in the Mauna Kea HSDP-2 dataset (Supplementary Figure A.2.9). Direct metal transfer from the liquid outer core into the silicate mantle would significantly elevate the abundances of siderophile elements in the affected mantle. For example, entrainment of core metal with 470 ppb W (McDonough, 2003) and $\mu^{182}W = -220$ (Kleine and Walker, 2017), into the lower mantle would require ~0.25 wt. % of core metal to generate a $\mu^{182}W$ of -18, which is within uncertainty of the largest $\mu^{182}W$ deficit observed in HSDP-2 (Supplementary Table S4). However, the addition of 0.25% of outer core metal with a Pt concentration of 5700 ppb (McDonough, 2003) would elevate the Pt abundance of the mantle source to ~22 ppb, which is unlikely to produce the range of Pt abundances observed in HSDP-2 lavas (0.5 to 4.8 ppb Pt).

As discussed above, core-mantle interaction may also involve a mechanism that does not directly transfer siderophile elements from the core to the silicate mantle, as would occur with metal infiltration. Previously proposed mechanisms include preferential transfer of W from the core relative to HSE, via oxide exsolution (Rizo et al., 2019), grain boundary diffusion of W from the core (Yoshino et al., 2020), or isotopic equilibration of W between the mantle and core without net mass transfer of W (Mundl-Petermeier et al., 2020; Ferrick and Korenaga, 2023). These mechanisms could occur at any time throughout Earth's history. A core-equilibrated mantle reservoir would not necessarily inherit elevated abundances of W and HSE or coupled ^{182}W-^{142}Nd signatures (Mundl-Petermeier et al., 2020).

Conversely, the presence of relatively unmodified, excess late accreted materials in the anomalous mantle source component would generate negative $\mu^{182}W$ and elevated abundances of siderophile elements in the mantle source. For example, an isolated, BSE-like mantle reservoir with 0.8 wt. % excess chondritic material with 1220 ppb Pt (Horan et al., 2003), 150 ppb W, and $\mu^{182}W = -190$ (Kleine et al., 2004a) would have a $\mu^{182}W$ of -16, similar to the maximum observed $\mu^{182}W$ deficit in Mauna Kea (Supplementary Table S4). The solid mantle mixture of BSE with an excess chondritic-like component would have 17 ppb Pt. Given that Pt is not substantially fractionated from the source composition, a mantle source with 17 ppb Pt is higher than may be presumed, given the Pt abundances observed in Mauna Kea melts, and estimated parental melt of 2.3 ± 0.2 ppb Pt (Ireland et al., 2009b). Isolation and preservation of an excess late accreted material in the deep mantle, thus, would likely elevate the HSE abundances to the extent that it would be detected.

In contrast to long- and short-lived isotope systems, as well as most lithophile and siderophile element abundances, $\mu^{182}W$ in the drill core lavas is characterized by robust correlations with certain high field strength elements (HFSE), consistent with the prior observation of excess HFSE accompanying elevated $^{3}He/^{4}He$ (Jackson et al., 2008). For example, within the HSDP-2 dataset there is a negative correlation between $\mu^{182}W$ and $^{208}Pb/^{204}Pb$ ($R^2 = 0.3$; p-value = 0.03) and positive correlation between $^{3}He/^{4}He$ and $^{208}Pb/^{204}Pb$ ($R^2 = 0.6$; p-value < 0.001; **Figure 2.5. C,F**). The expression of greater magnitude $\mu^{182}W$ deficits in Mauna Kea could thus be related to elevated abundances of the HFSE Th, as well as time-integrated Th/Pb of the source characterized by negative $\mu^{182}W$, compared to Mauna Kea lavas with normal $\mu^{182}W$. For the Mauna Kea suite there are also statistically significant negative correlations between $\mu^{182}W$ and Ti/Ti* ($Ti/Ti^*=Ti_N/(Sm_N*Tb_N)^{0.5}$), as well as Nb/Nb* ($Nb/Nb^*=Nb_N/(La_N*Th_N)^{0.5}$), linking negative

$\mu^{182}W$ anomalies to an excess of the refractory, HFSE Ti and Nb, relative to similarly incompatible elements (**Figure 2.5. A-B**). Consistent with the global dataset (Jackson et al., 2008), the correlations between $^{3}He/^{4}He$ and Ti/Ti* and Nb/Nb* are also significant (**Figure 2.5. D-E**).

Variations in Ti/Ti* and Nb/Nb* in OIB have been attributed to processes, such as partial melting and/or fractional crystallization and assimilation (Peters and Day, 2014), or may reflect mixing between mantle sources with different Ti and Nb concentrations (Prytulak and Elliott, 2007; Jackson et al., 2008). Assimilation and fractional crystallization (AFC) of oceanic crust during OIB petrogenesis can produce positive Ti/Ti* and Nb/Nb* that positively correlate with whole rock MgO wt. % and olivine and pyroxene modal abundances (Peters and Day, 2014). Within the HSDP-2 dataset, however, Ti/Ti* and Nb/Nb* do not correlate with MgO wt. %, or other major element systematics, such as CaO/Al_2O_3, an indicator of pyroxene fractionation (Supplementary Figure A.2.10). Further, it is unlikely that $\mu^{182}W$ and $^{3}He/^{4}He$ would be equivalently affected by AFC processes to produce the correlations observed in **Figure 2.5.**. Elevated Ti/Ti* and Nb/Nb* are also not likely due to an excess of a Ti-rich phase(s) in the Mauna Kea lavas, such as rutile, because Ti/Ti* and Nb/Nb* do not correlate with bulk rock TiO_2 wt. % (Supplementary Figure A.2.10).

The involvement of different phases related to depth of melting could also result in elevated Ti/Ti* and Nb/Nb*. Rare earth element systematics, for example small variations in Gd/Yb, of the HSDP-2 drill core indicate that the older, stratigraphically lower lavas, where the greatest $\mu^{182}W$ deficits and $^{3}He/^{4}He$ are observed, were produced by higher degree partial melts, and that the degree of partial melting tapered off over time as Gd/Yb increased stratigraphically upward (Feigenson et al., 2003). The expression of high $^{3}He/^{4}He$ and negative $\mu^{182}W$, in addition to elevated Ti/Ti* and Nb/Nb*, in the plume may be related to a higher degree of partial melting. The

$^{3}He/^{4}He$ of the drill core lavas anticorrelates with Gd/Yb (R^2 = 0.4; p-value = 0.007), although $\mu^{182}W$ is not well-correlated with Gd/Yb (R^2 = 0.2; p-value = 0.13) within the precision of the current dataset (Supplementary Figure A.2.11). The $\mu^{182}W$ and trace element systematics point to high temperature melting of a less fusible component in the generation of negative $\mu^{182}W$ and high $^{3}He/^{4}He$ in the erupted basalts. Therefore, we conclude elevated Ti/Ti* and Nb/Nb* are primary characteristics of the negative $\mu^{182}W$ mantle source. This conclusion then begs the question of how the elevated Ti/Ti* and Nb/Nb* (and potentially Th) were generated in relation to the anomalous W-He characteristics.

Subchondritic Ti/Zr and Nb/La in the DMM (and continental crust) has been taken as evidence for the existence of a complementary Ti- and Nb-rich reservoir, such as recycled crust in the form of eclogite accumulated in the lower mantle (McDonough, 1991; Jackson et al., 2008). Such material, however, would be unlikely to host low $\mu^{182}W$ and high $^{3}He/^{4}He$, given that most of this material would have accumulated subsequent to the disappearance of ^{182}Hf, and likely experienced He degassing. Thus, if the Ti, Nb, and potentially Th, enrichment in the anomalous component is associated with recycled crust, the correlations must be attributed to a physical juxtaposition of recycled eclogite and lower mantle domain(s) already characterized by anomalous $\mu^{182}W$ and $^{3}He/^{4}He$ (Jackson et al., 2008). Isotopic equilibration between recycled eclogite at the core-mantle boundary and the outer core could potentially produce a reservoir with high Ti/Ti*, Nb/Nb*, and negative $\mu^{182}W$. Diffusion of He from the core could also potentially transfer high $^{3}He/^{4}He$ to the recycled eclogitic component at the core-mantle boundary, as the recycled material itself would be unlikely to host high $^{3}He/^{4}He$ (Hanyu and Kaneoka, 1997; Moreira and Kurz, 2001; Moreira et al., 2003). Nevertheless, there is considerable debate with regard to the He content of the core as well as its isotopic composition (Bouhifd et al., 2013b; Roth et al., 2019; Ozgurel and

Caracas, 2023; Horton et al., 2023). Although the core formed early in Earth history, its $^{3}He/^{4}He$ may not be as high as in primitive materials, given that its composition through time would be dependent on the concentration of He relative to that of the ^{4}He producing elements, U, Th, and Pt present in the core (Ozgurel and Caracas, 2023). Furthermore, a high Re/Os eclogitic component in the mantle source would be expected to produce radiogenic $^{187}Os/^{188}Os$, which is in contrast to the relatively un-radiogenic $^{187}Os/^{188}Os$ of Mauna Kea compared to other Hawaiian volcanic centers; therefore, this is considered an unlikely model.

Another mechanism which could lead to elevated Ti/Ti* and Nb/Nb* in mantle-derived rocks is melt equilibration with a bridgmanite and Ca-perovskite bearing lithology in the lower mantle, due to the relatively low partition coefficients of Ti and Nb in perovskites compared to rare earth elements and U (Hirose et al., 2004; Jackson et al., 2008). A basal magma ocean with high Ti/Ti* and Nb/Nb* could experience isotopic equilibration with the core at any point in Earth's history to acquire negative $\mu^{182}W$ (Mundl-Petermeier et al., 2020). Alternatively, an early magma ocean that equilibrated with bridgmanite and Ca-perovskite while ^{182}Hf was extant may also be characterized by a low Hf/W, due to the preferential compatibility of Hf, relative to W, in the two perovskite phases (Corgne et al., 2005; Brown et al., 2014), and would therefore evolve to a lower $\mu^{182}W$ than the crystallizing solid. In this case, a single process might have generated high Ti/Ti* and Nb/Nb* and negative $\mu^{182}W$. The envisioned deep, primitive reservoir, however, must have retained isotopic signatures that pre-date the Moon-forming giant impact event. This early-formed reservoir might also have developed a low Sm/Nd, and therefore, evolve negative $\mu^{142}Nd$ (Brown et al., 2014). Limited available data do not show a correlation between $\mu^{182}W$ and $\mu^{142}Nd$ in Hawaii (Horan et al., 2018). It is also possible that the degree of fractionation between Sm and Nd was insufficient to generate discernable $\mu^{142}Nd$ variability, as the partition coefficients for Sm

and Nd in perovskite may be more similar compared to Hf and W (Brown et al., 2014). Additionally, recycling of lithospheric material with a high Nd/W would preferentially erase μ^{142}Nd variability compared to μ^{182}W. This may be likely due to the high Nd/W in mantle-derived rocks (Arevalo and McDonough, 2010) and bulk continental crust (Rudnick and Gao, 2003), as well as the fluid mobility of W during subduction that may remove W from the down-going slab (Bali et al., 2012). Therefore, if μ^{182}W and μ^{142}Nd were correlated in an early, deep mantle magma ocean, μ^{142}Nd variability may have since been overprinted.

We conclude that either diffusional equilibration of W and possibly He between the core and a HFSE-enriched portion of the mantle occurring at the core-mantle boundary, or very early crystal-liquid fractionation associated with magma ocean crystallization occurring in the deep mantle, can potentially account for the origin of the isotopically anomalous component identified in the Mauna Kea suite. Geophysical evidence supports the presence of a km-scale physically distinct layer, such as a remnant magma ocean or iron-enriched domain possibly related to ultra-low velocity zones, at the core-mantle boundary, where long-term storage of He and ancient geochemical signatures (*e.g.*, low μ^{182}W and high ^{3}He/^{4}He) and/or core-mantle interaction is also plausible (Williams and Garnero, 1996; Labrosse et al., 2007; Russell et al., 2023). Uncertainties in the concentration and isotopic composition of He in the core or an early magma ocean, diffusion characteristics of W and He at the CMB, and partitioning behaviors of Hf and W at high pressures and temperatures preclude a more definitive determination of the origin of the anomalous component.

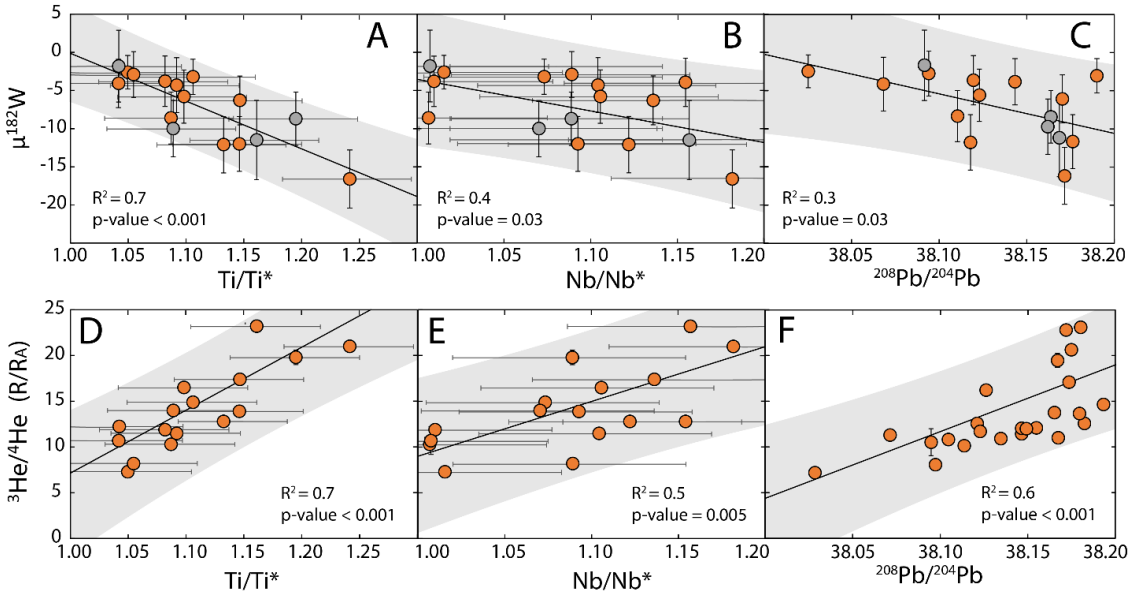

Figure 2.5. Tungsten and helium isotopic compositions correlate with Ti/Ti* (**A, D**), Nb/Nb* (**B, E**), and $^{208}Pb/^{204}Pb$ (**C, F**). Error bars represent the 2SE for $\mu^{182}W$ and $^{208}Pb/^{204}Pb$ and 1σ for $^{3}He/^{4}He$. Linear regressions are plotted as black lines with grey bands representing the 95% confidence interval of the regression. Grey circles are previously published $\mu^{182}W$ (Mundl et al., 2017; Mundl-Petermeier et al., 2020). Helium data is from Kurz et al. (2004). Trace element data are from Huang and Frey (2003) and Rhodes and Vollinger (2004). Error bars for Ti/Ti* and Nb/Nb*are calculated by propagating the 1SD of Ti, Nb, Sm, Tb, La, and Th measurements through each ratio.

2.5.4 Implications for plume structure and dynamics

The stratigraphic series of $\mu^{182}W$ presented here provides an opportunity to investigate plume structure and dynamics from a W isotopic perspective. Pre-existing plume models for Hawaii include a concentrically zoned plume in which primitive material containing high $^{3}He/^{4}He$ is located at the axis of the plume where the temperature is highest (DePaolo et al., 2001; Bryce et al., 2005). A contrasting model for the Hawaiian plume is a bilaterally zoned plume that produces

the geographic and chemical Kea and Loa trend volcanic chains (Abouchami et al., 2005). A third model, which is not mutually exclusive from either a concentrically or bilaterally zoned plume, includes vertical heterogeneity with "blobs" or elongated "filaments" of anomalous material (*e.g.,* recycled or primitive material) that can cause isotopic variations over time and space in Hawaiian volcanics (Blichert-Toft et al., 2003; Eisele et al., 2003; Bryce et al., 2005; Farnetani and Hofmann, 2009).

To test whether the $\mu^{182}W$ systematics of HSDP-2 can be explained by any of these plume models, we examine the stratigraphic data as a function of time and location of the Mauna Kea and Mauna Loa volcanoes relative to the inferred plume center. First, we consider a concentrically zoned plume to calculate the expected isotopic composition of the HSDP-2 core as Mauna Kea (and Mauna Loa) recede from the plume axis. In this model, the isotopic composition of the plume center is defined by the highest $^3He/^4He$ (32.2 R/R_A) and greatest magnitude $\mu^{182}W$ deficit (-25.6) measured in Hawaiian lavas (Kent et al., 1999; Mundl-Petermeier et al., 2020). The most distal portion of the plume is defined by "normal" mantle $^3He/^4He$ (~8 R/R_A) (Graham, 2002) and $\mu^{182}W$ (~0) (Kleine and Walker, 2017). To model the isotopic composition of the HSDP-2 drill core that would result from a concentrically zoned plume, we calculate the isotopic ratio of a given element (*i.e.,* He, Sr, Hf, W, Os, Pb) as a function of radial distance from the plume axis. The axis is assigned the maximum (or minimum) value for each isotopic ratio of interest and the ratio changes exponentially with radial distance according to $R = R_{min} + (R_{max} - R_{min}) \times e^{\frac{r^2}{a^2}}$, and expresses the isotopic ratio, R, of a given element as a function of radial distance, r, from the plume axis (Bryce et al., 2005). There is also a parameter for the length-scale of isotopic heterogeneity, a, that controls how rapidly the ratio changes with radius, r (Bryce et al., 2005). Further details on the calculation can be found in the supplementary material.

We find that a concentrically zoned plume with anomalous $^{3}He/^{4}He$ and $\mu^{182}W$ could produce the greatest magnitude anomalies and temporal decrease in the magnitude of $\mu^{182}W$ and $^{3}He/^{4}He$ in Mauna Kea (**Figure 2.6.**). The reappearance of $\mu^{182}W$ deficits and elevated $^{3}He/^{4}He$ in the Mauna Loa volcanics may be due to the relative proximity of Mauna Loa to the plume axis at ~200 ka compared to the Mauna Kea volcano sampled just prior in the stratigraphic column. The presence of "normal" $\mu^{182}W$ and moderate deficits throughout the entire Mauna Kea stratigraphic sequence requires that ambient mantle-like $^{3}He/^{4}He$ and $\mu^{182}W$ coexist in the melt region. Thus, the calculated isotopic compositions in the concentrically zoned plume model reflect only the maximum magnitude $^{3}He/^{4}He$ and $\mu^{182}W$ values (**Figure 2.6.**). Compositional zoning, and/or a temperature-dependent process, like relative partial melting of variably fusible components, are plausible as the distance of a volcano from the plume center also scales with a decrease in plume temperature.

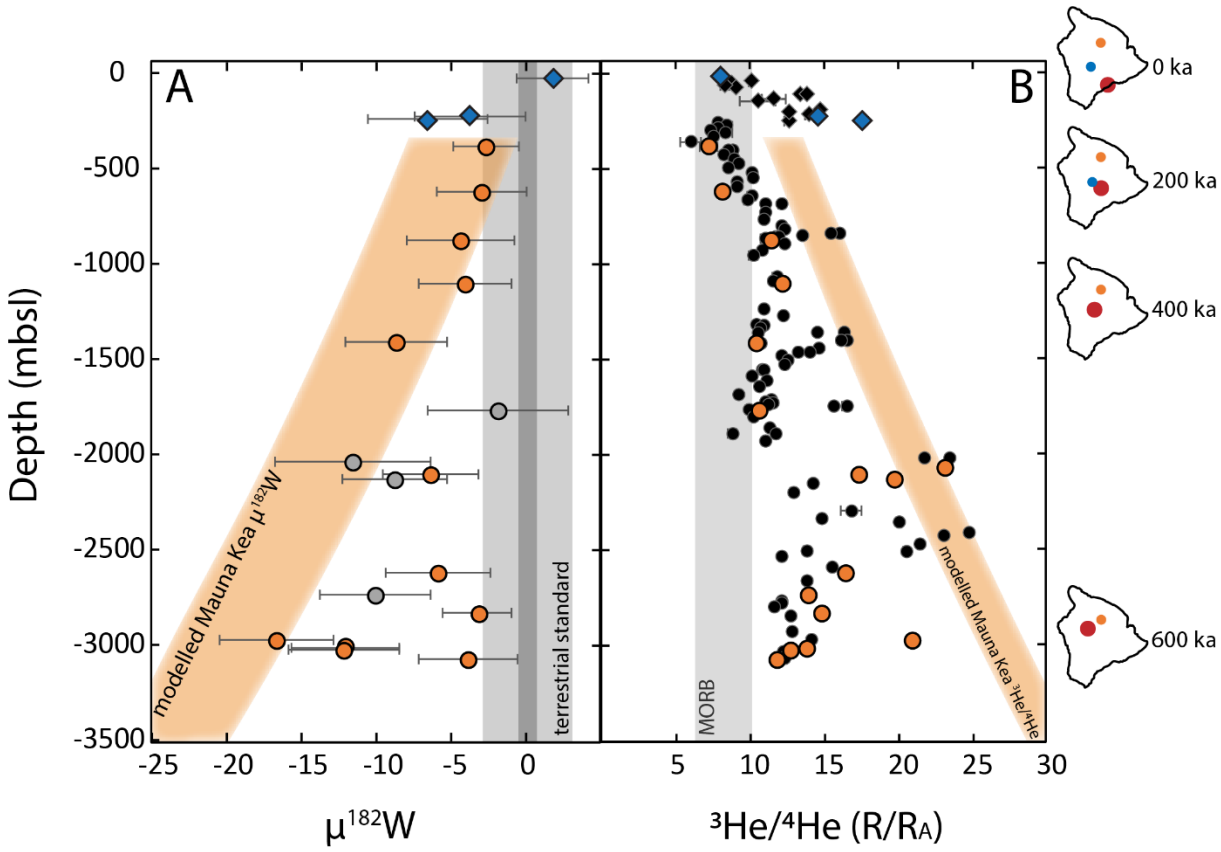

Figure 2.6. The orange fields represent the calculated isotopic composition of Mauna Kea in the drill core based on a concentrically zoned plume. Far right: The relative location of Mauna Kea (orange circle) and Mauna Loa (blue circle), respectively, from the inferred plume core (red circle). (**A**) Orange symbols are data from this study and grey symbols are previous $\mu^{182}W$ measurements (Mundl et al., 2017; Mundl-Petermeier et al., 2020). Blue diamonds are new $\mu^{182}W$ measurements for Mauna Loa volcanics from HSDP-2. Vertical grey bands reflect the 2SD (light grey) and 2SE (dark grey) external reproducibility of the Alfa Aesar W standard. (**B**) Orange and blue symbols represent the samples that have also been characterized for $\mu^{182}W$. Black circles and diamonds represent $^{3}He/^{4}He$ measurements that do not have paired $\mu^{182}W$ analyses. All He data are from Kurz et al. (2004). The vertical grey band reflects the typical range of $^{3}He/^{4}He$ (8 ± 2 R/R_A) observed in global MORB distal from mantle plumes (Graham, 2002).

A concentrically zoned plume fails to explain the lack of variation observed in $^{87}Sr/^{86}Sr$, $^{176}Hf/^{177}Hf$, $^{206}Pb/^{204}Pb$, $^{207}Pb/^{204}Pb$, and $^{187}Os/^{188}Os$ in the Mauna Kea stratigraphic column, since the ratios should systematically change with radial distance from the plume center (Supplementary Figure A.2.12). Of note, however, is that the model seems to better capture Mauna Loa Hf and Pb isotopic compositions (Supplementary Figure A.2.12). This requires a more complex plume structure than compositional concentric zoning to capture the isotope systematics of both volcanoes.

An alternative structural model for the Hawaiian mantle plume invokes a bilateral or azimuthal zonation that can explain the Loa and Kea trends observed across several Hawaiian islands (Abouchami et al., 2005). One interpretation is that the geochemically enriched Loa trend characteristics result from the entrainment of a physically distinct deep mantle component associated with recycled and/or primitive material, and the Kea trend samples the ambient, deep Pacific mantle (Weis et al., 2011, 2020; Harrison et al., 2017). Tungsten isotopic data for three Kea trend volcanoes (Kohala, Mauna Kea, and Kīlauea) and two Loa trend volcanoes (Mauna Loa and Kama‘ehuakanaloa) show that both trends produce rocks with negative $\mu^{182}W$ (Mundl et al., 2017; Mundl-Petermeier et al., 2020; Archer et al., 2023). Despite distinct componentry defining the lithophile isotopic compositions of the Kea and Loa trends, within HSDP-2, Mauna Loa samples have a $^{3}He/^{4}He$ versus $\mu^{182}W$ slope that is indistinguishable from Mauna Kea, indicating there is no bilateral difference in the W-He systematics of the Hawaiian plume. It is concluded that the component(s) hosting $\mu^{182}W$ deficits and high $^{3}He/^{4}He$ are sampled by both Loa and Kea trends and are thus independent of any bilateral zonation intrinsic to the plume. It remains likely, however, that the Loa trend samples a distinct deep component(s) with respect to radiogenic lithophile isotopic systems (Weis et al., 2011, 2020; Harrison et al., 2017). Strategic sampling from both

younger and older Loa and Kea trend volcanoes will be necessary to identify differences, if any, in W-He systematics between the two trends.

Vertical heterogeneity in the plume may also explain the temporal trends observed in HSDP-2. A vertical "pulse" or "blob" of anomalous material may produce high $^{3}He/^{4}He$ and $\mu^{182}W$ deficits in volcanic products for a period of time that correlates with the size of the "pulse" (Farnetani and Hofmann, 2009, 2010; Farnetani et al., 2018). It is possible that $\mu^{182}W$ deficits exist at equal or greater magnitude in the Mauna Kea volcanics below the HSDP-2 drill core stratigraphy, making it impossible to constrain the size of a hypothetical, anomalous "filament" or "blob" in the plume source. Of the characterized lavas, the first resolvable $\mu^{182}W$ deficit appears at ~620 ka and the last resolvable $\mu^{182}W$ deficit occurs at ~440 ka, giving a minimum ~180 kyr duration of sampling anomalous material at Mauna Kea. Assuming the vertical velocity of the plume is a maximum of 34 cm/yr at the axis and decreases exponentially to 2 cm/yr at the edge (Watson and McKenzie, 1991), integration across the ~180 kyr Mauna Kea record where resolvable $\mu^{182}W$ deficits are present may constrain the minimum vertical height of the isotopically anomalous portion of the solid plume that was sampled during that interval. The minimum approximate vertical height required to produce ~180 kyr of anomalous $\mu^{182}W$ is ~30 km (see supplementary material for calculation). A vertically heterogenous model would further require a coincidence to produce the systematic appearance and dissipation of $^{3}He/^{4}He$ and $\mu^{182}W$ anomalies in HSDP-2 in both Mauna Kea and Mauna Loa as they move away from the plume axis. A second "blob" is then required to reintroduce anomalous $\mu^{182}W$ at the beginning of the Mauna Loa stratigraphic section in HSDP-2. Therefore, although plausible, a "pulsing" plume appears unlikely to explain HSDP-2 $\mu^{182}W$ stratigraphy. It is more likely that vertical heterogeneity coexists within a concentrically and/or azimuthally zoned plume in the form of elongated filaments that span

beyond the timescale of the HSDP-2 drill core (Farnetani and Hofmann, 2009, 2010; Farnetani et al., 2018).

2.6. Conclusions

Mauna Kea volcanics are characterized by $\mu^{182}W$ values ranging from those similar to the modern BSE to negative $\mu^{182}W$ values that are well-resolved from the terrestrial standard. Generally, $\mu^{182}W$ is correlated with $^{3}He/^{4}He$ in Mauna Kea and the W-He systematics can be explained by two component mixing. The elevated Ti/Ti* and Nb/Nb* observed in lavas with $\mu^{182}W$ deficits indicates that a refractory component likely hosts the negative $\mu^{182}W$ and high $^{3}He/^{4}He$. This component may have originated solely as a result of early Earth crystal-liquid fractionation processes in the deep mantle, or as a result of diffusional equilibration of W and possibly He between the core and the mantle coupled with an early magma ocean fractionation product at the core-mantle boundary. The HSDP-2 stratigraphy shows that $\mu^{182}W$ deficits and $^{3}He/^{4}He$ are greatest when the Mauna Kea volcano was nearest the plume axis. The refractory component hosting negative $\mu^{182}W$ and high $^{3}He/^{4}He$ may be more easily melted at the plume axis where the temperature is highest compared to cooler, distal regions of the plume. The two defining type locality volcanoes for the Kea and Loa trends, Mauna Kea and Mauna Loa, respectively, do not show distinct $\mu^{182}W$ and $^{3}He/^{4}He$ systematics with the available data. This observation indicates that anomalous $\mu^{182}W$ is likely independent of the distinct mantle components that produce the Loa and Kea trend geochemical characteristics in Hawaii.

2.7. CRediT authorship contribution statement

Lori N Willhite: Conceptualization, Methodology, Investigation, Formal analysis, Data curation, Visualization, Writing – original draft, Writing – review & editing. **Valerie A Finlayson:** Conceptualization, Methodology, Investigation, Writing – review & editing, Funding acquisition. **Richard J Walker:** Conceptualization, Supervision, Investigation, Resources, Writing – review & editing, Funding acquisition.

2.8. Acknowledgements

This work was supported by NSF-EAR #2121979 to R. J. W. and V. A. F. The authors would like to thank Saebyul Choe for her assistance with drill core sampling and curation at the American Museum of Natural History, and Andrew Houston for his assistance with sample preparation at UMD. We thank Hanika Rizo and an anonymous reviewer for their comments that improved this manuscript. The authors thank Fang-Zhen Teng for the editorial handling of this manuscript.

2.9. Chapter 2 Appendix

2.9.1. Rock preparation and chemical separation for W isotopic composition

Samples were cut using a diamond-tipped rock saw blade, targeting the freshest portions of each sample. The cut rocks were then sanded to remove contamination from the saw blade prior to crushing with ceramic plates in a jaw crusher. An alumina shatterbox was used to powder the crushed samples. Between 13.5 and 31.7 grams of rock powder were digested using 2 mL of concentrated HNO_3 and 10 mL concentrated HF per gram of sample at 150 °C for at least 120 hours. Following sample digestion, the solution was dried down and brought up in 5 mL concentrated HF per gram of sample and left overnight at 150 °C to prevent high field strength elements (HFSE) from co-precipitating with fluoride salts (Blichert-Toft et al., 1997). Solid fluorides were then separated by centrifuging for ~30 min. The supernatant was dried down at ~120 °C. This step was repeated twice to extract W from the fluorides. Once dry, 6N HCl was added to the supernatant to convert it to chloride form. Once fully dissolved in 6N HCl, the solution was dried down. The sample was then brought up in 0.4M HCl + 0.5M HF (10 mL per 5 grams of sample).

Wet chemistry for primary W separation then followed a modified anion chromatography column procedure (Nagai and Yokoyama, 2014). The primary W separation was performed using 30 mL Bio-Rad column with 10 mL of Bio-Rad AG1-X8 (200-400 mesh) anion exchange resin. Resin cleaning steps included 100 mL 6M HCl followed by 50 mL 9M HCl + 3M HF, then 20 mL MilliQ® water, and 100 mL 6M HNO_3 + 3M HF. The sample was then loaded onto the resin followed by 30 mL of 0.4M HCl + 0.5M HF to remove the major matrix elements. The procedure then diverged from the Nagai and Yokoyama (2014) chemistry and did not use the 9M HCl + 0.05M HF step to separate Ti, Zr, and Hf because W tended to leak out of the column during this

step. Additionally, primary W collection used 9M HCl + 3M HF instead of 9M HCl + 1M HF because this yielded better separation of W and Nb. The W fraction was separated from Ti, Zr, Nb, and Hf in the clean-up column procedure subsequent to the primary column (Kleine et al., 2012). All samples required two or three iterations of the clean-up column procedure to purify W and reduce the Ti/W to below 0.5. Total analytical yields for W ranged from approximately 30 to 70%.

2.9.2. Sample preparation and chemical separation for determination of W concentration

Prior to sample digestion, the Teflon beakers were spiked with ~10 ng of ^{182}W spike per ~100 mg of rock powder. Powders were digested and equilibrated with the ^{182}W spike in 1 mL concentrated HNO_3 and 5 mL concentrated HF at ~150 °C for at least 24 hours. Digested samples were dried down and treated with 200 µL concentrated HNO_3 to break down fluoride salts, then re-dried. This step was repeated once. Next, 2 mL 6M HCl was added to each beaker and left to reflux for 48 hours. Samples were dried down and brought up in 5 mL 6M HCl and left to reflux for 24 hours. After 24 hours the samples were dried down. Two mL of 0.5M HCl + 0.5M HF were added to each sample and was dried down. Prior to loading onto the anion exchange column, 5 mL 0.5M HCl + 0.5M HF was added to each sample and refluxed for at least one hour then cooled to room temperature before chemical separation of W (Kleine et al., 2004b).

2.9.3. Chemical separation for analysis of highly-siderophile element concentrations and Os isotopic composition

Chemical procedures for purification of Ru, Pd, Ir, Pt, Re, and Os are based on techniques described in (Shirey and Walker, 1995; Ireland et al., 2009b). Teflon beakers were spiked with

^{190}Os enriched spike, ^{185}Re enriched spike, and a combined ^{99}Ru, ^{105}Pd, ^{191}Ir, and ^{194}Pt enriched spike. Concentrated HCl (3 mL) was added to each spiked beaker and then the contents of each beaker were added to borosilicate Carius tubes containing ~1.5 grams of sample powder. Before sealing the Carius tubes, 6 mL concentrated HNO_3 was added to each sample. Once sealed, the Carius tubes were placed in an oven at ~250 °C for at least 24 hours. Following sample digestion, Os was removed from the aqueous phase by CCl_4 solvent extraction followed by a HBr back extraction. The HBr fraction containing Os was dried down in preparation for Os microdistillation, which was then performed by adding chromic acid solution to the Os fraction and distilling Os to into an HBr trap. The other HSE were separated by anion exchange column chromatography as in Ireland et al. (2009).

2.9.4. Mixing scenarios and potential decoupling of $\mu^{182}W$ and $^3He/^4He$

In addition to the mixing model presented in the main text (*e.g.*, Figure 4), several plausible mixing scenarios have been investigated to assess the μ^{182}W and ^{3}He/^{4}He correlation for the HSDP-2 drill core samples and the greater Hawaiian suite (Supplementary Figure A.2.7). We present three additional scenarios here (parameters for all mixing scenarios are found in Supplementary Table S4). The first is a mixture of depleted mantle and a mantle reservoir that has been isotopically equilibrated with the outer core. The depleted mantle ^{4}He concentration is defined as 1×10^{-5} cm^3 STP/g and the mantle reservoir that is isotopically equilibrated (with respect to μ^{182}W) with the liquid outer core is given the ^{4}He concentration of the primitive mantle, approximately 2×10^{-5} cm^3 STP/g (Gonnermann and Mukhopadhyay, 2007). The ^{3}He/^{4}He of the depleted mantle and isotopically core-equilibrated mantle are defined as 7 R/R_A (Graham, 2002) and 120 R/R_A (Mahaffy et al., 1998), respectively. The He isotopic composition of the high

$^{3}He/^{4}He$ endmember is particularly difficult to constrain, given uncertainties in the abundance of radioactive nuclides in the metal core (Ozgurel and Caracas, 2023), as well as in silicate mantle, that undergo alpha decay and produce ^{4}He throughout geologic time. Here we employ the $^{3}He/^{4}He$ of Jupiter's atmosphere (Mahaffy et al., 1998) as an extreme endmember composition. Tungsten abundances of the depleted mantle and core-equilibrated mantle are 3 ppb and 13 ppb, respectively (Arevalo and McDonough, 2008). The $\mu^{182}W$ of the depleted mantle is 0 and a reservoir that has isotopically equilibrated with the outer core is given a $\mu^{182}W$ of -220 (Kleine et al., 2002). The resultant mixing curve is illustrated in Supplementary Figure A.2.7.

An alternative mixing model between depleted mantle and a component with chondritic-like $\mu^{182}W$ and $^{3}He/^{4}He$ with a high ^{4}He concentration (1×10^{-3} cm^3 STP/g) that was chosen in order to force the mixing curve through the Mauna Kea dataset (Supplementary Figure A.2.7) requires $0 - 0.25$ % by mass of a "chondritic component" to fit the majority of the Hawaiian data. The main difference between this model and the previous model with an isotopically core-equilibrated mantle is the high W concentration (and also, high Pt concentration) of the chondritic component (Supplementary Table S4). Additionally, the ^{4}He concentration of this model is defined to be 100 times more concentrated than the depleted mantle in order to illustrate the necessary ^{4}He abundance to explain the Hawaiian data in such a scenario. The high ^{4}He abundance required for a chondritic W composition to generate the $\mu^{182}W$ observed in Hawaii is unlikely given recent evidence for a degassed high $^{3}He/^{4}He$ reservoir (Parai, 2022).

The third mixing scenario is between BSE and a chondritic-like component (low $\mu^{182}W$ and high $^{3}He/^{4}He$) that has a lower ^{4}He concentration than the BSE endmember. The ^{4}He concentration of the chondritic component is four times less the BSE. This is based on the concept of a "dry plume mantle" that experienced less processing (*e.g.*, convective mixing) compared to

the ambient upper mantle and thus, better preserved primitive geochemical signatures over time (Parai, 2022). This model is illustrated in Supplementary Figure A.2.7. Many of these two component mixing models fail to capture the Hawaiian data or have unlikely endmember compositions (*e.g.*, the high ^{4}He concentration chondritic component). Though possible, it is difficult to explain the Hawaiian μ^{182}W and ^{3}He/^{4}He systematics with simple, two component mixing.

One way to probe the possible causes of complexity in the W-He systematics of Hawaiian volcanoes is by assessing whether the deviations from a simple two-component mixing curve among volcanic centers are related to lithophile elemental or isotopic systematics. For example, the presence of W-rich recycled lithospheric materials with normal μ^{182}W in the plume source of these rocks could lead to attenuation of μ^{182}W anomalies. In this case, samples with less negative μ^{182}W at a given ^{3}He/^{4}He might be expected to have distinct lithophile isotopic compositions, such as ^{87}Sr/^{86}Sr, ^{176}Hf/^{177}Hf, ^{187}Os/^{188}Os, ^{206,207,208}Pb/^{204}Pb, etc., due to mixing with the recycled component(s). There is, however, no relationship between the magnitude of μ^{182}W at a given ^{3}He/^{4}He (*i.e.*, μ^{182}W divided by ^{3}He/^{4}He R/R_A) and ^{87}Sr/^{86}Sr, ^{176}Hf/^{177}Hf, ^{187}Os/^{188}Os, and ^{206,207,208}Pb/^{204}Pb (Supplementary Figure A.2.13). This suggests that the relationship between μ^{182}W and ^{3}He/^{4}He is not detectibly perturbed by the presence of distinct components in the mantle source. This does not preclude the possibility that all observed μ^{182}W values have been attenuated by recycled components in the Hawaiian plume, though it is difficult to understand how the relationship between μ^{182}W and ^{3}He/^{4}He is retained if significant amounts of recycled material are present in the plume.

An alternative scenario is decoupling of μ^{182}W and ^{3}He/^{4}He during shallow plume processes, such as by variable partial melting of different components, crystal-liquid fractionation,

etc. While both elements are highly incompatible during mantle partial melting, W and He behave quite differently in magmatic systems. For example, W is primarily carried by silicate melt, and its concentration is determined by its incompatibility associated with partial melting (Greaney et al., 2017). Conversely, the atmophile He is primarily carried by CO_2 (O'Nions and Oxburgh, 1988; Gonnermann and Mukhopadhyay, 2007). Thus, W and He that originate from the same mantle source may be decoupled as the carrier phases of W and He are likely to be physically separated during partial melting, melt extraction, and crystallization processes, potentially creating variation in the spatio-temporal $\mu^{182}W$ and $^{3}He/^{4}He$ record of erupted basalts. For example, high $^{3}He/^{4}He$ in pre-shield lavas has been interpreted to result from the rapid separation velocity of CO_2-rich fluids or carbonatite liquid from peridotite, causing high $^{3}He/^{4}He$ that originates in the plume center to be carried to the leading edge of the plume (Valbracht et al., 1996; Hofmann et al., 2011). Processes like these may decouple $^{3}He/^{4}He$ from $\mu^{182}W$. Such processes, however, would likely not decouple $\mu^{182}W$ from isotopic ratios of other refractory elements, like $^{87}Sr/^{86}Sr$, $^{176}Hf/^{177}Hf$, $^{187}Os/^{188}Os$, $^{206,207,208}Pb/^{204}Pb$. Therefore, the magnitude of $\mu^{182}W$ at a given $^{3}He/^{4}He$ would vary independently from other refractory element ratios and isotopic compositions, as appears to be the case for the HSDP-2 lavas. Though the HSDP-2 lavas exhibit variability in $^{87}Sr/^{86}Sr$, $^{176}Hf/^{177}Hf$, $^{187}Os/^{188}Os$, $^{206,207,208}Pb/^{204}Pb$ that indicate the presence of multiple mantle components (Eisele et al., 2003; Bryce et al., 2005; Nobre Silva et al., 2013), the componentry does not appear to have any relationship to the $\mu^{182}W$ and $^{3}He/^{4}He$ systematics. This observation may indicate decoupling of $\mu^{182}W$ and $^{3}He/^{4}He$ in shallow plume processes.

2.9.5. Concentric plume model

As discussed in the main text, we investigate a concentrically zoned plume model to explain the observed $\mu^{182}W$ and $^{3}He/^{4}He$ of the HSDP-2 stratigraphic section. The model invoked here is based on the approach of (Bryce et al., 2005) that calculated the isotopic composition of the Hawaiian plume based on a maximum (or minimum) isotopic ratio at the plume axis that decreases (or increases) with radial distance from the axis. As described in the main text, the relationship between the isotopic ratio, R, of a given element and radial distance from the plume axis is, r, is given by $R = R_{min} + (R_{max} - R_{min}) \times e^{\frac{r^2}{a^2}}$ where a determines how rapidly R changes with respect to r. In this study, we define the isotopic composition of the plume axis as the most extreme $^{3}He/^{4}He$ (32.2 R/R_A) and $\mu^{182}W$ deficit (-25.6) observed in any Hawaiian volcano (Kent et al., 1999; Mundl et al., 2017; Mundl-Petermeier et al., 2020). The distal composition is defined by a $^{3}He/^{4}He$ ~8 R/R_A (Graham, 2002) and $\mu^{182}W$ of 0 (Kleine et al., 2002). We also model the Sr, Hf, Os, Pb isotopic compositions as a function of radial distance from the plume axis (Supplementary Figure A.2.12).

Bryce et al. (2005) defined R_{MAX} as the most "anomalous" isotopic ratio observed in Hawaii, and R_{AMB} as "ambient" mantle that they equated to Pacific MORB values using data from the East Pacific Rise. In our model, we use only the maximum and minimum ratio observed in Hawaiian lavas to define R_{max} and R_{min}. Helium isotopes in Hawaii range from a MORB-like value of ~8 to a maximum of 32.2 R/R_A (Mundl et al., 2017). The greatest magnitude $\mu^{182}W$ observed in Hawaii so far is -25.6 (Mundl-Petermeier et al., 2020), which is used as the R_{max} and the R_{min} for $\mu^{182}W$ is defined as zero. For $^{87}Sr/^{86}Sr$, R_{max} and R_{min} are 0.70439 and 0.70311, respectively. The $^{176}Hf/^{177}Hf$ ratios are bracketed by 0.283148 and 0.282959; $^{187}Os/^{188}Os$ is

bracketed by 0.1310 and 0.1282. The R_{max} for $^{206}Pb/^{204}Pb$, $^{207}Pb/^{204}Pb$, and $^{208}Pb/^{204}Pb$, are 18.64, 15.52, and 38.22, respectively. The R_{min} for $^{206}Pb/^{204}Pb$, $^{207}Pb/^{204}Pb$, and $^{208}Pb/^{204}Pb$, are 17.85, 15.42, and 37.77, respectively. Further, the approach of (Bryce et al., 2005) was to vary a (*i.e.* the distance required for the isotope ratio of interest to change from R_{max} to R_{min}) from the full length of the thermal anomaly at melting depth (~100 km) to less than the length of the melt zone itself (~25 km). They found that their data best fit an a value of ~50-100 km for $^{87}Sr/^{86}Sr$, $^{176}Hf/^{177}Hf$, $^{187}Os/^{188}Os$, $^{206}Pb/^{204}Pb$, $^{207}Pb/^{204}Pb$ and a shorter length scale, a = ~25 km, for $^{3}He/^{4}He$ and $^{208}Pb/^{204}Pb$. Instead of varying a for each isotopic ratio, in this model we fit a to our $\mu^{182}W$ data and find that ~30 km captures the $\mu^{182}W$ stratigraphy well. We then fix a at 30 km for all isotopic ratios to test whether the plume is similar zoned for He-Sr-Hf-Os-Pb. The results for $^{3}He/^{4}He$ and $\mu^{182}W$ are shown in Figure 6 of the main text, and all other isotope ratios are plotted in Supplementary Figure A.2.12.

2.9.6. Calculation of vertical height of anomalous "filament" or "blob" in plume

According to (Watson and McKenzie, 1991), the maximum vertical velocity of the Hawaiian plume is at the axis and is 34 cm/yr. The vertical velocity exponentially decays to ~2 cm/yr over the radius of the thermal anomaly, which varies by depth, but is approximated to be ~80 km at the depth of melting (Bryce et al., 2005). Equation S1 shows the exponential decay function of the plume's vertical velocity, v, solving for the decay rate, k, over a radius, r, of 80 km (Supplementary Figure A.2.14).

$$\text{Eq. S1} \quad \ln\frac{V}{V_0} \times r = -k$$

Over the interval of time recorded by the HSDP-2 drill core, the Mauna Kea volcano moves from ~14 km from the plume axis at 600 ka to a distance of ~40 km at 200 ka (DePaolo et al., 2001). Using the decay rate calculated in Eq. S1, the vertical velocity underneath Mauna Kea can be calculated as a function of distance from the plume axis using Eq. S2.

$$\text{Eq. S2} \quad V = V_0 e^{-kr}$$

This calculation yields a vertical velocity of 20.7 cm/yr at 14 km radial distance from the plume axis and 8.2 cm/yr at 40 km from the plume axis. We then use Eq. S1 to calculate the decay rate of the vertical velocity as a function time in kyr. The decay function is shown in Supplementary Figure A.2.15. We then integrate the calculated decay rate as a function of time (Eq. S3) over the ~180 kyr interval of time in which resolvable $\mu^{182}W$ deficits are present in the Mauna Kea section of HSDP-2 (orange field in Supplementary Figure A.2.15). Equation S3 yields a plume height of ~30 km sampled by Mauna Kea between ~600 ka and ~420 ka, which resulted in resolvable $\mu^{182}W$ deficits in HSDP-2.

$$\text{Eq. S3} \quad \int_0^{180} V_0 e^{-0.0023t} dt$$

2.9.7 Supplementary Figures

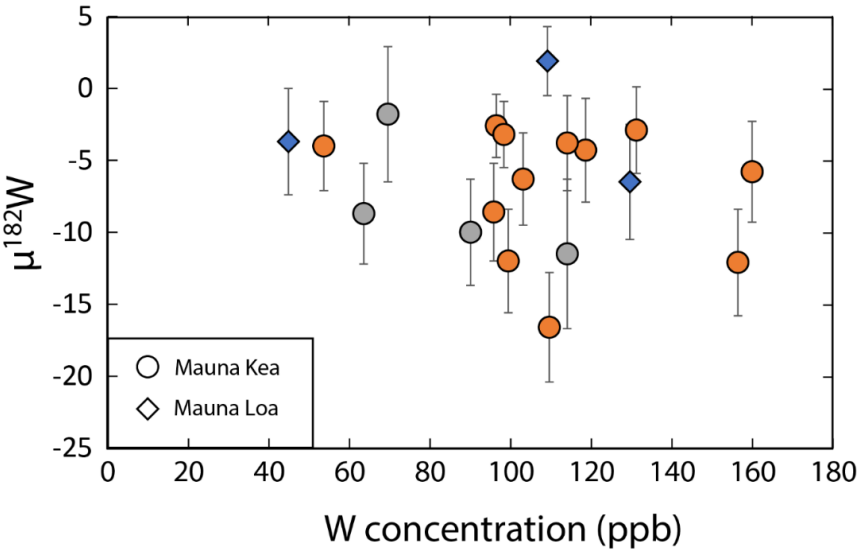

Supplementary Figure A.2.1. W concentration versus $\mu^{182}W$ in HSDP-2. The orange circles are new Mauna Kea $\mu^{182}W$ measurements and the grey circles are previously published Mauna Kea measurements (Mundl et al., 2017; Mundl-Petermeier et al., 2020). Blue diamonds are new $\mu^{182}W$ measurements from Mauna Loa samples.

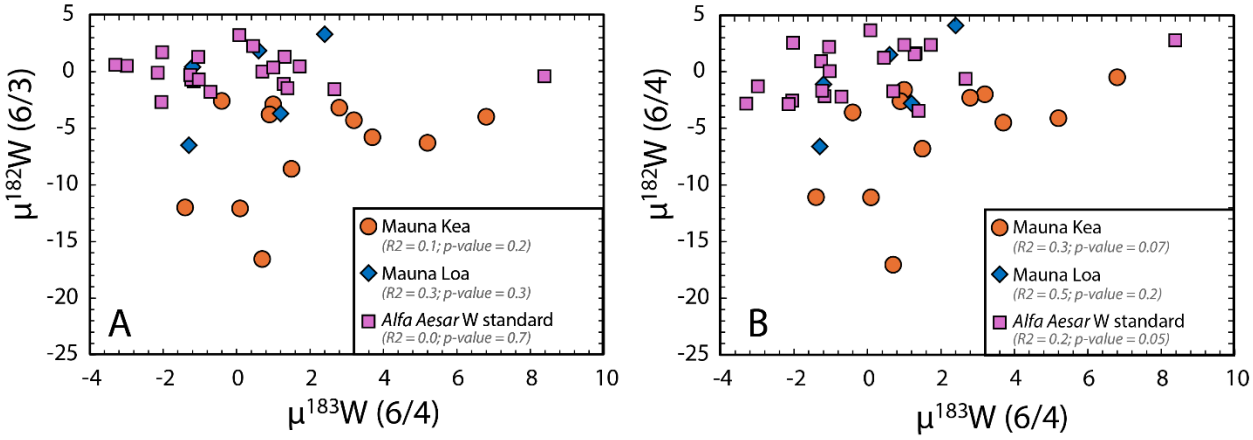

Supplementary Figure A.2.2. **(A)** $\mu^{182}W$, regardless of whether the $^{186}W/^{183}W$ or $^{186}W/^{184}W$ ratio is used for normalization, does not correlate with $\mu^{183}W$ (6/4) in Mauna Kea, Mauna Loa, or the *Alfa Aesar* W standard analyzed in this study. Tungsten isotopic compositions plotted here are from this study only.

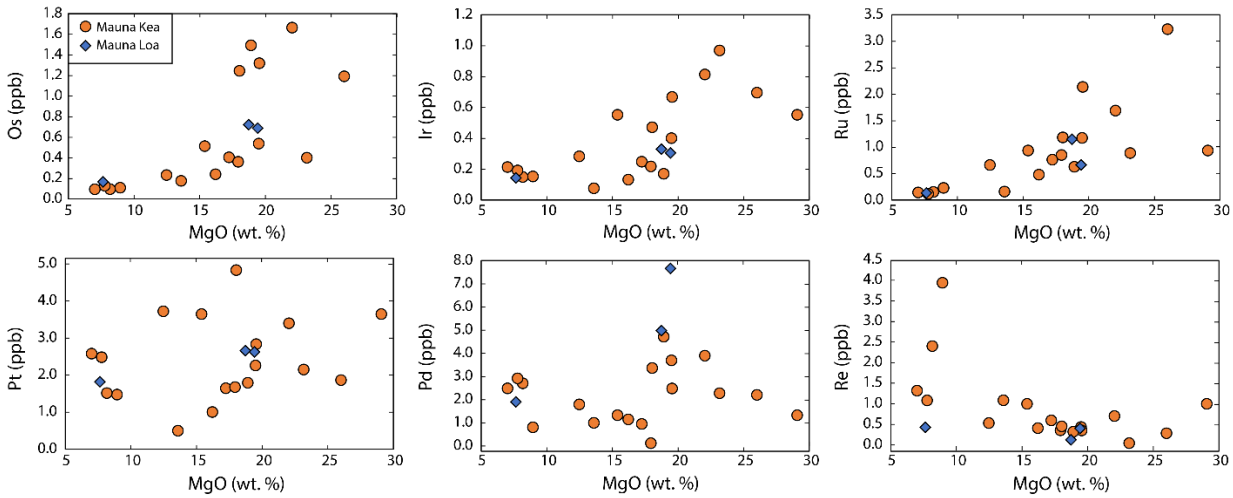

Supplementary Figure A.2.3. Highly siderophile element abundances versus MgO in HSDP-2. The positive correlations between the HSE Os, Ir, and Ru and MgO wt. % reflect their compatibility during mantle melting and crystal liquid fractionation processes, as shown for Kilauea Iki in (Pitcher et al., 2009). Platinum and Pd do not correlate with MgO wt. %. Rhenium negatively correlates with MgO, reflecting its incompatibility during mantle melting.

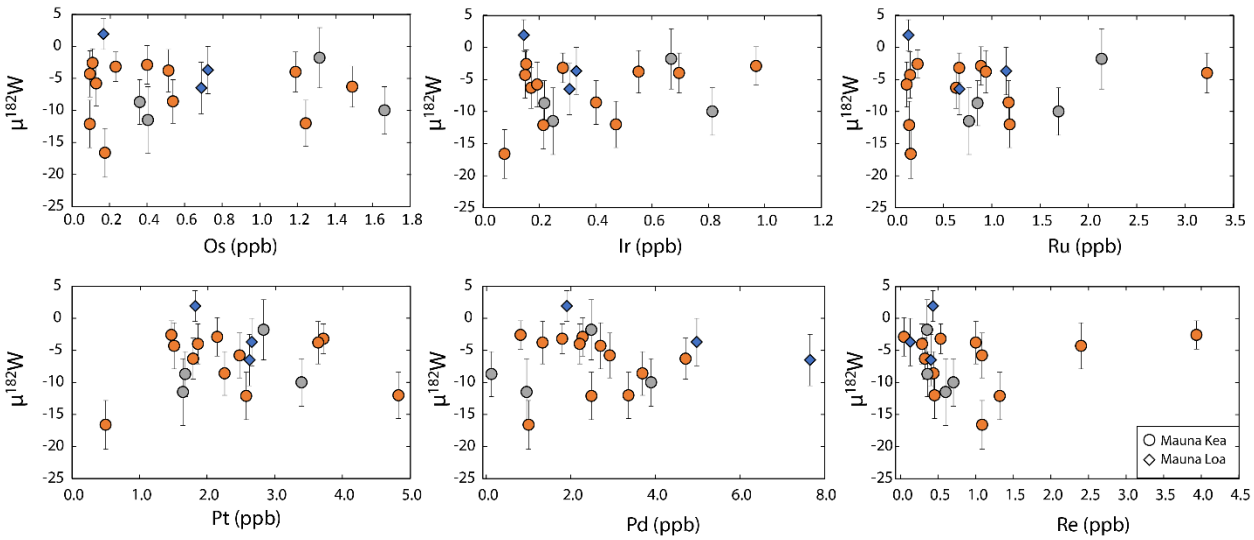

Supplementary Figure A.2.4. Tungsten isotopic composition versus highly siderophile element abundances in HSDP-2. The orange circles are new Mauna Kea $\mu^{182}W$ measurements and the grey circles are previously published Mauna Kea measurements (Mundl et al., 2017; Mundl-Petermeier et al., 2020). Blue diamonds are new $\mu^{182}W$ measurements from Mauna Loa samples.

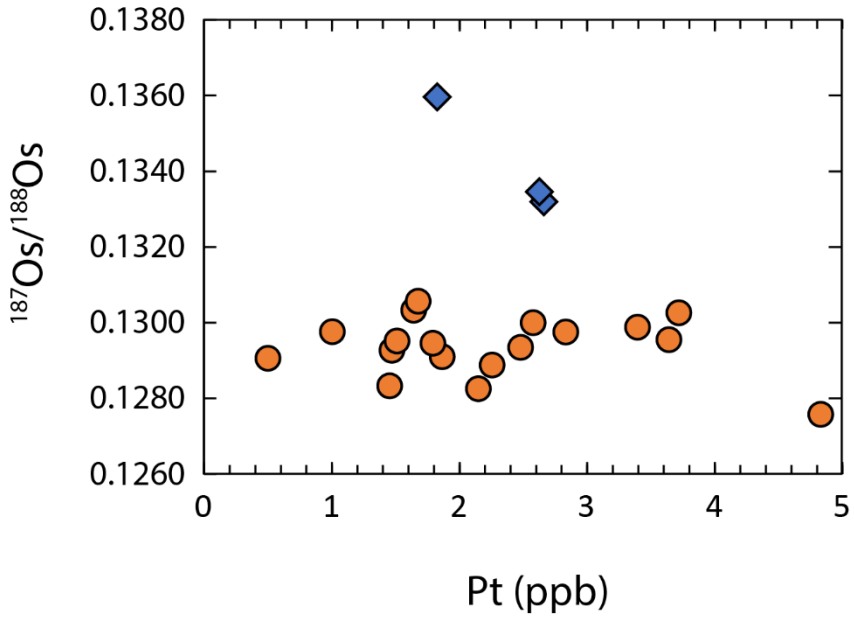

Supplementary Figure A.2.5. Osmium isotopic composition versus Pt abundance in HSDP-2. Mauna Kea samples (orange circles) are less radiogenic than Mauna Loa samples (blue diamonds). Data are from this study and Ireland et al. (2009).

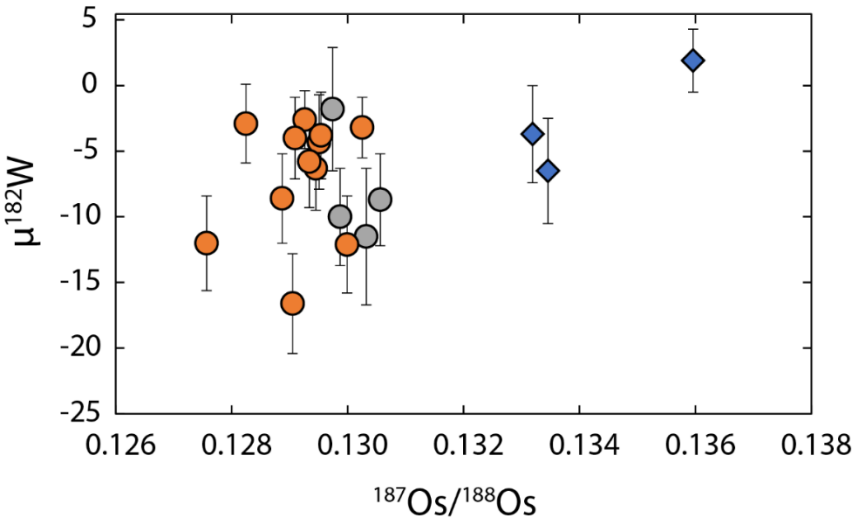

Supplementary Figure A.2.6. Tungsten isotopic composition versus $^{187}Os/^{188}Os$ in HSDP-2. The orange circles are new Mauna Kea $\mu^{182}W$ measurements and the grey circles are previously published Mauna Kea measurements (Mundl et al., 2017; Mundl-Petermeier et al., 2020). Within the Mauna Kea dataset, there is no correlation between $\mu^{182}W$ and $^{187}Os/^{188}Os$. Blue diamonds are new $\mu^{182}W$ measurements from Mauna Loa samples. Given that there are only three Mauna Loa samples with paired $\mu^{182}W$ and $^{187}Os/^{188}Os$, it is not possible to assess whether a statistically robust correlation exists between the two geochemical parameters.

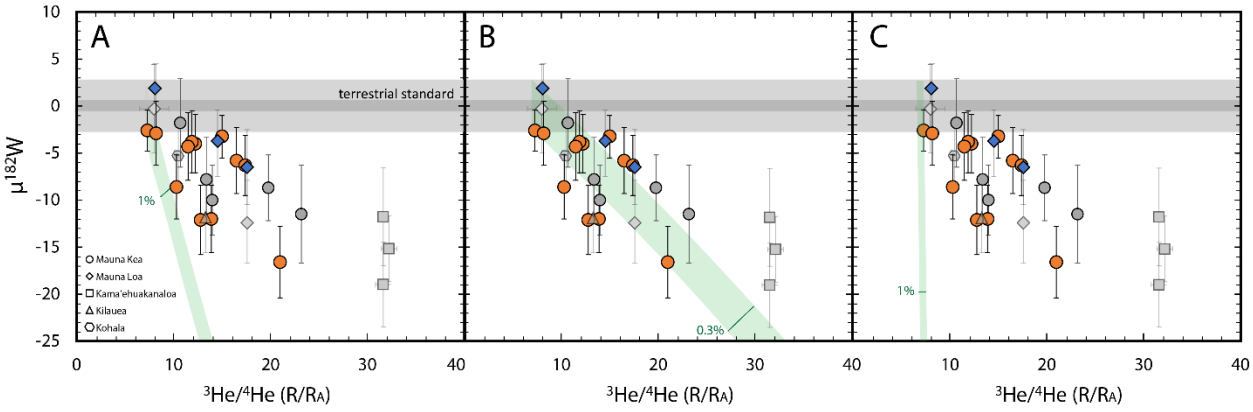

Supplementary Figure A.2.7. Tungsten isotopic composition versus $^{3}He/^{4}He$ for Hawaiian lavas. The orange circles are new Mauna Kea $\mu^{182}W$ measurements and the grey circles are previous Mauna Kea measurements (Mundl et al., 2017; Mundl-Petermeier et al., 2020). Blue diamonds are new $\mu^{182}W$ measurements from Mauna Loa samples. Helium data are from Kurz et al. (2004). **(A)** The green band represents the mixing curve between depleted mantle and a mantle reservoir that is isotopically equilibrated with the core (with respect to $\mu^{182}W$). A tick mark is shown for the composition with 1% core-equilibrated material. **(B)** The green band represents the mixing curve between depleted mantle and a chondritic-like component with a ^{4}He concentration that is 100 times higher than the depleted mantle. A tick mark is shown for the composition with 0.3% excess chondritic-like component. **(C)** The green band represents a mixture between BSE and a chondritic-like component with a ^{4}He concentration four times lower than BSE.

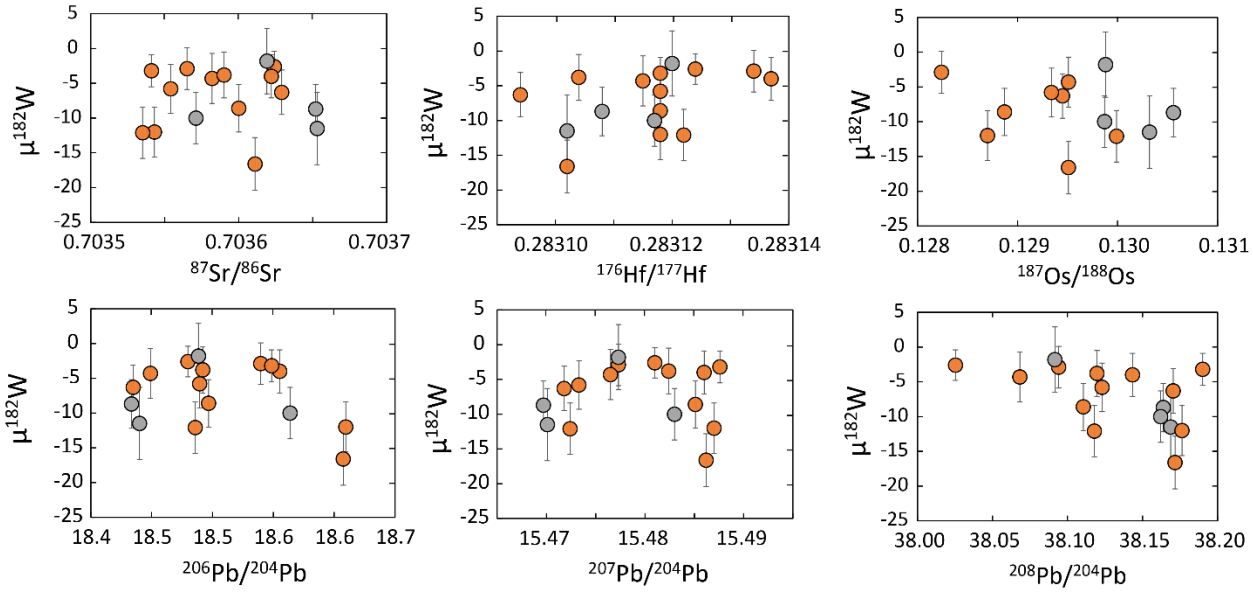

Supplementary Figure A.2.8. Tungsten isotopic composition versus Sr-Hf-Os-Pb isotopic compositions (Blichert-Toft et al., 2003; Eisele et al., 2003; Bryce et al., 2005; Ireland et al., 2009b) in Mauna Kea samples from HSDP-2. The orange circles are new $\mu^{182}W$ measurements, while the grey circles are previously published $\mu^{182}W$ (Mundl et al., 2017; Mundl-Petermeier et al., 2020).

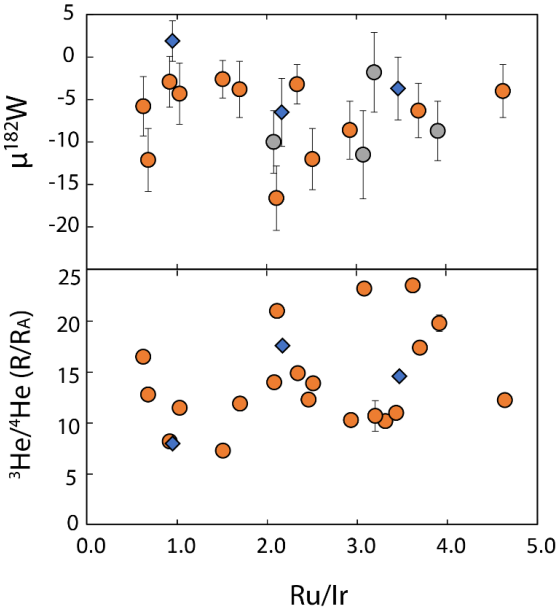

Supplementary Figure A.2.9. Tungsten and He isotopic compositions versus Ru/Ir in HSDP-2. The orange circles are new $\mu^{182}W$ measurements and the grey circles are previously published $\mu^{182}W$ (Mundl et al., 2017; Mundl-Petermeier et al., 2020). Blue diamonds represent Mauna Loa samples.

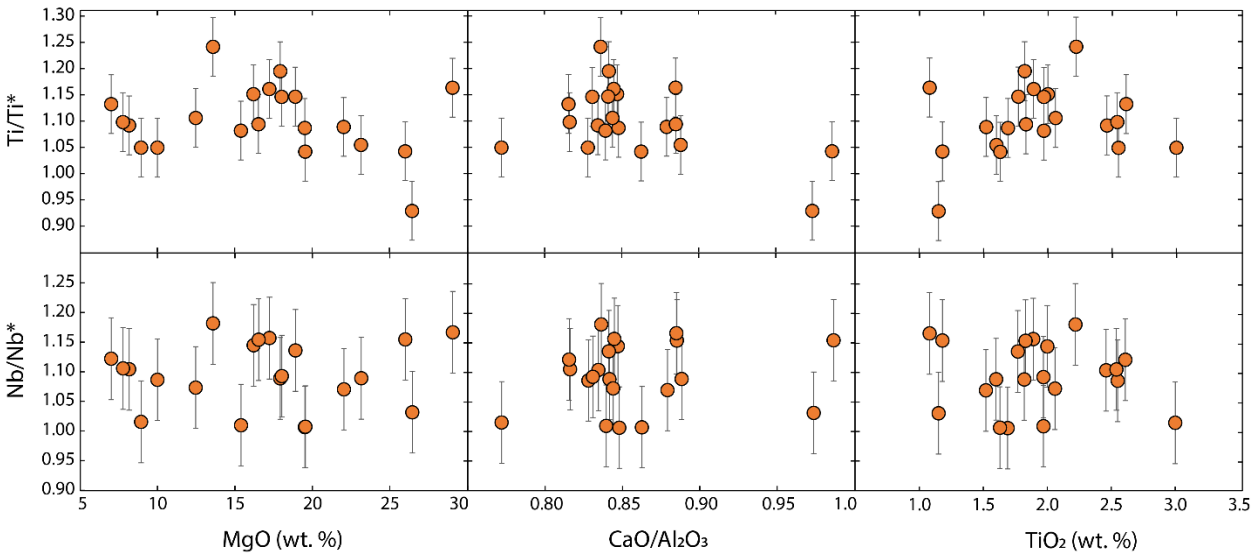

Supplementary Figure A.2.10. Whole rock Ti/Ti* ($Ti/Ti^*=Ti/(Sm_N*Tb_N)^{0.5}$, where the N subscript denotes normalization to primitive mantle) and Nb/Nb* ($Nb/Nb^*=Nb/(La_N*Th_N)^{0.5}$) versus whole rock MgO wt. %, CaO/Al_2O_3, and TiO_2 wt. % in Mauna Kea samples from HSDP-2. Error bars represent the 1SD for Ti, Nb, Sm, Tb, La, and Th propagated through each ratio. Major and trace element data are from Huang and Frey (2003) and Rhodes and Vollinger (2004).

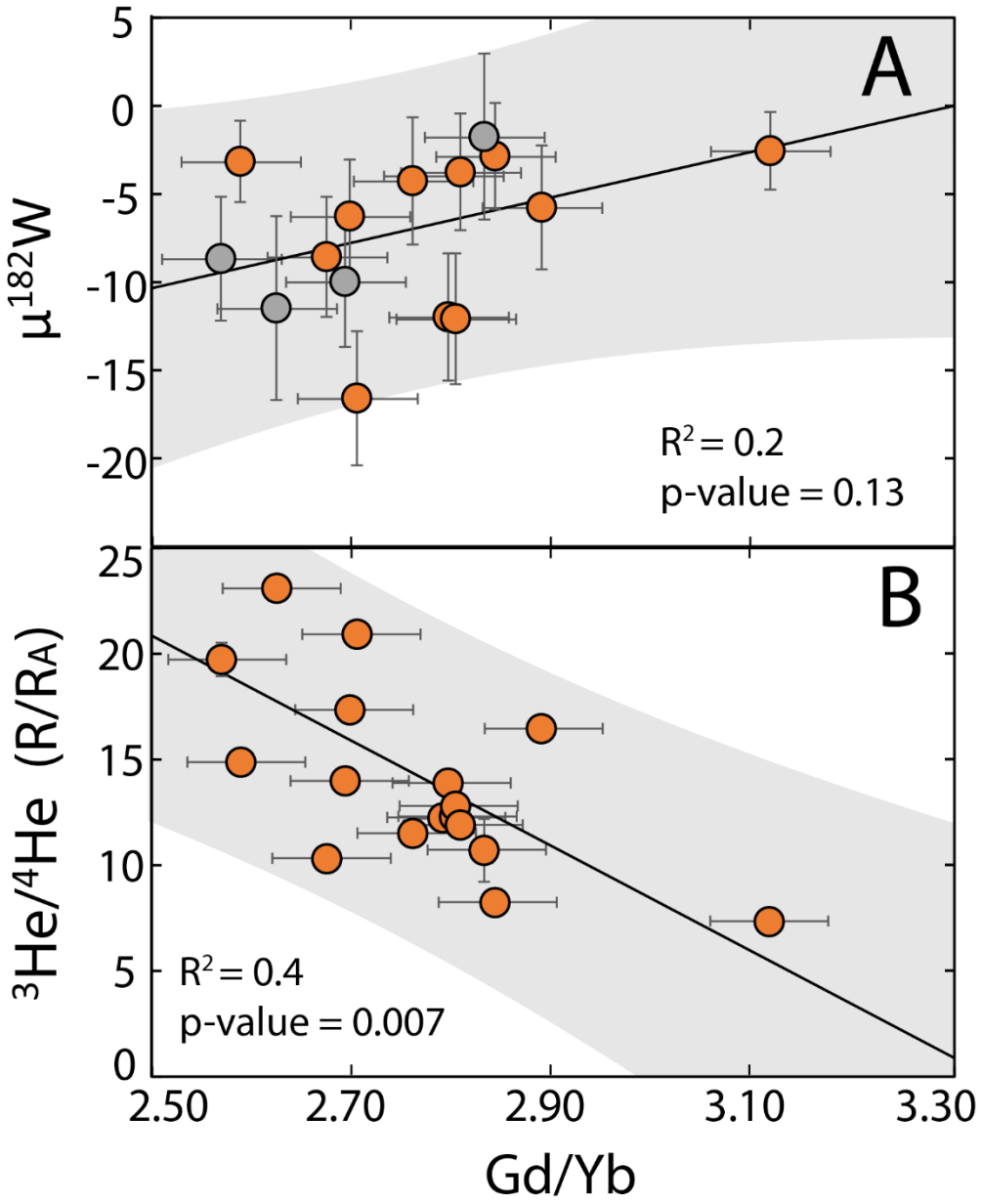

Supplementary Figure A.2.11. Tungsten and He isotopic compositions versus Gd/Yb in HSDP-2. The orange circles are new $\mu^{182}W$ measurements and the grey circles are previously published $\mu^{182}W$ (Mundl et al., 2017; Mundl-Petermeier et al., 2020). Blue diamonds represent Mauna Loa samples. Helium data are from Kurz et al. (2004) and Gd, Yb data are from Feigenson et al., (2003).

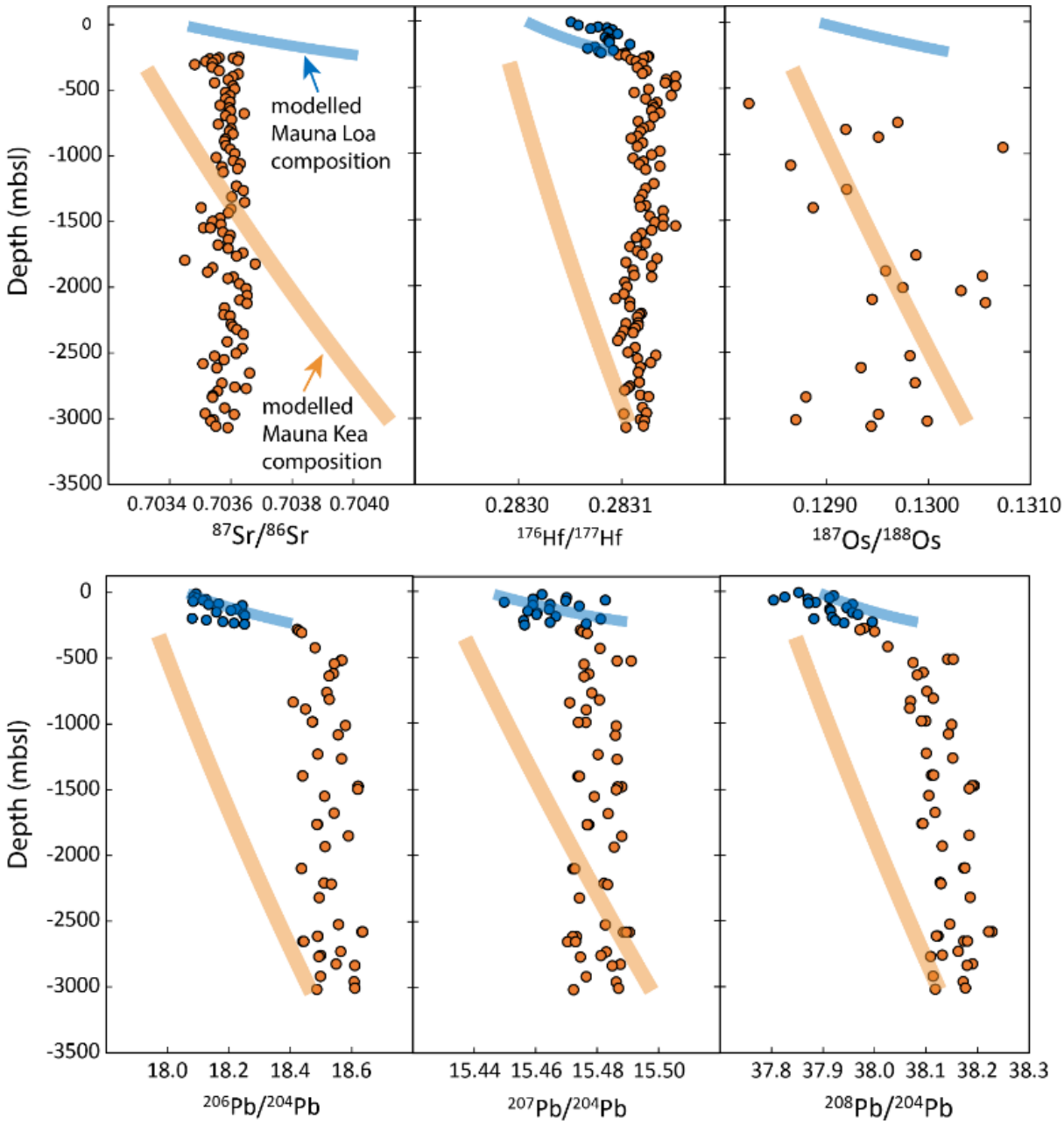

Supplementary Figure A.2.12. Strontium, Hf, Os, and Pb isotopic compositions versus depth (meters below sea level) in the HSDP-2 drill core. Orange circles represent measured Mauna Kea data; blue circles represent measured Mauna Loa samples. Isotopic compositions are from Blichert-Toft et al. (2003); Bryce et al. (2005); Eisele et al. (2003); Ireland et al. (2009), and this study. The orange bands are the calculated isotopic compositions for Mauna Kea in HSDP-2 and blue bands are the calculated compositions for Mauna Loa in HSDP-2 based on a concentrically zoned plume model (Supplementary Material S.5). The modelled compositions are calculated by tracking the distance of Mauna Kea (and Mauna Loa) from the inferred plume center over the time interval captured by the HSDP-2 core. Assuming the maximum value observed in Hawaii for each isotopic system is found at the plume center and exponentially decreases with distance from the center, it is possible to model how each isotopic system would change throughout the drill core.

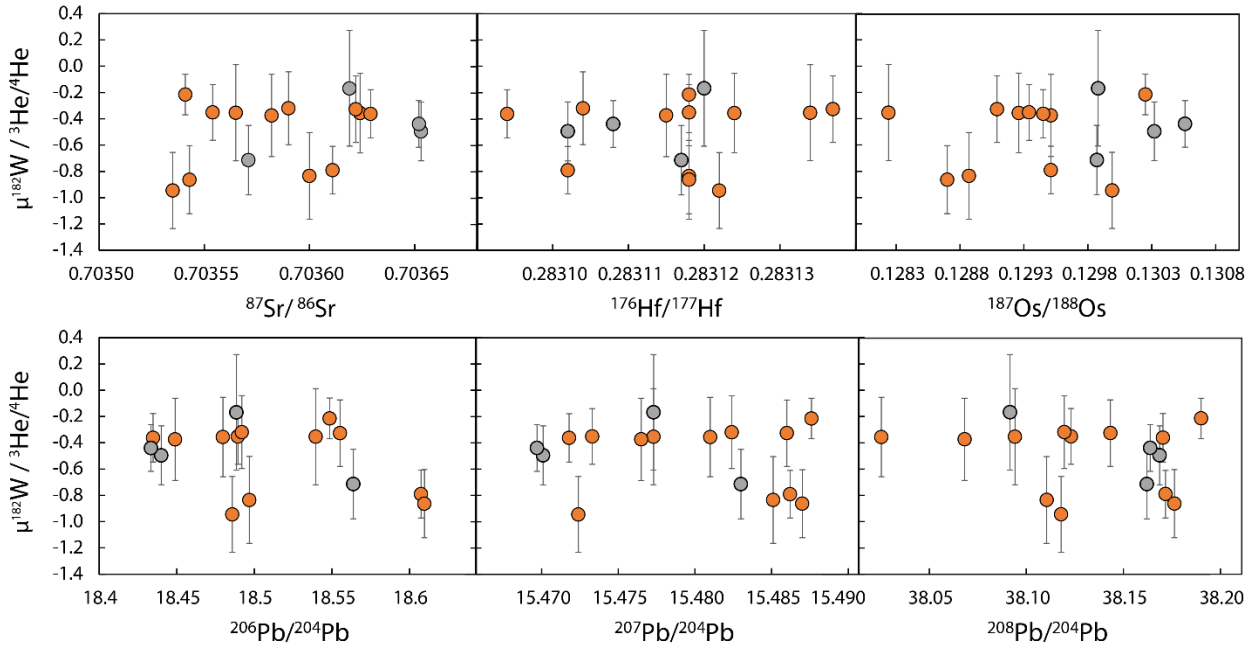

Supplementary Figure A.2.13. The magnitude of $\mu^{182}W$ divided by the $^{3}He/^{4}He$ in each sample versus the Sr, Hf, Os, and Pb isotopic compositions in the HSDP-2 drill core. Orange circles represent new Mauna Kea $\mu^{182}W$ measurements and grey circles represent previous $\mu^{182}W$ data (Mundl et al., 2017; Mundl-Petermeier et al., 2020). Isotopic compositions of Sr, Hf, Os, and Pb are from Blichert-Toft et al. (2003); Bryce et al. (2005); Eisele et al. (2003); Ireland et al. (2009), and this study

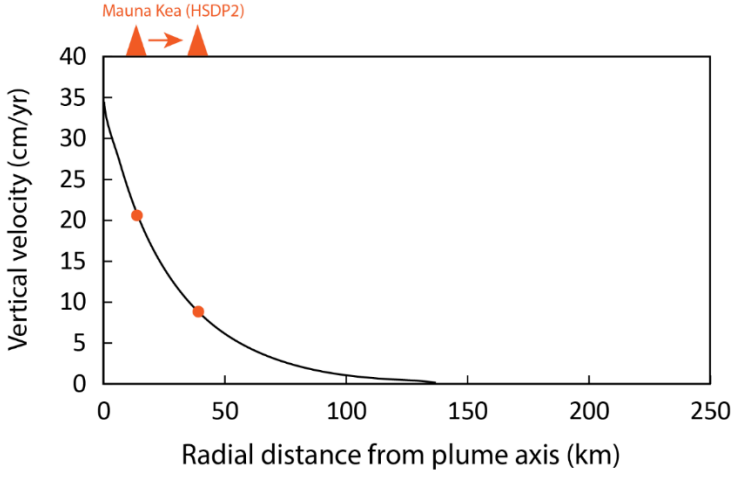

Supplementary Figure A.2.14. Vertical velocity (cm/yr) of the solid plume as a function of radial distance from the axis. The axis of the plume has the greatest ascent velocity. The orange circles reflect the radial distances of Mauna Kea from the plume axis at the initial and final times captured by the HSDP-2 drill core.

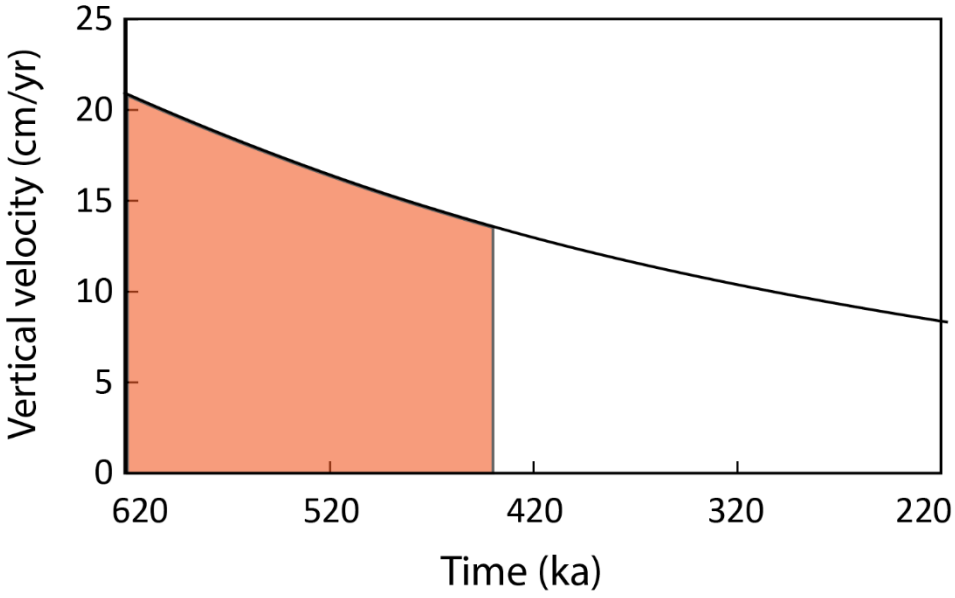

Supplementary Figure A.2.15. Vertical velocity (cm/yr) of the solid plume beneath the Mauna Kea volcano as a function of time. The integral bounded by the duration of time in which $\mu^{182}W$ deficits appear in the Mauna Kea section of the HSDP-2 drill core is represented by the orange field. The integral is equal to the vertical length of solid plume sampled by Mauna Kea over the ~180 kyr interval (~30 km).

Chapter 3: Acid leaching effects on the tungsten-182 of Hawaiian lavas

Lori Willhite[1], Michelle Jordan[2], Nicole Williamson[2], Igor Puchtel[1], Val Finlayson[1], Dominique Weis[2], Richard Walker[1]

[1]University of Maryland, College Park, MD, USA 20742

[2]Carnegie Earth and Planets Laboratory

[3]Pacific Centre for Isotopic and Geochemical Research, University of British Columbia, Vancouver, BC, Canada

3.1 Abstract

Variations in the radiogenic tungsten isotopic composition ($^{182}Hf \rightarrow ^{182}W$ isotope system; $t_{1/2} = 8.9$ Myr) of ocean island basalts (OIB) may reveal insights into potential core-mantle interactions, long-term storage of mantle domains, and mantle plume dynamics. Due to parts-per-million level differences among Earth materials, accurate and precise $\mu^{182}W$ (the parts-per-million deviation of $^{182}W/^{184}W$ from the terrestrial standard) measurements are critical to the utility of this isotope tracer. OIB erupt in subaerial and submarine environments, leading to potential post-eruptive disruption of certain isotopic compositions (e.g., Sr, Pb) by weathering and/or crustal contamination. Whether $\mu^{182}W$ values are affected by subaerial or submarine alteration is unknown, but given the fluid mobility of W in the near surface environment, there is potential for W to be mobilized by rain or seawater. Six Hawaiian shield-stage lavas were selected to investigate the effect of acid leaching on the $\mu^{182}W$ of OIB. Four subaerial tholeiites from Kaua‘i and one submarine tholeiite from a drill core of Mauna Kea were cut, sanded, crushed, powdered, and leached using 1M HCl followed by 3M HNO_3. The leachates were analyzed for elemental abundances and the leached sample residues were analyzed for $\mu^{182}W$. For comparison, an unleached aliquot of each sample was also analyzed for $\mu^{182}W$. Acid leaching of subaerial samples led to $\mu^{182}W$ values consistently within analytical uncertainty of the unleached aliquots. The results for the subaerial Kaua‘i samples show that $\mu^{182}W$ in minimally altered OIB are likely reliable within current analytical precision. Further investigation is required for highly weathered samples. The submarine drill core sample was the only sample in which acid leaching led to a resolvable difference in $\mu^{182}W$ and for this sample, the leached sample had a greater $\mu^{182}W$ composition than the residue. The difference may be the result of contamination from drilling

mud, as has been observed in Sr and Pb isotopic compositions of samples from the same lava flow in the same drill core.

3.2 Introduction

Determination of accurate radiogenic isotopic compositions of oceanic lavas is instrumental to tracking mantle evolution and determining the chemical and physical structure of Earth's mantle. The short-lived ^{182}Hf-^{182}W isotope system ($t_{1/2}$ = 8.9 Myr; Vockenhuber et al., 2004) can be used to probe early Earth and deep mantle processes. The μ^{182}W (the parts-per-million deviation of ^{182}W/^{184}W from the terrestrial standard) of ocean island basalts (OIB) varies from compositions similar to the bulk silicate Earth (BSE), thought to be μ^{182}W = 0 ± 3.5, to negative values of approximately -25 (Chapter 2 of this dissertation, Mundl et al., 2017; Rizo et al., 2019; Mundl-Petermeier et al., 2020). The negative μ^{182}W compositions observed in a subset of OIB may reflect the presence of a mantle component that either underwent isotopic equilibration between the metal core and rocky mantle, or is a remnant of early silicate fractionation (Rizo et al., 2019; Mundl-Petermeier et al., 2020).

To effectively use the μ^{182}W of OIB to investigate these potential processes, accurate and reproducible W isotopic measurements are required. For example, variability of μ^{182}W in OIB is limited, with a total range of ~25 ppm (*n* = 131; Chapter 2 of this dissertation, Mundl et al., 2017; Rizo et al., 2019; Mundl-Petermeier et al., 2019, 2020; Jackson et al., 2020; Peters et al., 2021; Archer et al., 2023). Due to eruption in submarine or oceanic subaerial environments, OIB are susceptible to seawater interactions and alteration (e.g., Hart et al., 1974). The isotopic compositions of certain elements, such as Sr and Pb, have been shown to be modified post-eruption

by submarine and/or subaerial alteration in OIB (Nobre Silva et al., 2009, 2010). The effect that seawater, alteration, and contamination by local sediments has on the $\mu^{182}W$ composition of OIB is unknown. To obtain isotopic compositions that accurately reflect the mantle source, acid leaching has been employed to remove phases associated with chemical alteration and contamination by sediments (Hart et al., 1974; McDonough and Chauvel, 1991; Nobre Silva et al., 2009, 2010). If W behaves similarly to other high-field strength elements, such as Hf, alteration effects may be minimal (Nobre Silva et al., 2010). Conversely, it is possible that alteration phases and/or contamination by seawater, mud, loess, etc., may create W isotopic variations within a volcanic rock, leading to poor external reproducibility or inaccuracy when measuring W isotopic compositions of OIB. To assess whether leaching may have an effect on the $\mu^{182}W$ value of OIB with varying degrees of alteration, five Hawaiian basalts were leached, initially with 1M HCl, followed by 3M HNO_3, prior to chemical separation of W and isotopic analysis. A complete duplicate analysis, with no acid leaching, of an additional sample was performed to assess the reproducibility of the $\mu^{182}W$ measurement of altered OIB without acid leaching.

3.3. Samples and analytical methods

3.3.1 Sample descriptions

Five tholeiitic basalts from Kauaʻi are subaerial, shield stage samples from the ~5 Ma Nāpali member of the Waimea Canyon Basalt group (Figure 3.1). The Kauaʻi samples span a range of MgO from 7.6 to 14.3 wt. % (Williamson et al., 2021, 2023). The Nāpali member has been subdivided into distinct geochemical groups (i.e., East, West, and North Nāpali) based on Sr-Nd-Hf-Pb isotopic compositions (Williamson et al., 2019, 2023). Three of the Nāpali samples studied here are from East Nāpali (KAU-2015-007, KAU-2015-014, KAU-2015-017) and two are from West Nāpali (KAU-2015-035 and KAU-2015-036). One additional sample, KAU-2015-036,

was not leached, but was instead analyzed to demonstrate the reproducibility of a complete duplicate analysis. Constraints from K-Ar dating of the Nāpali member place the eruption of West Nāpali at approximately 4.68 Ma, and East Nāpali at approximately 4.36 Ma (McDougall, 1979; Garcia et al., 2010; Williamson et al., 2019). Post-magmatic alteration occurring in tropical climates with high rainfall can lead to loss of K and other alkali elements (Chen and Frey, 1985; Frey et al., 1994). An indicator of loss of K by natural leaching in Hawaiian settings is K_2O/P_2O_5 < 1.0 (Frey et al., 1994). The Nāpali samples have K_2O/P_2O_5 of 0.5 to 1.2, indicating some samples may have experienced loss of K relative to P by natural leaching in the tropical climate of Hawaii. The Nāpali samples have loss on ignition (mass percent lost during heating for major element analyses) ranging from 0.03 to 2.16, indicating these samples are minimally altered.

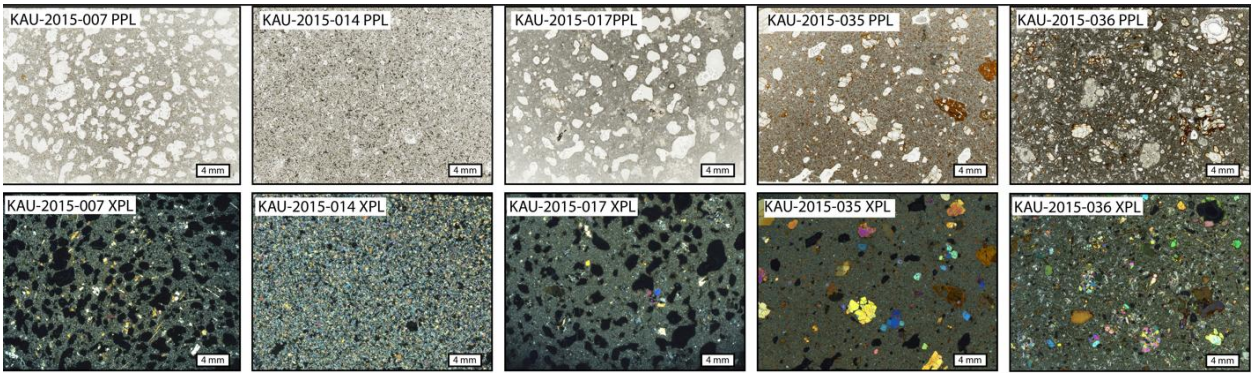

Figure 3.1. Photomicrographs of Kauaʻi samples in this study. **Top:** plain polarized light. **Bottom:** cross-polarized light.

In addition to the samples from Kauaʻi , a submarine tholeiite from the Mauna Kea section of Hawaiian Scientific Drilling Project phase 2 (HSDP-2) drill core was selected for acid leaching to compare this younger (~617 Ka; Kurz et al., 2004) sample with the older (~4.5 Ma) subaerially exposed rocks from the Nāpali member of Kauaʻi. The drill core sample, SR0954-7.4 is from a section of the drill core that has been previously studied in the context of acid leaching for Sr-Nd-

Hf-Pb isotopic compositions (Nobre Silva et al., 2009, 2010; Hanano et al., 2015). The submarine Mauna Kea lava hosts phenocrysts and groundmass comprising olivine, clinopyroxene, plagioclase, and ilmenite. The HSDP-2 sample has an MgO of 18.0 wt. %. The HSDP-2 sample has a K_2O/P_2O_5 of 1.14 and LOI of 0.85%, indicating that it is relatively fresh, compared to a subset of the Kaua‘i lavas that have lower K_2O/P_2O_5 and higher LOI.

3.3.2 Sample preparation and leaching protocol

The samples were first cut with a diamond-tipped rock saw in order to access only interior portions of the rocks. Once cut, the pieces were sanded with coarse, medium, and fine grit sandpaper and rinsed with deionized water to remove possible contamination from the saw blade. The sanded rock fragments were then crushed using an alumina jaw crusher and powdered using an alumina shatterbox. To assess whether acid leaching affects the measured W isotopic composition of weathered OIB, two leaching steps were performed on sample powders prior to digestion and chemical separation of W. The W isotopic compositions of the leached powders were then measured by thermal ionization mass spectrometry and compared to the isotopic composition determined in an unleached aliquot of the same sample powder, which was processed in the same manner.

The first leaching step included the addition of 1 mL 1M HCl per gram of sample powder in a pre-weighed Teflon vial, which was placed on a hotplate at 80 °C for 20 minutes. After 20 minutes, the sample was cooled to room temperature before being placed in an ultra-sonic bath for 15 minutes. The sample was then centrifuged to facilitate separation of the aqueous HCl leachate from the residual powder. The HCl leachate was added to a separate, pre-weighed Teflon vial. The

sample was then rinsed with 18.2 MΩ · cm de-ionized water, and centrifuged to remove the water rinse, which was added to the Teflon vial containing the HCl leachate. This was repeated two additional times. The leachate was then dried down.

The sample powder was then leached with 3M HNO_3 on a hotplate at 80 °C for 20 minutes. The leachate was separated by centrifuging and placed in a separate, pre-weighed Teflon vial. The sample was then rinsed with 18.2 MΩ · cm de-ionized water and centrifuged to remove the water, which was added to the Teflon vial containing the HNO_3 leachate. The water rinse step was repeated two additional times and then the vial was dried. The residual sample powder was dried, and the sample vial was weighed to determine the mass lost during the leaching procedure. The leached sample residue was then digested using 1 mL of concentrated HNO_3 and 5 mL concentrated HF per gram of sample at 150 °C for at least five days. An aliquot of each sample underwent digestion and chemical separation with no acid leaching steps to compare the isotopic compositions of leached and unleached powders. The unleached powders and leached residues then underwent chemical purification of W, as described in Willhite et al. (2024) and references therein.

3.3.3 Measurement of leachate elemental composition

Thirty-two elements were measured in the leachate solutions by single quadrupole inductively coupled plasma mass spectrometry on a *Thermo Fisher iCAP Q* at the Carnegie Earth and Planets Laboratory. The dried leachates were first brought up in 10 mL of 0.8M HNO_3 + 0.02M HF. These solutions were then diluted to maintain a total ion concentration of 5 ppm to avoid saturating the detector. The analytes included the following isotopes for each element: ^{23}Na, ^{39}K, ^{44}Ca, ^{48}Ti, ^{53}Cr, ^{57}Fe, ^{60}Ni, ^{63}Cu, ^{85}Rb, ^{88}Sr, ^{90}Zr, ^{95}Mo, ^{115}In, ^{140}Ce, ^{141}Pr, ^{146}Nd, ^{147}Sm, ^{153}Eu, ^{157}Gd, ^{159}Tb, ^{163}Dy, ^{165}Ho, ^{166}Er, ^{169}Tm, ^{172}Yb, ^{175}Lu, ^{178}Hf, ^{182}W, ^{185}Re, ^{206}Pb, ^{207}Pb, ^{208}Pb, ^{209}Bi,

^{232}Th. Indium and Bi were used as internal standards. Six calibration solutions of varying concentrations were made, including all of the analytes. Two USGS reference materials, BHVO-1 and BCR-1, were included in the analysis. The average measurement uncertainty based on rare earth element compositions in the reference materials was 30% (Raczek et al., 2001).

3.3.4 Tungsten isotopic analysis of unleached and leached powders

Tungsten isotopic measurements were conducted using negative-ion thermal ionization mass spectrometry (N-TIMS) on a Thermo Scientific Triton™ multi-collector thermal ionization mass spectrometer at the University of Maryland's Isotope Geochemistry Laboratory following the protocol outlined in Willhite et al. (2024) and references therein. In brief, the W fraction of each sample was loaded onto Re filaments in 1 μL of 0.5M HCl + 0.5M HF solution. Mass spectrometric measurements were performed using the Faraday cup and amplifier configuration, along with a per-integration oxide correction, following Archer et al. (2017). Analyses typically consist of a beam intensity of 1 V on mass $^{184}WO_3$ (using a 10^{11} Ω resistor amplifier). Each analysis time was 12 hours and 15 minutes, including 45 minutes of baseline measurements. Final isotopic ratios were corrected for mass fractionation using an exponential law. The Alfa Aesar W standard (Lot No.: 211576G) was analyzed repeatedly throughout the sessions with an average $^{182}W/^{184}W$ (normalized to $^{186}W/^{183}W = 1.9859$) of 0.864861, and an external reproducibility of 3.9 ppm (2SD) and 0.7 ppm (2SE) (where $n = 42$).

3.4 Results and Discussion

3.4.1 Composition of the leachates

The initial 1M HCl leaching procedure removed a greater total mass of material than the subsequent 3M HNO_3 leaching procedure. In all cases, Fe was the most abundant element of those

measured in the leachates (Table 3.1). The next most abundant elements measured in the leachates were Ca, Na, K, Ni, and Ti. The most abundant trace elements measured in the leachates were Ce, Sr, and Nd.

Table 3.1. Leachate trace element compositions.

Sample	KAU-2015-007	KAU-2015-007	KAU-2015-014	KAU-2015-014	KAU-2015-017	KAU-2015-017	KAU-2015-035	KAU-2015-035	SR0954	SR0954
Leaching acid	HCl	HCl	HCl	HCl	HCl	HNO_3	HNO_3	HNO_3	HNO_3	HNO_3
Na (µg)	3400	2100	8200	3900	16400	1100	1200	1300	1300	2200
K (µg)	1700	400	1900	1700	4500	400	100	300	300	1500
Ca (µg)	32000	22000	45000	49000	48000	5000	5000	5000	5000	8000
Ti (µg)	830	430	1390	920	650	710	310	1080	450	480
Cr (µg)	190	20	40	160	440	120	10	10	120	280
Fe (µg)	115500	35200	29800	86200	120900	59200	17700	7700	64100	69000
Ni (µg)	1140	160	320	1480	1890	730	110	90	1020	2500
Cu (µg)	160	500	220	80	160	50	80	40	40	590
Sr (µg)	190	100	250	220	230	30	30	50	50	50
Zr (ng)	24000	1000	6000	2000	5000	23000	16000	8000	26000	11000
Rb (ng)	1300	1000	2100	2100	12500	800	300	600	600	8800
Mo (ng)	6300	300	400	300	600	300	200	200	200	1200
Ce (ng)	270000	170000	310000	390000	330000	30000	10000	20000	20000	40000
Pr (ng)	49000	25700	45300	56600	47800	5900	1400	2700	3200	5700
Nd (ng)	220000	120000	210000	260000	210000	30000	10000	10000	10000	30000
Sm (ng)	56000	31000	52000	61000	52000	7000	2000	3000	3000	6000
Eu (ng)	15700	6900	8400	12000	13000	1800	380	510	760	1500
Gd (ng)	63000	35000	54000	62000	54000	7000	2000	3000	3000	6000
Tb (ng)	8800	4800	7200	8000	7300	900	200	400	400	800
Dy (ng)	52000	28000	40000	43000	43000	5000	1000	2000	2000	5000
Ho (ng)	9400	4950	6860	7090	7450	950	250	380	440	830
Er (ng)	26000	14000	18000	18000	21000	2700	700	1100	1300	2300
Tm (ng)	3100	1600	2100	1900	2500	300	80	120	140	280
Yb (ng)	18000	9000	12000	10000	15000	2000	500	700	800	1700
Lu (ng)	2610	1250	1540	1360	2040	260	60	90	120	240
Hf (ng)	990	170	280	280	340	650	270	180	510	240
W (ng)	1000	1000	600	2300	700	400	1700	300	300	300
Re (ng)	10	10	10	10	10	3	5	1	1	4
Pb (ng)	5200	3500	3800	1500	3000	1100	400	600	1000	1800
Th (ng)	2500	1200	1700	4400	5700	100	900	1800	900	1800

Generally, a greater percentage of the light rare earth elements (REE), with the exception of Eu, was leached from the powders compared to the heavy REEs (Figure 3.2). Between 25% to 90% of the measured REEs were leached from the samples during the 1M HCl leaching step. Europium was less effectively leached compared to the other light REEs. The relative depletion of Eu in the leachate may reflect the retention of plagioclase in the residual powder (Figure 3.2).

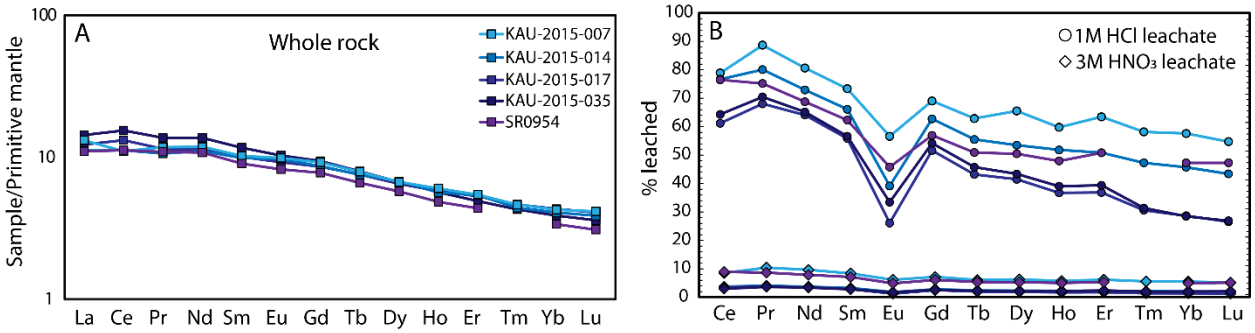

Figure 3.2. (A) Whole rock rare earth element (REE) diagram. Samples are normalized to primitive mantle (McDonough and Sun, 1995). **(B)** REE compositions of leachates in percent removed from whole rock. The 1M HCl leachates (circles) removed a greater percentage of REE than the subsequent 3M HNO_3 leachates (diamonds).

3.4.2 W isotopic compositions of Hawaiian lavas with and without acid leaching

Leached samples from Kaua‘i have $\mu^{182}W$ values within analytical uncertainty of their unleached counterparts (Table 3.2). Nevertheless, each of the leached powders are consistently offset by 2 to 6 ppm toward more negative $\mu^{182}W$ values compared to the aliquots that were not leached (Figure 3.3). A sign test (a non-parametric statistical test used to determine whether the direction of offset between two sets of data is statistically significant), indicates that the consistent

drop in $\mu^{182}W$ to more negative values is not significant at the 95% confidence level. Nevertheless, the possibility remains that alteration introduces a small amount of radiogenic W to OIB.

Table 3.2. Tungsten isotopic compositions of the unleached and leached lavas in this study.

Sample name	Island	Volcanic center	Age (Ma)	$\mu^{182}W$	2SE (internal)
KAU-2015-007	Kauaʻi	East Nāpali	5	-20.0	3.4
KAU-2015-007 leached	Kauaʻi	East Nāpali	5	-22.1	3.2
KAU-2015-014	Kauaʻi	East Nāpali	5	-16.8	4.2
KAU-2015-014 leached	Kauaʻi	East Nāpali	5	-21.4	4.6
KAU-2015-017	Kauaʻi	East Nāpali	5	-13.1	2.7
KAU-2015-017 leached	Kauaʻi	East Nāpali	5	-19.1	3.5
KAU-2015-035	Kauaʻi	West Nāpali	5	-5.6	3.3
KAU-2015-035 leached	Kauaʻi	West Nāpali	5	-11.2	1.6
KAU-2015-036	Kauaʻi	West Nāpali	5	-18.4	2.9
KAU-2015-036 duplicate	Kauaʻi	West Nāpali	5	-18.8	3.9
SR0954-7.4	Hawaii	Mauna Kea	0.6	-12.0	3.6
SR0954-7.4 leached	Hawaii	Mauna Kea	0.6	-3.5	3.0

The magnitude of the offset in the measured $\mu^{182}W$ between the leached and unleached aliquots is independent of the magnitude of the $\mu^{182}W$ of the sample. For example, KAU-2015-035 has a $\mu^{182}W$ of -5.6 ± 3.3 (unleached aliquot) and the leached aliquot had a $\mu^{182}W$ of -11.2 ± 1.6, resulting in a total offset of -5.6 ppm. KAU-2015-017 had a larger initial $\mu^{182}W$ deficit of -13.1 ± 2.7 in the unleached aliquot, and -19.1 ± 3.5 in the leached aliquot, resulting in an offset of -6.0 ppm. Therefore, regardless of the initial $\mu^{182}W$ of the bulk sample powder, there is potential for the W isotopic composition to change as a result of acid leaching. There may be a correlation between the absolute value of the offset between the $\mu^{182}W$ of the leached and unleached powders and the starting concentration of W in the sample; however, uncertainties make it impossible to definitively establish a relationship.

One of the Nāpali samples (KAU-2015-036) was selected for duplicate W isotopic analyses with no acid leaching for comparison of $\mu^{182}W$ reproducibility without acid leaching to the results from the acid leached samples. The duplicate $\mu^{182}W$ measurements of KAU-2017-036 differed by only 0.4 ppm. The reproducibility of $\mu^{182}W$ of two separate digestions of KAU-2017-036 indicate that $\mu^{182}W$ can be precisely determined in minimally altered OIB, even without acid leaching. The offset is less than that of the leached and unleached paired analyses, which may support the hypothesis that alteration can add a small amount of W with normal $\mu^{182}W$. Though the null hypothesis, that alteration has no effect on $\mu^{182}W$ in minimally, subaerially altered OIB, cannot be rejected.

There is no evidence for the addition of a significant amount of W to the lavas in this study. All lavas have W/Th between 0.10 and 0.15, which are within the estimated W/Th range for the BSE, 0.19 ± 0.15 (Arevalo and McDonough, 2008). Furthermore, all lavas have minimal to moderate evidence for alteration in their LOI (0.03 to 2.16 wt. %). The Hawaiian sample with a

LOI of only 0.03, KAU-2015-014, still showed an offset of -4.6 ppm between the measured $\mu^{182}W$ in the unleached and leached powders.

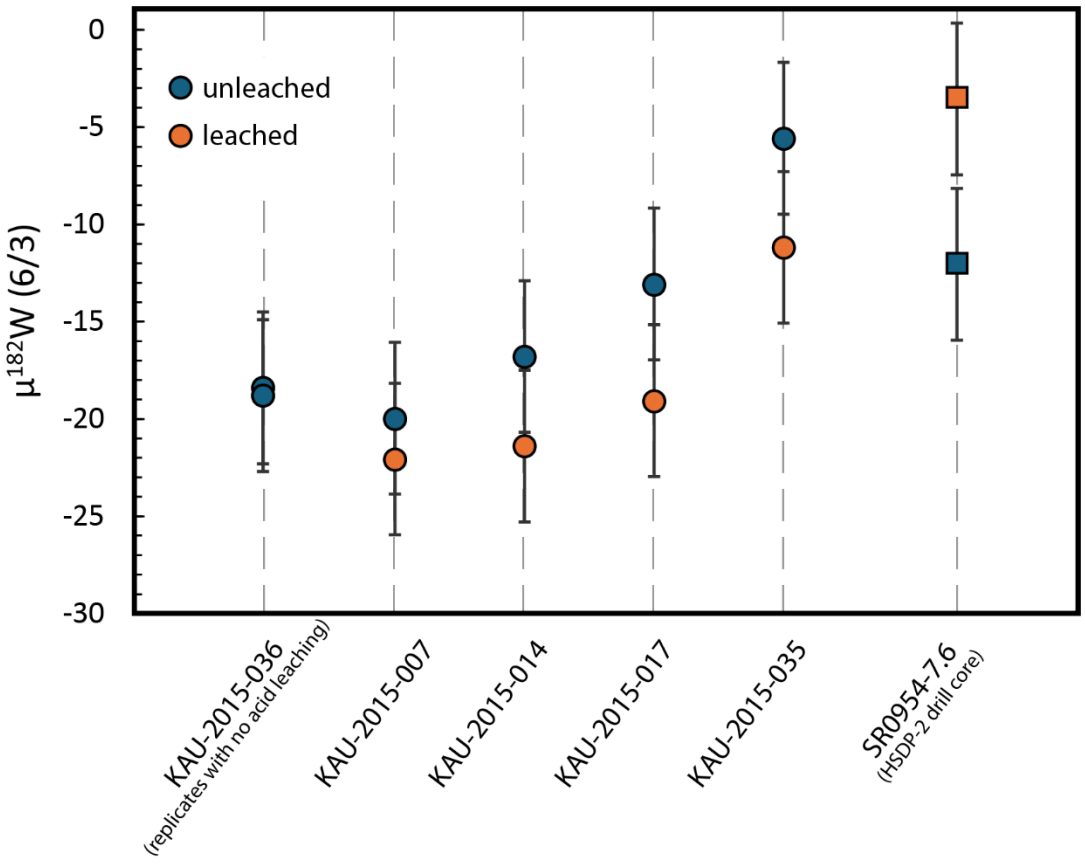

Figure 3.3. Tungsten isotopic compositions of the unleached (blue) and leached (orange) samples. Kaua‘i samples (circles) exhibit a systematic offset to greater magnitude $\mu^{182}W$ deficits in the leached samples compared to the unleached aliquots. Sample KAU-2015-036 did not undergo acid leaching and a complete replicate analysis of this sample demonstrates sub-ppm reproducibility of the total analytical procedure. Acid leaching of the submarine Mauna Kea drill core sample (squares) resulted in a lesser magnitude $\mu^{182}W$ deficit.

The submarine Mauna Kea sample from the HSDP-2 drill core shows a different behavior from the subaerial Kaua‘i samples post-leaching. The leached Mauna Kea sample resulted in a resolvable, *less* negative $\mu^{182}W$ than the unleached aliquot (Figure 3.3). It is not clear why the leached powder resulted in a relatively radiogenic $\mu^{182}W$ compared to the unleached sample. This sample, SR0954-7.4, is from the same lava flow (SR0954-8.00) that has been previously studied with regard to acid leaching of alteration phases and the effects on Sr-Nd-Hf-Pb isotopic compositions (Nobre Silva et al., 2009, 2010; Hanano et al., 2015). The LOI of this sample is 0.85 wt. %, and the K_2O/P_2O5 is 1.14, an indicator minor alteration, and little to no mobilization of K (Frey et al., 1994; Rhodes and Vollinger, 2004; Hanano et al., 2015). Alteration phases are present in the form of talc along fractured olivine surfaces, in addition to minor amounts of interstitial smectite, barite, and celestite (Hanano et al., 2015). In prior studies, leaching of SR0954-8.00 powder with 6M HCl resulted in a shift of Pb isotopic compositions towards less radiogenic ratios (Nobre Silva et al., 2009). The bulk leachate solution had radiogenic Pb and Sr isotopic compositions relative to the unleached and leached sample, leading to the conclusion that the drill core lava was contaminated with drilling mud, in addition to possible interactions with seawater, Fe-Mn oxides, loess, etc. (Abouchami et al., 2000; Nobre Silva et al., 2009, 2010). The W concentration and isotopic composition of the HSDP-2 drilling mud is unknown; however, it is unlikely that drilling tools would contain W with negative $\mu^{182}W$ compositions. It will be advantageous for future studies to acid leach drilled OIB samples prior to chemical separation of W for $\mu^{182}W$ measurement.

Seawater may alter the $\mu^{182}W$ of submarine samples via direct interaction or through mobilization of W from nearby basalts (e.g., Reifenröther et al., 2021). The concentration of W in seawater is approximately 50 pmol/kg (Fujiwara et al., 2020). Given the limited range of LOI

values in the submarine drill core samples (0 to 4.5 wt. %), it is unlikely that seawater itself is the source of exogenous W in the Mauna Kea drill core sample that has a W concentration many orders of magnitude (i.e., ~20,000x) greater than seawater. Tungsten is mobilized in oxic oceans as WO_4^{2-} and adsorbs onto Fe-Mn oxides, which precipitate onto submarine rock outcrops (Sohrin et al., 1987; Fujiwara et al., 2020). The concentration of W in Fe-Mn oxides is ~100,000 ppb (Kashiwabara et al., 2013), which is 1000 times that of the 99.4 ppb W submarine HSDP-2 sample studied here (Chapter 2 of this dissertation). Iron and Mn-oxides may, therefore also be a major source of exogenous W to submarine basalts.

The Mauna Kea pillow basalt studied here, SR0954-7.4, is located within 10 meters of a contact with an intrusive lava flow that has a $\mu^{182}W$ of -12.1 ± 3.7 (Rhodes and Vollinger, 2004; Chapter 2 of this dissertation). Given the nearly identical $\mu^{182}W$ of the unleached powder from SR0954-7.4, it is possible that the intrusion introduced or mobilized W with $\mu^{182}W$ of approximately -12. In this case, the anomalous W is from the Mauna Kea mantle source, but the timing and location of the erupted $\mu^{182}W$ anomaly might not be represented accurately in the stratigraphic section.

3.5 Conclusions

The results of acid leaching subaerial Hawaiian tholeiites indicate that the $\mu^{182}W$ of minimally altered ocean island basalts can reliably trace mantle processes such as potential core-mantle interactions, long-term mantle storage, and mantle plume entrainment and melting processes. All subaerial samples resulted in $\mu^{182}W$ within analytical uncertainty with and without acid leaching. The consistent offset towards more negative $\mu^{182}W$ after acid leaching, though not analytically resolvable, may result from addition of a small amount of exogenous, radiogenic W during subaerial weathering. The Kauaʻi samples analyzed in this study are minimally altered as

indicated by LOI less than 2 wt. %. Further investigation of OIB with a greater degree of alteration (e.g., higher LOI or greater petrographic evidence for alteration phases) is warranted to understand how greater degrees of weathering may alter the $\mu^{182}W$ of mantle-derived rocks.

The submarine drill core sample from Mauna Kea resulted in distinct $\mu^{182}W$ between the unleached and leached sample aliquots. The leached aliquot (-3.5 ± 3.0) had a smaller magnitude $\mu^{182}W$ deficit compared to the unleached aliquot (-12.0 ± 3.6). The small difference (≥1.9 ppm) may be the result of mobilization of W from nearby submarine basalts with anomalous $\mu^{182}W$, an analytical artifact, or contamination from drilling mud, which has been observed in Sr and Pb isotopic compositions of samples from the same lava flow in the same drill core—although it is unlikely that drilling mud would introduce anomalous $\mu^{182}W$.

3.6 Authorship credit statement

Lori Willhite: Conceptualization, Methodology, Investigation, Formal analysis, Data curation, Visualization, Writing – original draft, Writing – review & editing. **Michelle Jordan:** Methodology, Formal analysis, Data curation. **Nicole Williamson:** Investigation, Resources. **Igor Puchtel:** Conceptualization, Investigation, Resources. **Valerie A Finlayson:** Conceptualization, Methodology, Funding acquisition. **Dominique Weis:** Conceptualization, Investigation, Resources, Supervision. **Richard J Walker:** Conceptualization, Supervision, Investigation, Resources, Writing – review & editing, Funding acquisition.

Chapter 4: Pulsing plume or mantle mixing?: dynamics of the Hawaiian plume through the lens of $\mu^{182}W$

Lori Willhite[1], Nicole Williamson[2], Val Finlayson[1], Dominique Weis[2], Richard Walker[1]

[1]University of Maryland, College Park, MD, USA 20742

[2]Pacific Centre for Isotopic and Geochemical Research, University of British Columbia, Vancouver, BC, Canada

4.1 Abstract

Tungsten-182 isotopic compositions provide insight into processes that occurred in the first ~60 Myr of the Solar System. Variations in $\mu^{182}W$ (μ is the parts-per-million deviation from a terrestrial standard assumed to be representative of the bulk silicate Earth) in terrestrial rocks can be used to study very early metal-silicate and silicate-silicate differentiation, as well as grainy late accretion, and potential long-term core-mantle interactions. Ocean island basalts have $\mu^{182}W$ similar to the modern bulk silicate Earth (BSE), as well as a range of $\mu^{182}W$ deficits from BSE (~0) to approximately -25. It is not clear what processes control the presence and magnitude of $\mu^{182}W$ expressed in modern lavas at Earth's surface. Variation in $\mu^{182}W$ in mantle plume-derived rocks may be related to plume structure, dynamics, and interaction with additional components in the plume, such as recycled materials. The Hawaiian mantle plume is well characterized with respect to chemical and isotopic variations, as well as magmatic flux, over the ~5 Myr rock record composing the archipelago. When paired with new $\mu^{182}W$ values, chemical and Sr-Nd-Hf-Os-Pb isotopic compositions are used to demonstrate that the Hawaiian plume likely experienced pulses of anomalous material, such that the component that hosts negative $\mu^{182}W$ was either not always present, or did not always contribute to melt production. The previously identified Loa and Kea trends, and their geochemical subgroups, are characterized for $\mu^{182}W$ compositions to explore the relationship between $\mu^{182}W$ and mantle componentry and show no difference. The Hawaiian plume expresses large $\mu^{182}W$ deficits during two distinct time periods (~5 Ma, and <1 Ma), and lacks appreciable $\mu^{182}W$ deficits for a duration of ~3.5 Myr between the two minima. The temporal variation of $\mu^{182}W$ is inversely correlated with magmatic flux, and $^{208}Pb/^{204}Pb$. The Hawaiian mantle plume seems to experience pulses of higher mantle potential temperatures and magmatic flux that correspond to the presence of the anomalous component in the plume. Though some

volcanic centers and lava flows may express BSE-like $\mu^{182}W$ due to attenuation caused by the incorporation of W-rich, anomaly-free recycled materials, it is likely that volcanism during the 3.5 Myr interval did not consistently sample the anomalous component because it was irregularly entrained in the mantle plume.

4.2 Introduction

The short-lived $^{182}Hf \rightarrow ^{182}W$ radiogenic isotope system provides a tool for probing early formed chemical reservoirs, and subsequent evolution of those reservoirs. The parent nuclide, ^{182}Hf, has a half-life of 8.9 Myr, and was therefore only extant for the first ~60 Myr of Solar System history (Vockenhuber et al., 2004). Observed $\mu^{182}W$ (μ is the parts-per-million deviation from the terrestrial standard) variability in modern ocean island basalts (OIB) provides evidence for the storage of materials characterized by primitive isotopic signatures in Earth's interior for over 4.5 Gyr. Additionally, there is a statistically significant anticorrelation between $\mu^{182}W$ and $^{3}He/^{4}He$ (R_A, relative to Earth's atmosphere) in some OIB systems (Mundl et al., 2017; Mundl-Petermeier et al., 2020). Elevated $^{3}He/^{4}He$ R_A is a signature of the early Solar System (e.g., Mahaffy et al., 1998), and provides corroborative evidence that mantle plumes entrain material with primitive isotopic signatures.

The negative $\mu^{182}W$ compositions in mantle sources of OIB may have resulted from early silicate differentiation during the lifetime of ^{182}Hf (Touboul et al., 2012; Chapter 2 of this dissertation), or grainy late accretion of material with broadly chondritic ($\mu^{182}W \approx -200$) compositions (Puchtel et al., 2016; Archer et al., 2023). An alternative process to generate $\mu^{182}W$ deficits in the mantle is isotopic equilibration with the core (Rizo et al., 2019; Mundl-Petermeier et al., 2020; Ferrick and Korenaga, 2023). The core is characterized by low $\mu^{182}W$ (~-220) due to the fractionation of the lithophile element Hf and the moderately siderophile element W during

core formation while ^{182}Hf was extant (Kleine and Walker, 2017). The origin of μ^{182}W deficits in global OIB remains unknown and many questions remain regarding the chemical and physical properties of the anomalous μ^{182}W component in mantle plumes. Detailed analysis of μ^{182}W systematics in a suite of well characterized samples that represent variable spatial and temporal sampling of a single plume may reveal additional constraints on the component with negative μ^{182}W.

The Hawaiian mantle plume is the best sampled plume localities globally (e.g., Harðardóttir and Jackson, 2024). The Hawaiian Islands of Kauaʻi, Oʻahu, Lānaʻi, Maui, and Hawaiʻi, as well the submarine West Kaʻena Ridge and Kamaʻehuakanaloa seamount, represent >500 km and ~5 Myr of volcanic products from the plume. Prior studies have reported that Hawaiian volcanic rocks have a range of μ^{182}W from compositions similar to the presumed composition of the bulk silicate Earth (BSE, ~0) to among the most extreme negative μ^{182}W observed in OIB, -26 (Mundl et al., 2017; Mundl-Petermeier et al., 2020; Chapter 2 of this dissertation). The anticorrelations between μ^{182}W and ^{3}He/^{4}He observed in individual OIB systems globally is maintained in the Hawaiian plume (R^2 = 0.65, p value = 1E-08; Chapter 2 of this dissertation, Mundl-Petermeier et al., 2020).

Tomographic evidence suggests that the Hawaiian plume is rooted at the core-mantle boundary associated with an ultra-low velocity zone (ULVZ), as well as near the edge of a large low shear wave velocity province (LLSVP). The plume therefore plumbs what are likely physically and chemically heterogeneous mantle reservoirs (Cottaar and Romanowicz, 2012; Zhao et al., 2015; Kim et al., 2020). Additionally, it has been established that volcanoes along the archipelago comprise two parallel geographic and geochemical trends, the Loa and Kea trends, which have been interpreted to reflect distinct deep mantle sources (Harrison et al., 2017; Weis et al., 2020).

The Loa trend is typically geochemically enriched compared to Kea, possibly due to the incorporation of recycled materials housed in the LLSVP (Weis et al., 2011, 2020). The Kea trend is generally geochemically depleted and less heterogeneous than the Loa trend, but is distinct from the compositions of regional Pacific mid-ocean ridge basalts (MORB), leading to the hypothesis that Kea reflects the ambient deep Pacific mantle (Weis et al., 2011, 2020).

Heterogeneity within the Loa and Kea trends has been further classified into six geochemical groups using Sr-Nd-Hf-Pb isotopic compositions and linear discrimination analysis (Weis et al., 2020). Within the main Loa group there is Average Loa, which comprises the Mauna Loa, Māhukona, Hualālai, W. Molokaʻi, Penguin Bank, Waiʻanae, Koʻolau (except the Makapuʻu section of Koʼolau), West Kaʻena, and East Kauaʻi volcanic centers. Another subgroup of Loa includes Enriched Loa (Koʻolau Makapuʻu section, Lānaʻi, and Kahoʻolawe). The Kamaʻehuakanaloa seamount (formerly Lōʻihi) forms its own Loa subgroup. In addition to the main Kea group (Mauna Kea, Kīlauea, Hilina, Hāna Ridge, and West Kauaʻi), other subgroups of Kea include Transitional Kea (including West Maui and East Molokaʻi) and the Kohala group composed of Kohala and Haleakalā (Weis et al., 2020).

Thus far, the Hawaiian lavas that have been characterized for $\mu^{182}W$ represent a limited spatial and temporal range. All are from the Big Island of Hawaiʻi (Mauna Loa, Kīlauea, Mauna Kea, Kohala) and the Kamaʻehuakanaloa Seamount, and are less than 1 Ma (Chapter 2 of this dissertation; Mundl et al., 2017; Mundl-Petermeier et al., 2020; Archer et al., 2023). Of these lavas, only four of the six subgroups (Average Loa, Kea, Kohala, and Lōʻihi, where the name Lōʻihi refers to the subgroup defined by Kamaʻehuakanaloa) are represented. Three groups, Average Loa, Kea, and Lōʻihi, show $\mu^{182}W$ deficits are present in their mantle sources, though BSE-like compositions are also present. Interaction between the anomalous $\mu^{182}W$-bearing component and

recycled materials is examined alongside new and compiled Sr-Nd-Hf-Pb isotopic compositions and trace element abundances. New highly siderophile element (HSE) data and $^{187}Os/^{188}Os$ are used to discern whether late accreted material or core mantle interactions have affected the HSE and $\mu^{182}W$ of the Hawaiian mantle plume. Here, variations in $\mu^{182}W$ are characterized in the context of the Kea and Loa trends, as well as each of the six subgroups, to test what portions of the plume are likeliest to carry an anomalous $\mu^{182}W$ signature, and what subsequent processes and materials effect the expression of the $\mu^{182}W$ in erupted lavas.

4.3 Materials and methods

4.3.1 Sample descriptions

New $\mu^{182}W$ data are provided for tholeiitic, shield-stage lavas from volcanic centers across the Hawaiians Islands. Samples from the submarine Kama‘ehuakanaloa Seamount are exceptions to the shield stage sampling criteria used in this study, as the seamount is the youngest volcanic center among the Hawaiian chain, and represents pre-shield and early-shield volcanism. One sample from Kama‘ehuakanaloa, in which $\mu^{182}W$ was measured in a previous study (Mundl et al., 2017), is considered an alkali basalt. Samples in this study were selected because they are tholeiitic and shield stage samples. All samples in this study have Mg# > 51 and MgO >6 wt. %, and are classified as basalts, with the exception of two picro-basalts from Mauna Kea and Kama‘ehuakanaloa, and three basaltic andesites from Ko’olau – Makapu’u (Figure 4.1). The samples characterized here are relatively fresh, with a maximum loss on ignition (LOI) value of 2.2 wt %.

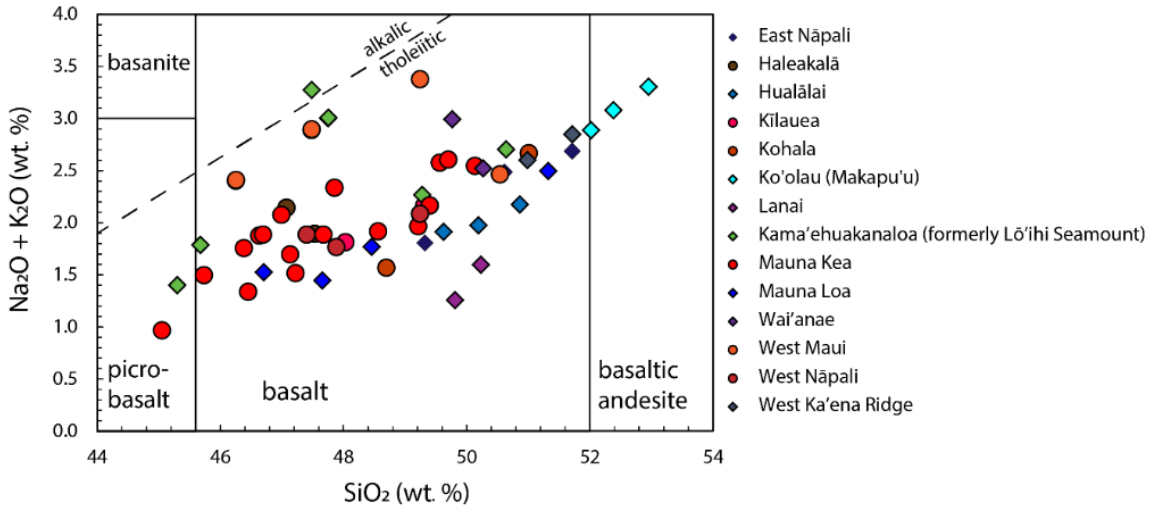

Figure 4.1. Total alkali-silica diagram (based on Le Bas et al., 1986) for Hawaiian samples that have $\mu^{182}W$ data. Circles represent samples from the Kea trend and diamonds represent samples from the Loa trend. Tholeiitic and alkalic subdivision line from Macdonald and Katsura (1964).

4.3.2. Sample preparation and chemical separation for $\mu^{182}W$ and W concentration analyses

Rocks were received from multiple sources as hand samples and were cut with a rock saw and sanded before crushing in a jaw crusher with alumina plates, which were cleaned before each use. An alumina shatterbox was cleaned before each use and was then used to powder the crushed samples. For $\mu^{182}W$ measurements, starting sample masses ranged from 13.8 to 26.9 grams. Acid digestion was performed using 1 mL of concentrated HNO_3 and 5 mL concentrated HF per gram of rock powder. After 5 days at approximately 150 °C the digested sample was evaporated to dryness and brought up in 5 mL of 1M HF per gram of sample. The 1M HF solution was then sonicated for 30 minutes and left overnight at approximately 130 °C. The solution was subsequently centrifuged and the supernatant was decanted into a clean beaker and dried down.

This step was repeated twice. The fluoride solids were then disposed of. Following fluoride extraction, 30 mL of 6M HCl was added to the dried sample until complete dissolution. The 6M HCl sample solution was dried down, and the sample was brought up in the column loading solution, 0.4M HCl + 0.5M HF (20 mL per 5 grams of sample). The W separation procedure was performed using 10 mL AG1-X8 anion exchange resin, following the protocols described in Willhite et al. (2024) and references therein. Secondary columns, following the procedure of Kleine et al. (2012) further purified W from the matrix. Total analytical yields for $\mu^{182}W$ analyses ranged from approximately 35 to 70%.

A separate chemical separation was performed on approximately 100 mg aliquots of the same sample powders used for $\mu^{182}W$ analyses in order to determine W abundances. Approximately 10 ng of ^{182}W spike was added to dedicated Teflon vessels for W isotope dilution analyses. To achieve digestion of sample powder and equilibration with the W spike, 1 mL concentrated HNO_3 and 5 mL concentrated HF was added to the Teflon vessels and they were left at ~150 °C for 24 hours. The sample-spike solution was then dried and 200 µL concentrated HNO_3 was added and dried down. Two iterations of the concentration HNO_3 step were performed. Next, 2 mL 6M HCl was added to each beaker and left to reflux for 48 hours. Each sample was dried then re-dissolved in 5 mL 6M HCl and left to reflux for overnight and then dried. Two mL of the column loading solution (0.5M HCl + 0.5M HF) were then added to each sample and was dried down to convert the sample for the loading solution. For loading onto the column, 5 mL 0.5M HCl + 0.5M HF was added to each Teflon vessel and refluxed for at least one hour. Once cooled to room temperature, the loading solution was added to each column for final separation of W (Kleine et al., 2004b). The total procedural blanks for W isotope dilution measurements ranged from 7 to

12 pg, which is less than 0.2% of the W mass from any sample and has no appreciable effect on the tungsten isotopic composition.

4.3.3 Thermal ionization mass spectrometry of tungsten isotopic compositions

Tungsten isotopic measurements were performed via negative-ion thermal ionization mass spectrometry (N-TIMS) on a *Thermo Scientific Triton*™ multicollector thermal ionization mass spectrometer in the Isotope Geochemistry Laboratory at the University of Maryland, College Park. To prepare each sample for mass spectrometric analysis, the chemically separated W fraction was loaded onto Re filaments using 1 µL of 0.5M HCl + 0.5M HF. A current of 0.7 A was applied and slowly increased to approximately 1.8 A to dry the sample onto the filament. Aliquots of the *Alfa Aesar* W standard that had not been through column chemistry, turned white or remained clear on the filament during the drying process. Samples that had been through column chemistry turned black around the edges of the sample droplet at this stage. The filament is glowed at 1.8 A until the black rim, which is thought to be organic material, turned white or clear (usually less than three seconds). The W sample on the filament was usually blue on the filament at this stage. The sample was then left on the filament for at least 24 hours before 1 µL of La (9 ng/µL) and Gd (3 ng/µL) activator was added and dried by slowly increasing current up to ~1.8 A. Mass spectrometric measurements followed the Faraday cup and amplifier configuration and per-integration oxide correction from Archer et al. (2017). In this configuration, tungsten oxide isotopologues that have ^{18}O (e.g., $^{186}W^{16}O_2{}^{18}O$) were measured using 10^{12} Ω resistor amplifiers to improve signal to noise of low abundance oxides and correct for O isotope variability (Archer et al., 2017). Isobaric interference from $^{180}TaO_3$ was monitored by measuring the $^{181}TaO_3$ signal throughout analyses, the measured signal was negligible, and no corrections were made for $^{180}TaO_3$ interference. Typical

beam intensities were ~1 V on mass $^{184}WO_3$ using a 10^{11} Ω resistor amplifier, and the total analysis time was 12 hours and 15 minutes, which included 45 minutes of baseline measurements. Final isotopic ratios were determined using the exponential law to correct for mass fractionation. The *Alfa Aesar* W standard (Lot No.: 211576G) was analyzed repeatedly throughout the analytical sessions (n = 38) with an average $^{182}W/^{184}W$ (normalized to $^{186}W/^{183}W$ = 1.98594) of 0.864861 and an external reproducibility of 3.6 ppm (2SD) and 0.73 ppm (2SE). The average $^{183}W/^{184}W$ of the standards was 0.467152 with an external reproducibility of 2.8 ppm (2SD) and 0.56 ppm (2SE) (Supplementary Table A.4.1).

4.3.4 Measurement of W concentrations

Following chemical purification of W isotope dilution aliquots (described in Section 2.2), the W concentration of each spiked sample was determined by multi-collector inductively-coupled-plasma mass spectrometry (MC-ICP-MS) using a *Thermo Scientific Neptune Plus* instrument in the Plasma Laboratory at the University of Maryland, College Park. Using a canonical $^{186}W/^{184}W$ value of 0.92767, fractionation correction was performed using exponential law via interspersed *Alfa Aesar* W standards. Analytical uncertainties were less than 5%.

4.3.5 Chemical purification and mass spectrometric analysis of highly siderophile element abundances and Os isotopic composition

Purification of the highly siderophile elements (HSE) Ru, Pd, Ir, Pt, Re, and Os followed the protocol outlined by Shirey and Walker (1995) and Ireland et al. (2009). Approximately 1.5 grams of sample powder was added to a borosilicate Carius tube. Teflon vessels were spiked with

approximately 0.5 ng of ^{190}Os, 0.8 ng of ^{185}Re, 2 ng of ^{99}Ru, ^{105}Pd, ^{191}Ir, and 4 ng of ^{194}Pt. After the addition of 3 mL concentrated HCl to the HSE spike mixture, the contents of the Teflon vessels were added to each Carius tube. The Carius tubes were placed in an ice bath before adding 6 mL concentrated HNO_3, to avoid oxidative loss of Os in HNO_3. Carius tubes were then sealed and heated to ~250 °C for at least 48 hours to achieve sample digestion and equilibration with the HSE spikes. After the Carius tubes were cooled and opened, any solid phases present were removed by centrifuging the solution. The supernatant was then added to CCl_4 to perform solvent extraction of Os followed by HBr back extraction to quantitatively remove Os. The HBr fraction was dried down. Further purification of Os was done via microdistillation with chromic acid and HBr. The final HBr solution containing purified Os was dried down and prepared for thermal ionization mass spectrometry. The Os fraction was analyzed via N-TIMS using the *Thermo Scientific Triton* in the Isotope Geochemistry Laboratory at the University of Maryland, College Park to obtain Os concentration and $^{187}Os/^{188}Os$. Analytical precision (internal 2SE) for $^{187}Os/^{188}Os$ measurements was better than 0.1 %. A total procedural blank was measurement for Os and resulted in an average blank of 6 pg. The $^{187}Os/^{188}Os$ of each sample was then blank corrected using the total Os mass and $^{187}Os/^{188}Os$ of the blank. Separation of Ru, Pd, Ir, Pt, Re was done by anion exchange column chromatography (Ireland et al., 2009). Once purified, Ru, Pd, Ir, Pt, Re abundances were measured by inductively coupled plasma mass spectrometry using the *Thermo Scientific Neptune Plus* MC-ICPMS instrument in the Plasma Laboratory at the University of Maryland, College Park. Average total procedural blanks for Re, Ru, Pt, Ir, and Pd were 2, 16, 16, 4, and 18 pg, respectively.

4.3.6 Chemical purification and mass spectrometric analysis of Sr-Nd-Hf-Pb isotopic compositions

New Sr-Nd-Hf-Pb isotopic analyses were performed on a subset of samples at the Pacific Centre for Isotopic and Geochemical Research (PCIGR), University of British Columbia (Vancouver, Canada) using aliquots of the same sample powders used for $\mu^{182}W$, $^{187}Os/^{188}Os$, and HSE measurements. New Sr-Nd-Hf-Pb data for twelve samples from seven volcanic centers are reported in Supplementary Table 4.2. Total procedural duplicates were performed ($n = 2$), as well as analytical replicates ($n = 1$), and all are in agreement within analytical uncertainty (Supplementary Table A.4.2). Prior to chemical digestion, sample powders were leached using 6M HCl to remove phases associated with weathering and alteration (e.g., Nobre Silva et al., 2009, 2010). Then, between 150 and 200 mg of sample powder was digested using a concentrated HF-HNO_3 mixture on a hotplate at 130°C in Teflon vials. The same sample dissolution was used to purify Sr, Nd, Hf, Pb by ion exchange column chromatography (Weis et al., 2006; Fourny et al., 2016).

Strontium isotopic compositions were measured by thermal ionization mass spectrometry on a *Nu Instruments TIMS* following instrument protocols described in Fourney et al. (2016). The SRM 987 standard reference material was analyzed repeatedly throughout the analytical session and had an average $^{87}Sr/^{86}Sr$ of 0.710251 ± 0.000013 ($n = 8$), which was within uncertainty of the preferred value, 0.710248 (Weis et al., 2006). Two Hawaiian rocks were analyzed as in house reference materials (KIL93 and KOO'LAU). After correction to the preferred NBS987 value, the average measured $^{87}Sr/^{86}Sr$ for KIL93 was 0.703590 (± 0.000008) and for KO'OLAU was 0.704093 (± 0.000007). The measured $^{87}Sr/^{88}Sr$ values of KIL93 and KO'OLAU were within

uncertainty of those reported in Nobre Silva et al. (2013): 0.703589 ± 0.000015 and 0.704101 ± 0.000022, respectively.

Neodymium and Hf isotopes were measured by multi-collector inductively coupled plasma mass spectrometry (MC-ICP-MS) sing a *Nu Plasma II 214* (Fourny et al., 2016). The $^{143}Nd/^{144}Nd$ standard, JNDi, was analyzed repeatedly throughout the analytical session and had an average $^{143}Nd/^{144}Nd$ of 0.512083 ± 0.000006 (n = 13). The JNDi value used for sample-standard bracketing correction was 0.512116 (per *Nu Instruments* specification). Reference materials, the Hawaiian rocks KIL93 and KO'OLAU, yielded $^{143}Nd/^{144}Nd$ of 0.512989 ± 0.000005 and 0.512773 ± 0.000006, respectively. Both values were within uncertainty of the preferred $^{143}Nd/^{144}Nd$, 0.512975 ± 0.000020 and 0.512758 ± 0.000009, respectively. For $^{176}Hf/^{177}Hf$, the JMC-475 standard reference material was analyzed repeatedly throughout Hf analytical sessions. The measured JMC 475 value was 0.282166 ± 0.000004 (n = 13). The JMC 475 value used for sample-standard bracketing correction was 0.282160 ± 0.000009 (Blichert-Toft et al., 1997). New Hf-isotopic data are reported in Table 4.1. The measured $^{176}Hf/^{177}Hf$ of the two Hawaiian reference materials, KIL93 and KO'OLAU, was 0.283096 ± 0.000004 and 0.282955 ± 0.000004, respectively, which are within the preferred values of 0.283104 0.000007 and 0.282959 0.000019 (Nobre Silva et al., 2013).

Lead isotopic compositions were measured by MC-ICP-MS on a *Nu Plasma 1700* (Fourny et al., 2016; Williamson et al., 2023). Pb isotopic compositions were corrected for mass bias by Tl-addition, assuming an exponential law and a $^{205}Tl/^{203}Tl$ ratio of 2.388. The ^{202}Hg isotope was monitored to make the isobaric correction for ^{204}Hg on mass 204. The standard reference material NBS 981 was analyzed throughout the analytical session, resulting in $^{208}Pb/^{204}Pb$ of 36.7191 ± 0.0019, $^{207}Pb/^{204}Pb$ of 15.4976 ± 0.0007, and $^{206}Pb/^{204}Pb$ of 16.9414 ± 0.0007 (n = 24). The

Hawaiian reference materials, KIL93 and KO'OLAU, resulted in $^{208}Pb/^{204}Pb$, $^{207}Pb/^{204}Pb$, and $^{206}Pb/^{204}Pb$ within uncertainty of preferred values from Nobre Silva et al. (2013).

4.3.7 Trace element analyses

A suite of 26 trace elements (Cs, Rb, Ba, Th, U, Nb, Ta, La, Ce, Pb, Pr, Nd, Sr, Zr, Hf, Sm, Eu, Gd, Tb, Dy, Ho, Y, Er, Tm, Yb, Lu) were measured on a subset of samples by ICP-MS on a *Thermo Scientific Element 2* at the Pacific Centre for Isotopic and Geochemical Research (PCIGR), University of British Columbia (Vancouver, Canada). Sample preparation followed Fourny et al. (2016). Drift correction was performed using BCR-2 for sample-standard bracketing. For the BCR-2 reference materials analyzed in this study, most trace element concentrations are within 5-10% of the preferred values from Jochum et al. (2016). New trace element data are reported in Supplementary Table A.4.3.

4.4 Results

4.4.1 Tungsten isotopic compositions of Hawaiian volcanics

New $\mu^{182}W$ data are presented here for thirteen Hawaiian volcanic centers including West and East Nāpali (Kauaʻi), W. Kaʻena Ridge (submarine seamounts), Waiʻanae (Oʻahu), Koʻolau (Oʻahu), West Maui (Maui), Haleakalā (Maui), Lānaʻi, Kohala (Hawaiʻi), Hualālai (Hawaiʻi), Mauna Loa (Hawaiʻi), Kīlauea (Hawaiʻi), and Kamaʻehuakanaloa (submarine seamount) (Table 4.1; Figure 4.2). Lavas from the ~5 Ma East Nāpali formation on Kauaʻi have negative $\mu^{182}W$ compositions ranging from -13.1 to -20.0. Similarly, ~5 Ma West Nāpali lavas have negative $\mu^{182}W$ values from -5.6 to -18.4. By comparison, volcanic centers between Kauaʻi and Hawaiʻi are

characterized by a limited range of $\mu^{182}W$ values. Two lavas have been characterized from the submarine West Kaʻena ridge and display $\mu^{182}W$ values of -2.1 and -6.3. Two lavas from the Waiʻanae volcano on Oʻahu do not show resolvable deficits $\mu^{182}W$ with values of -2.9 and +3.4. Three Koʻolau lavas are characterized by $\mu^{182}W$ ranging from -4.5 to -7.5. The $\mu^{182}W$ values of Lānaʻi samples range from +1.2 and -1.9. New data from the volcanoes on the island of Hawaiʻi are consistent with previously published $\mu^{182}W$ values. One new sample from Kohala has a BSE-like $\mu^{182}W$ value of -0.5. A new sample from Hualālai indicates a resurgence of negative $\mu^{182}W$ within the Hawaiian plume, with a $\mu^{182}W$ value of -7.7. New analyses from Mauna Loa and Kīlauea are BSE-like with a $\mu^{182}W$ of -4.5 and -5.3, respectively. It is important to note that all volcanic centers with resolvable $\mu^{182}W$ deficits also have lavas with BSE-like compositions. Hence, the BSE dominant composition appears to be present in all volcanic centers, while the anomalous component is not always present.

In combination with previously published $\mu^{182}W$, the data show that resolvable $\mu^{182}W$ deficits are present at 5 Ma in the Nāpali volcanic center and then disappear for over 3 Myr of the plume lifetime, as only BSE-like values are present until a resurgence to negative $\mu^{182}W$ in Hualālai, Mauna Kea, Mauna Loa, Kīlauea, and Kamaʻehuakanaloa lavas.

Table 4.1. New (**bold**) and previously published $\mu^{182}W$ and $^{187}Os/^{188}Os$ in Hawaiian lavas.

Sample	Island	Volcanic center	Distance from Kilauea (km)	Loa/Kea	Group	$\mu^{182}W$ (6/3)	2SE
KAU-2015-007	**Kauai**	**East Nāpali**	**519**	**Loa**	**Average Loa**	**-20.0**	**3.4**
KAU-2015-007 leached	**Kauai**	**East Nāpali**	**519**	**Loa**	**Average Loa**	**-22.1**	**3.2**
KAU-2015-014	**Kauai**	**East Nāpali**	**519**	**Loa**	**Average Loa**	**-16.8**	**4.2**
KAU-2015-014 leached	**Kauai**	**East Nāpali**	**519**	**Loa**	**Average Loa**	**-21.4**	**4.6**
KAU-2015-017	**Kauai**	**East Nāpali**	**519**	**Loa**	**Average Loa**	**-13.1**	**2.7**
KAU-2015-017 leached	**Kauai**	**East Nāpali**	**519**	**Loa**	**Average Loa**	**-19.1**	**3.5**
C-121	**Maui**	**Haleakala**	**175**	**Kea**	**Kohala**	**-1.5**	**3.4**
H2	Hawaii	Hualalai	64	Loa	Average Loa	-13.4	2.9
H27	**Hawaii**	**Hualalai**	**64**	**Loa**	**Average Loa**	**-7.7**	**2.8**
KIL-1-17	**Hawaii**	**Kilauea**	**0**	**Kea**	**Kea**	**-5.3**	**4.1**
KIL3-1	Hawaii	Kilauea	0	Kea	Kea	-8.8	3.8
KIL1840-2	Hawaii	Kilauea	0	Kea	Kea	-11.9	4.4
Kilauea 1712b	Hawaii	Kilauea	0	Kea	Kea	-3.4	4.3
KI81-2-88.6	Hawaii	Kilauea Iki	0	Kea	Kea	-11.4	3.6
KI81-2-88.6 dup	Hawaii	Kilauea Iki	0	Kea	Kea	-11.4	3.3
KI67-2-85.7	Hawaii	Kilauea Iki	0	Kea	Kea	-9.5	2.9
KI67-2-85.7 dup	Hawaii	Kilauea Iki	0	Kea	Kea	-10.4	3.5
KO-1-20	**Hawaii**	**Kohala**	**100**	**Kea**	**Kohala**	**-0.5**	**5.6**
KOH 1-28	Hawaii	Kohala	100	Kea	Kohala	-5.3	3.6
KOOb-015	**Oahu**	**Koolau-Makapuu**	**339**	**Loa**	**Enriched Loa**	**-7.5**	**3.6**
KOOb-016	**Oahu**	**Koolau-Makapuu**	**339**	**Loa**	**Enriched Loa**	**-4.5**	**2.9**
WH-489	**Oahu**	**Koolau-Makapuu**	**339**	**Loa**	**Enriched Loa**	**-5.4**	**3.0**
85-LAN-4	**Lanai**	**Lanai**	**226**	**Loa**	**Enriched Loa**	**-1.9**	**5.4**
85-LAN-7	**Lanai**	**Lanai**	**226**	**Loa**	**Enriched Loa**	**1.2**	**4.3**
LO-02-02	submarine	Loihi	-40	Loa	Loihi	-9.7	3.5
LO-02-02	submarine	Loihi	-40	Loa	Loihi	-13.8	3.6
J2-374-R5	submarine	Loihi	-40	Loa	Loihi	-18.4	6.2
J2-374-R5	submarine	Loihi	-40	Loa	Loihi	-11.9	3.8
LO-02-04	submarine	Loihi	-40	Loa	Loihi	-19	5
LO-02-04	submarine	Loihi	-40	Loa	Loihi	-16.1	1.9
LO-02-04	submarine	Loihi	-40	Loa	Loihi	-25.6	2.9
KK16-1	submarine	Loihi	-40	Loa	Loihi	-20.8	6.2
KK 25-4	submarine	Loihi	-40	Loa	Loihi	-14.8	8.9

Table 4.1. continued

SR0167-5.7	**Hawaii**	**Mauna Kea**	**54**	**Kea**	**Kea**	**-2.6**	**2.2**
SR0267-6.3	**Hawaii**	**Mauna Kea**	**54**	**Kea**	**Kea**	**-2.9**	**3.0**
SR0372-3.2	**Hawaii**	**Mauna Kea**	**54**	**Kea**	**Kea**	**-4.3**	**3.6**
SR0455-6.8	**Hawaii**	**Mauna Kea**	**54**	**Kea**	**Kea**	**-4.0**	**3.1**
SR0548-8.0	**Hawaii**	**Mauna Kea**	**54**	**Kea**	**Kea**	**-8.6**	**3.4**
SR0756-14.3	**Hawaii**	**Mauna Kea**	**54**	**Kea**	**Kea**	**-6.3**	**3.2**
SR0860-6.5	**Hawaii**	**Mauna Kea**	**54**	**Kea**	**Kea**	**-5.8**	**3.5**
SR0913-2.3	**Hawaii**	**Mauna Kea**	**54**	**Kea**	**Kea**	**-3.2**	**2.3**
SR0940-7.7	**Hawaii**	**Mauna Kea**	**54**	**Kea**	**Kea**	**-16.6**	**3.8**
SR0954-7.4	**Hawaii**	**Mauna Kea**	**54**	**Kea**	**Kea**	**-12.0**	**3.6**
SR0956-9.3	**Hawaii**	**Mauna Kea**	**54**	**Kea**	**Kea**	**-12.1**	**3.7**
SR0967-2.8	**Hawaii**	**Mauna Kea**	**54**	**Kea**	**Kea**	**-3.8**	**3.3**
SR0683-5.75	Hawaii	Mauna Kea	54	Kea	Kea	-1.8	4.7
SR0891-15.10	Hawaii	Mauna Kea	54	Kea	Kea	-10	3.7
SR0750-12.45	Hawaii	Mauna Kea	54	Kea	Kea	-11.5	5.2
SR0762-4.6	Hawaii	Mauna Kea	54	Kea	Kea	-8.7	3.5
MK 1-6	Hawaii	Mauna Kea	54	Kea	Kea	-2.3	3.1
MK 1-6	Hawaii	Mauna Kea	54	Kea	Kea	-7.8	6.1
SR0008-4.2	**Hawaii**	**Mauna Loa**	**35**	**Loa**	**Average Loa**	**1.9**	**3.3**
SR0113-6.1	**Hawaii**	**Mauna Loa**	**35**	**Loa**	**Average Loa**	**-3.7**	**3.7**
SR0117-3.8	**Hawaii**	**Mauna Loa**	**35**	**Loa**	**Average Loa**	**-6.5**	**4.0**
ML 1868-9	Hawaii	Mauna Loa	35	Loa	Average Loa	-0.3	3.1
ML 2-50	Hawaii	Mauna Loa	35	Loa	Average Loa	-12.3	4.3
ML-2-12	**Hawaii**	**Mauna Loa**	**35**	**Loa**	**Average Loa**	**-4.5**	**4.5**
J2-305-04	**submarine**	**W. Kaena Ridge**	**414**	**Loa**	**Average Loa**	**-2.1**	**2.8**
J2-306-15	**submarine**	**W. Kaena Ridge**	**414**	**Loa**	**Average Loa**	**-6.3**	**3.4**
WA-2017-02	**Oahu**	**Waianae**	**374**	**Loa**	**Average Loa**	**-2.9**	**3.4**
WA-2017-03	**Oahu**	**Waianae**	**374**	**Loa**	**Average Loa**	**3.4**	**2.4**
02-WA-10	**Maui**	**West Maui**	**221**	**Kea**	**Transitional Kea**	**-2.1**	**2.7**
KAU-2015-032	**Kauai**	**West Nāpali**	**519**	**Kea**	**Kea**	**-16.3**	**2.9**
KAU-2015-035	**Kauai**	**West Nāpali**	**519**	**Kea**	**Kea**	**-5.6**	**3.3**
KAU-2015-035 leached	**Kauai**	**West Nāpali**	**519**	**Kea**	**Kea**	**-11.2**	**1.6**
KAU-2015-036	**Kauai**	**West Nāpali**	**519**	**Kea**	**Kea**	**-18.4**	**2.9**
KAU-2015-036 duplicate	**Kauai**	**West Nāpali**	**519**	**Kea**	**Kea**	**-18.8**	**3.9**

$\mu^{182}W$ is the deviation of $^{182}W/^{184}W$ of a sample from that of the average of repeated measurements of an Alfa Aesar tungsten standard (2SD = 3.6; *n* = 38). New data are presented in bold. For $\mu^{182}W$ 2SE represents the internal standard error of a single analysis. All $\mu^{182}W$ values are normalized to $^{186}W/^{183}W$. Data not in bold are previous $\mu^{182}W$ from Mundl et al. (2017) and Mundl-Petermeier et al. (2020).

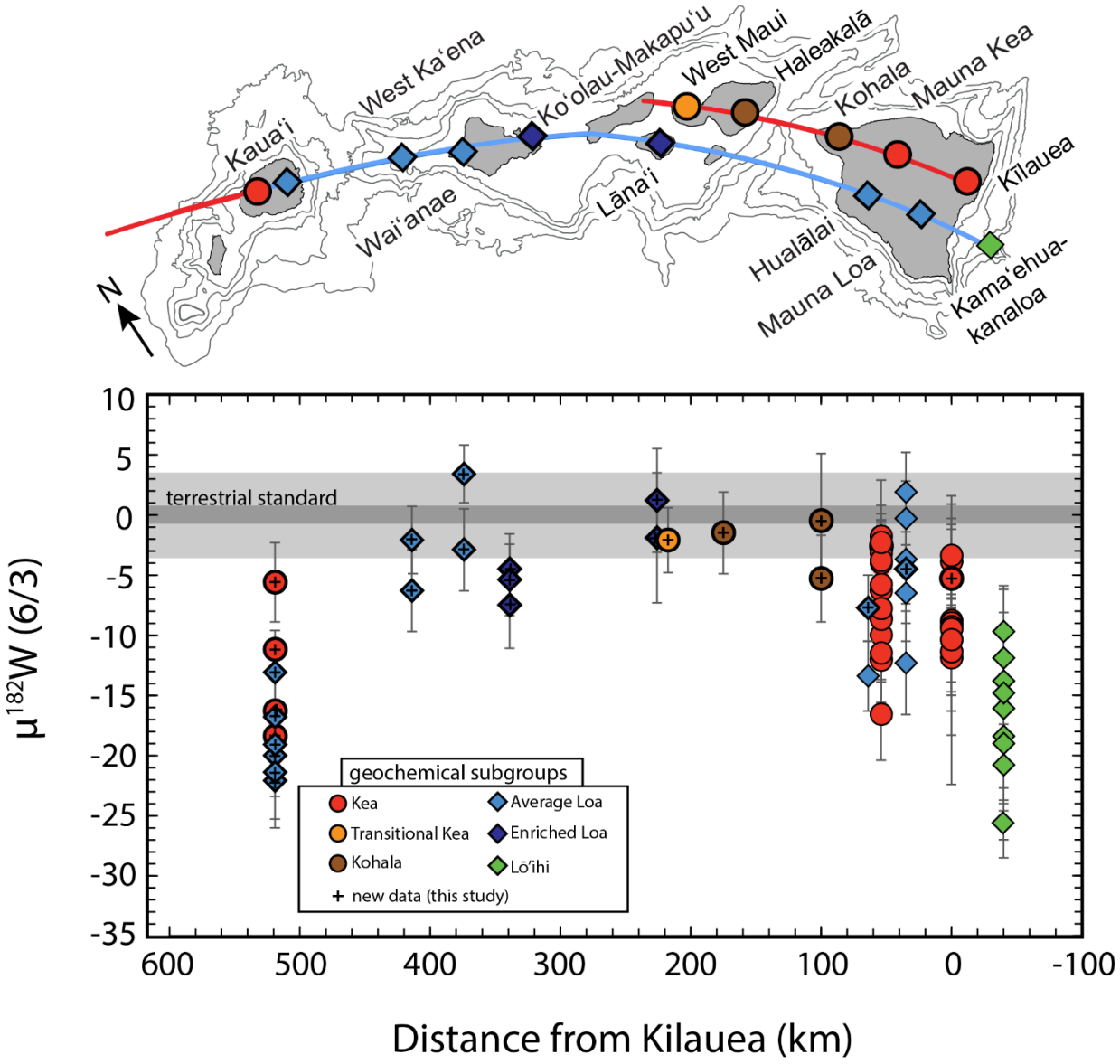

Figure 4.2. $\mu^{182}W$ values (normalized to $^{186}W/^{183}W$) as a function of distance from Kīlauea. The colors represent geochemical subgroups defined using Sr-Nd-Hf-Pb isotopic compositions (Weis et al., 2020). Blue and green diamonds are subgroups from the Loa trend, and red, orange, and brown circles are from the Kea trend. These colors and symbols are maintained in all of the following figures. Data symbols with crosses are from this study, while all other data are from previous studies (Mundl et al., 2017; Mundl-Petermeier et al., 2020).

4.4.2 Osmium isotopic compositions and HSE abundances

East Nāpali volcanics from Kauaʻi, which are classified as part of the average Loa geochemical group, have more radiogenic $^{187}Os/^{188}Os$ (0.1419 to 0.1597) compared to West Nāpali (0.1333 to 0.1352), which have Kea trend characteristics. Applying a 5 Myr age correction to the $^{187}Os/^{188}Os$ ratios using measured Re/Os yields ratios ranging from 0.1404 to 0.1571 in East Nāpali and 0.1329 to 0.1351 in West Nāpali (Table 4.1). The more radiogenic ratios observed in East Nāpali are among highest $^{187}Os/^{188}Os$ in any Hawaiian shield; however, the radiogenic Os isotopic composition of sample KAU-2015-017 (0.1597) should be treated with caution due to the low Os concentration (0.049 ppb) and the potential for contamination by crustal and/or sedimentary Os (e.g., Lassiter and Hauri, 1998). Osmium abundances in the other East and West Nāpali samples overlap range from 0.170 to 0.558 ppb (Table 4.2). Rhenium is distinctly lower in West Nāpali (0.050 to 0.131 ppb) compared to East Nāpali (0.276 to 0.582 ppb), yielding higher Re/Os (~1 to 6) in East Nāpali compared to West Nāpali (~0.2 to 0.25). Platinum abundances are comparable at both East and West Nāpali, with ranges from 2.323 to 3.893 ppb, and 2.474 to 4.788 ppb, respectively.

The submarine West Kaʻena Ridge sample has an Os concentration of 0.852 ppb and $^{187}Os/^{188}Os$ ~0.1310, which is less radiogenic compared to most Loa trend volcanic centers. The Waiʻanae volcanic center has Os concentrations of 0.190 and 0.252 ppb, and $^{187}Os/^{188}Os$ compositions of 0.1348 and 0.1354. Koʻolau lavas in this study have measured $^{187}Os/^{188}Os$ from 0.1414 to 0.1417, and age correction to 2.6 Ma yields $^{187}Os/^{188}Os$ from 0.1403 to 0.1412, consistent with previous studies of $^{187}Os/^{188}Os$ in Koʻolau with age corrected values ranging from 0.1406 to 0.1477 (Lassiter and Hauri, 1998). Similar to East Nāpali, Koʻolau has high Re/Os, ranging from ~1 to 6. Lānaʻi $^{187}Os/^{188}Os$ ranges from 0.1348 to 0.1384. The Kea trend volcanoes on Maui,

including the West Maui volcanic center and Haleakalā have $^{187}Os/^{188}Os$ of 0.1252 and 0.1300, respectively. The West Maui sample, WA-10, has the lowest Os concentration in the Hawaiian suite (0.031 ppb), and therefore, the $^{187}Os/^{188}Os$ may be affected by crustal assimilation or weathering processes, and should be treated with caution.

Kohala has $^{187}Os/^{188}Os$ ranging from 0.1329 to 0.1431. The radiogenic $^{187}Os/^{188}Os$ in one sample from Kohala is the highest $^{187}Os/^{188}Os$ in any Kea trend volcano. Hualālai, a Loa trend volcano, has $^{187}Os/^{188}Os$ of 0.1344 to 0.1369. Mauna Kea has the least radiogenic $^{187}Os/^{188}Os$ among all Hawaiian volcanic centers (except potentially West Maui, if the $^{187}Os/^{188}Os$ is unaffected in the low Os concentration sample). Mauna Kea $^{187}Os/^{188}Os$ ranges from 0.1276 to 0.1300. The Mauna Loa volcano is radiogenic compared to Mauna Kea, with $^{187}Os/^{188}Os$ from 0.1332 to 0.1360. The youngest Hawaiian volcanic center, the Kamaʻehuakanaloa seamount, has $^{187}Os/^{188}Os$ overlapping Mauna Loa, with a range of 0.1338 to 0.1352. This seamount also has Pd abundances (2.3 to 7.3) and distinctly higher Pt abundances (~5.8 to 6.5 ppb) compared to other Hawaiian volcanic centers (Table 4.2).

The $^{187}Os/^{188}Os$ of lavas from Loa geochemical groups are statistically higher than Kea trend lavas. The most radiogenic $^{187}Os/^{188}Os$ among all geochemical groups comes from average Loa (only from East Nāpali) and enriched Loa (Koʻolau). Other Average Loa group lavas, such as those from Mauna Loa and Hualālai, have only moderate $^{187}Os/^{188}Os$. The least radiogenic Os isotopic compositions are associated with lavas from the Kea subgroup, especially those from Mauna Kea. The Kohala subgroup is intermediate, and so is the Lōʻihi subgroup.

The HSE abundances of Hawaiian lavas studied here are summarized in Figure 4.3.

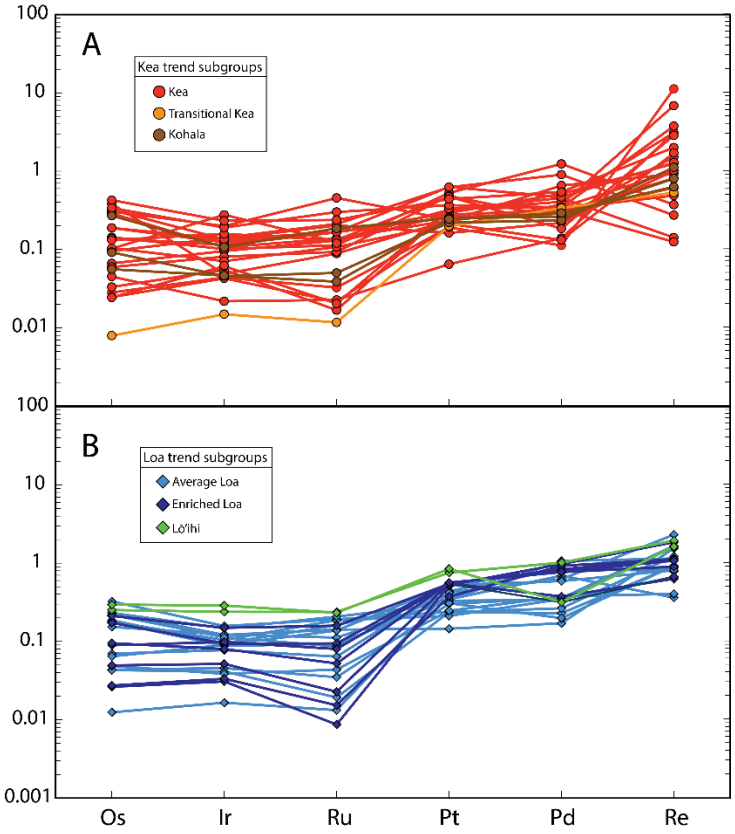

Figure 4.3. Highly siderophile element abundances of Hawaiian shield basalts from (A) Kea trend subgroups, and (B) Loa trend subgroups. Data are from this study and Ireland et al. (2009).

Table 4.2. New (**bold**) and compiled osmium isotopic compositions and HSE abundances in Hawaiian lavas.

Sample	Island	Volcanic center	$^{187}Os/^{188}Os$ (m)	Os (ppb)	Ir	Ru	Pt	Pd	Re
KAU-2015-007	**Kauai**	**East Nāpali**	***0.1442***	**0.272**	**0.271**	**0.454**	**3.893**	**6.192**	**0.276**
KAU-2015-014	**Kauai**	**East Nāpali**	***0.1404***	**0.170**	**0.160**	**0.248**	**2.323**	**2.566**	**0.582**
KAU-2015-017	**Kauai**	**East Nāpali**	***0.1571***	**0.049**	**0.058**	**0.094**	**3.386**	**6.067**	**0.303**
C-121	**Maui**	**Haleakala**	**0.1300**	**0.218**	**0.163**	**0.276**	**1.873**	**2.104**	**0.221**
H2	Hawaii	Hualalai	0.13685	0.910	0.423	1.007	1.120	1.228	0.542
H27	**Hawaii**	**Hualalai**	0.13437	1.262	0.550	1.359	1.834	1.647	0.321
H9	**Hawaii**	**Hualalai**	0.13624	0.598	0.429	0.796	2.538	2.470	0.567
KIL3-1	Hawaii	Kilauea	0.13031	0.733	0.434	1.182	1.975	2.128	0.215
KIL1840-2	Hawaii	Kilauea	0.13086	1.129	0.373	0.984	1.807	2.384	0.171
KO-1-20	**Hawaii**	**Kohala**	0.14310	0.358	0.160	0.356	1.695	1.695	0.392
KOH 1-28	Hawaii	Kohala	0.13294	1.052	0.376	1.321	1.929	1.896	0.282
KOOb-015	**Oahu**	**Koolau-Makapuu**	***0.1412***	**0.371**	**0.280**	**0.371**	**4.346**	**5.574**	**0.376**
KOOb-016	**Oahu**	**Koolau-Makapuu**	***0.1407***	**0.107**	**0.117**	**0.108**	**2.885**	**6.648**	**0.393**
WH-489	**Oahu**	**Koolau-Makapuu**	***0.1403***	**0.103**	**0.108**	**0.062**	**4.039**	**7.013**	**0.647**
LWAW-4	**Lanai**	**Lanai**	0.13843	0.827	0.522	1.129	4.171	2.281	0.236
LWAW-7	**Lanai**	**Lanai**	0.13760	0.349	0.344	0.568	4.234	2.701	0.221
85-LAN-4	**Lanai**	**Lanai**	**0.1348**	**0.193**	**0.181**	**0.161**	**4.221**	**5.985**	**0.398**
85-LAN-7	**Lanai**	**Lanai**	**0.1369**	**0.674**	**0.328**	**0.670**	**4.338**	**5.520**	**0.316**
LO-02-02	Hawaii	Kamaʻehuakanaloa	0.13518	0.984	0.836	1.689	5.825	7.301	0.679
LO-02-02	Hawaii	Kamaʻehuakanaloa	0.13518	0.984	0.836	1.689	5.825	7.301	0.679
LO-02-04	Hawaii	Kamaʻehuakanaloa	0.13377	1.150	1.006	1.649	6.526	2.288	0.567
LO-02-04	Hawaii	Kamaʻehuakanaloa	0.13377	1.150	1.006	1.649	6.526	2.288	0.567
LO-02-04	Hawaii	Kamaʻehuakanaloa	0.13377	1.150	1.006	1.649	6.526	2.288	0.567

Table 4.2. continued

SR0167-5.7	Hawaii	Mauna Kea	0.1293	**0.110**	**0.154**	**0.231**	**1.471**	**0.811**	**3.937**
SR0267-6.3	Hawaii	Mauna Kea	0.1282	**0.401**	**0.970**	**0.888**	**2.150**	**2.278**	**0.044**
SR0372-3.2	Hawaii	Mauna Kea	0.1295	**0.096**	**0.150**	**0.154**	**1.513**	**2.705**	**2.401**
SR0455-6.8	Hawaii	Mauna Kea	0.1291	**1.191**	**0.696**	**3.228**	**1.865**	**2.210**	**0.284**
SR0548-8.0	Hawaii	Mauna Kea	0.1289	**0.538**	**0.401**	**1.175**	**2.258**	**3.694**	**0.436**
SR0756-14.3	Hawaii	Mauna Kea	0.1295	1.493	**0.171**	**0.630**	**1.793**	**4.717**	**0.322**
SR0860-6.5	Hawaii	Mauna Kea	0.1293	**0.129**	**0.192**	**0.119**	**2.480**	**2.922**	**1.082**
SR0913-2.3	Hawaii	Mauna Kea	0.1303	**0.233**	**0.283**	**0.663**	**3.720**	**1.796**	**0.532**
SR0940-7.7	Hawaii	Mauna Kea	0.1291	**0.176**	**0.076**	**0.161**	**0.500**	**1.001**	**1.084**
SR0954-7.4	Hawaii	Mauna Kea	0.1276	**1.245**	**0.472**	**1.185**	**4.831**	**3.364**	**0.451**
SR0956-9.3	Hawaii	Mauna Kea	0.1300	**0.095**	**0.214**	**0.145**	**2.578**	**2.488**	**1.318**
SR0967-2.8	Hawaii	Mauna Kea	0.1295	**0.514**	**0.552**	**0.938**	**3.643**	**1.332**	**1.000**
SR0683-5.75	Hawaii	Mauna Kea	0.1297	**1.319**	**0.668**	**2.137**	**2.835**	**2.484**	**0.352**
SR0891-15.10	Hawaii	Mauna Kea	0.1299	1.665	0.814	1.691	3.397	3.899	0.702
SR0750-12.45	Hawaii	Mauna Kea	0.1296	0.405	**0.249**	**0.765**	**1.643**	**0.953**	**0.597**
SR0762-4.6	Hawaii	Mauna Kea	0.1301	0.361	**0.218**	**0.853**	**1.676**	**0.121**	**0.355**
MK 1-6	Hawaii	Mauna Kea	0.12924	0.736	0.476	1.444	1.254	1.572	0.353
MK 1-6	Hawaii	Mauna Kea	0.12924	0.736	0.476	1.444	1.254	1.572	0.353
SR0008-4.2	Hawaii	Mauna Loa	0.1360	**0.168**	**0.144**	**0.137**	**1.824**	**1.906**	**0.429**
SR0113-6.1	Hawaii	Mauna Loa	0.1332	**0.724**	**0.331**	**1.148**	**2.660**	**4.978**	**0.127**
SR0117-3.8	Hawaii	Mauna Loa	0.1335	**0.689**	**0.307**	**0.665**	**2.626**	**7.661**	**0.401**
ML 1868-9	Hawaii	Mauna Loa	0.13491	0.701	0.365	1.327	1.629	2.498	0.230
ML 2-50	Hawaii	Mauna Loa	0.13419	0.902	0.515	1.474	2.373	1.426	0.324
J2-306-15		**W. Kaena Ridge**	**0.1309**	**0.852**	**0.396**	**0.612**	**3.224**	**4.490**	**0.808**
WA-2017-02	**Oahu**	**Waianae**	**0.1348**	**0.190**	**0.135**	**0.311**	**1.900**	**2.704**	**0.142**
WA-2017-03	**Oahu**	**Waianae**	**0.1354**	**0.252**	**0.316**	**0.980**	**4.027**	**4.241**	**0.284**
02-WA-10	**Maui**	**West Maui**	**0.1252**	**0.031**	**0.052**	**0.083**	**1.520**	**2.442**	**0.186**
KAU-2015-032	**Kauai**	**West Nāpali**	***0.1342***	**0.373**	**0.495**	**1.505**	**4.788**	**6.497**	**0.096**
KAU-2015-035	**Kauai**	**West Nāpali**	***0.1351***	**0.259**	**0.335**	**0.926**	**2.474**	**3.281**	**0.050**
KAU-2015-036	**Kauai**	**West Nāpali**	***0.1329***	**0.558**	**0.355**	**0.804**	4.061	8.911	0.131

Data in bold are new measurements. Data that are not in bold are from Ireland et al. (2009). The $^{187}Os/^{188}Os$ are measured values (m), except for the italicized data from East and West Nāpali and Koʻolau, which have been age corrected to ~5 Ma and 2.6 Ma, respectively.

4.4.3 Sr-Nd-Hf-Pb isotopic compositions

The $^{87}Sr/^{86}Sr$ of the four Lānaʻi samples is between 0.704071 and 0.704331. Two West Maui samples were analyzed and have $^{87}Sr/^{86}Sr$ between 0.703410 and 0.703459. One Kohala was analyzed and has a $^{87}Sr/^{86}Sr$ of 0.703721. Two samples were analyzed from Hualālai, H27 and H9. Sample H9 has a $^{87}Sr/^{86}Sr$ of 0.703748. Replicate measurements of H27 (i.e., replicate measurement of the same sample solution after chemical purification) resulted in $^{87}Sr/^{86}Sr$ of 0.703754 and 0.703755. A full duplicate analysis (i.e., separate digestion, chemical purification, and measurement) of H27 resulted in $^{87}Sr/^{86}Sr$ of 0.703751. One Mauna Loa sample was analyzed and has a $^{87}Sr/^{86}Sr$ of 0.703721. One Kīlauea sample was analyzed and has a $^{87}Sr/^{86}Sr$ of 0.703564, and one Kamaʻehuakanaloa sample has a $^{87}Sr/^{86}Sr$ of 0.703591.

The $^{143}Nd/^{144}Nd$ of the four Lānaʻi samples is between 0.512763 and 0.512852. The two West Maui samples analyzed have $^{143}Nd/^{144}Nd$ between 0.513045 and 0.513052. The Kohala sample has $^{143}Nd/^{144}Nd$ of 0.512973. The full duplicate analysis of H27 (Hualālai) resulted in $^{143}Nd/^{144}Nd$ of 0.512927 and 0.512917. Replicate measurements of H9 resulted in $^{143}Nd/^{144}Nd$ of 0.512912 and 0.512916. The Mauna Loa sample underwent replicate $^{143}Nd/^{144}Nd$ analyses that resulted in $^{143}Nd/^{144}Nd$ of 0.512922 and 0.512929. One Kīlauea sample was analyzed and has a $^{143}Nd/^{144}Nd$ of 0.512992, and one Kamaʻehuakanaloa sample has a $^{143}Nd/^{144}Nd$ of 0.512951.

The $^{176}Hf/^{177}Hf$ of the four Lānaʻi samples is between 0.282952 and 0.283020. The two West Maui samples have $^{176}Hf/^{177}Hf$ of 0.283129 and 0.283136 and the Kohala sample has $^{176}Hf/^{177}Hf$ of 0.283099. The full duplicate analysis of H27 (Hualālai) resulted in $^{176}Hf/^{177}Hf$ of 0.283056 and 0.283058. Replicate measurements of H9 resulted in $^{176}Hf/^{177}Hf$ of 0.283057 and 0.283063. Replicate analyses of the Mauna Loa sample resulted in $^{176}Hf/^{177}Hf$ of 0.283070 and

0.283074. The $^{176}Hf/^{177}Hf$ of the Kīlauea sample is 0.283098. The Kama‘ehuakanaloa sample has $^{176}Hf/^{177}Hf$ of 0.283093.

The four Lāna‘i samples have the least radiogenic $^{208}Pb/^{204}Pb$ (37.75 to 37.78), $^{207}Pb/^{204}Pb$ (15.43 to 15.45) and $^{206}Pb/^{204}Pb$ (17.88 to 17.98) of the new samples analyzed. West Maui samples have $^{208}Pb/^{204}Pb$ from 37.89 to 38.03, $^{207}Pb/^{204}Pb$ from 15.47 to 15.49, and $^{206}Pb/^{204}Pb$ of 18.35 to 18.50. The West Maui sample, OL-33a, has the most radiogenic $^{206}Pb/^{204}Pb$ and $^{207}Pb/^{204}Pb$, but not $^{208}Pb/^{204}Pb$, among the new analyses. The Kohala sample has intermediate Pb isotopic values among the new samples analyzed. The two Hualālai samples have similar Pb isotopic compositions, and the replicate and duplicate values for all Pb isotopes are within analytical uncertainty. The Mauna Loa sample has Pb isotopic compositions within uncertainty of the Hualālai samples, and replicate analyses of the Mauna Loa sample are in good agreement. The Kīlauea sample has relatively radiogenic Pb compared to the all other new samples, except the sample from Kama‘ehuakanaloa, which has the most radiogenic $^{208}Pb/^{204}Pb$ (~38.16).

4.4.4 Trace element compositions

New trace element data are presented in Supplementary Table 4.2. Rare earth element (REE) systematics show that most samples are geochemically enriched relative to BSE. For example all but three samples have primitive mantle normalized La/Sm ($[La/Sm]_N$) > 1.2. The exceptions include three Lāna‘i samples, with relatively flat REE and $[La/Sm]_N$ between 0.9 and 1.2. Two Lāna‘i lavas exhibit relatively large depletions in the fluid mobile elements Cs, Rb, and U, compared to the smaller depletions observed in the other samples. All samples have a depletion in Pb, as is common in mantle-derived basalts (Hart and Gaetani, 2006). Lāna‘i has distinctly low

Nb/Th (14.2 to 15.7) relative to this suite of Hawaiian lavas, while Kama‘ehuakanaloa’s Nb/Th is distinctly high (18.3). The Nb/Th of all other samples in this suite fall between 15.8 and 17.4. Lāna‘i samples are also elevated in Sr/Nb (39 to 45) compared to the rest of the suite (20 to 30). The Nb/Y relative to Zr/Y of all samples is typical of Hawaiian shield basalts (e.g., Williamson et al., 2023).

4.5 Discussion

4.5.1 Hawaiian plume: Pulsing or persistent anomalous material?

To understand which processes and materials affect the expression of $\mu^{182}W$ anomalies in mantle-derived lavas, ^{182}W measurements for the Hawaiian mantle plume are paired with chemical compositions, including HSE systematics, and radiogenic Sr-Nd-Hf-Os-Pb isotopic compositions. The $\mu^{182}W$ of a single volcano can vary with time as a result of the thermal structure of the plume. For example, in Chapter 2 it was shown that in a stratigraphic section of shield stage Mauna Kea, the magnitude of $\mu^{182}W$ anomalies decreased over a duration of ~300 kyr. That study also showed that the $\mu^{182}W$ values in Mauna Kea do not vary systematically with Sr-Hf-Os isotopic compositions. Instead, $\mu^{182}W$ in Mauna Kea corresponds to the relative location of the volcano and plume axis, such that the largest $\mu^{182}W$ anomalies appeared when the volcano was proximal to the plume axis and the mantle potential temperature was highest.

There is an anticorrelation between $\mu^{182}W$, Ti/Ti*, Nb/Nb*, and $^{208}Pb/^{206}Pb$ in Mauna Kea, interpreted to reflect the refractory nature of a high field strength element (HFSE) enriched component that hosts $\mu^{182}W$ anomalies (Chapter 2 of this dissertation). Normal and anomalous $\mu^{182}W$ are in lavas when the volcano was proximal to the plume axis, demonstrating that the

anomalous component may present small volumes, and is not always melted, even when the volcano is proximal to the plume axis. In this case, the thermal structure of the plume is interpreted to control the probability of $\mu^{182}W$ anomalies expressed in lavas of a given volcano and indicates that a relatively high temperature and melt flux may be required to sample the anomalous component.

Using the Mauna Kea shield stage as a model, a kernel probability density function predicts a 62% chance of a shield stage melt sampling the anomalous component and expressing a resolvable $\mu^{182}W$ (defined as $\mu^{182}W \leq -5$) (Figure 4.4). The Mauna Kea model is based on lavas that were selected because they have a range of $^3He/^4He$ from normal (i.e., ~8 ± 2 R_A; Graham, 2002) to 23 R_A and a limited range of MgO and SiO_2 wt. % throughout the shield stage. Therefore, though the samples were not randomly selected, the $\mu^{182}W$ data are not biased toward a specific $^3He/^4He$. A slight bias toward negative values may result from a higher frequency of sampling of the lower half of the stratigraphic section (n =10) compared to the upper half of the section (n = 6). As a comparison, a model was created using $^3He/^4He$ in the same drill core, which is correlated with $\mu^{182}W$, and was measured at a higher frequency sampling rate in the Mauna Kea stratigraphic section (n = 114) compared to $\mu^{182}W$ (Figure 4.4). The $^3He/^4He$ model indicates a 48% probability of sampling a high $^3He/^4He$ (>12 R_A) relative to the average of mid-ocean ridge basalts (Graham, 2002).

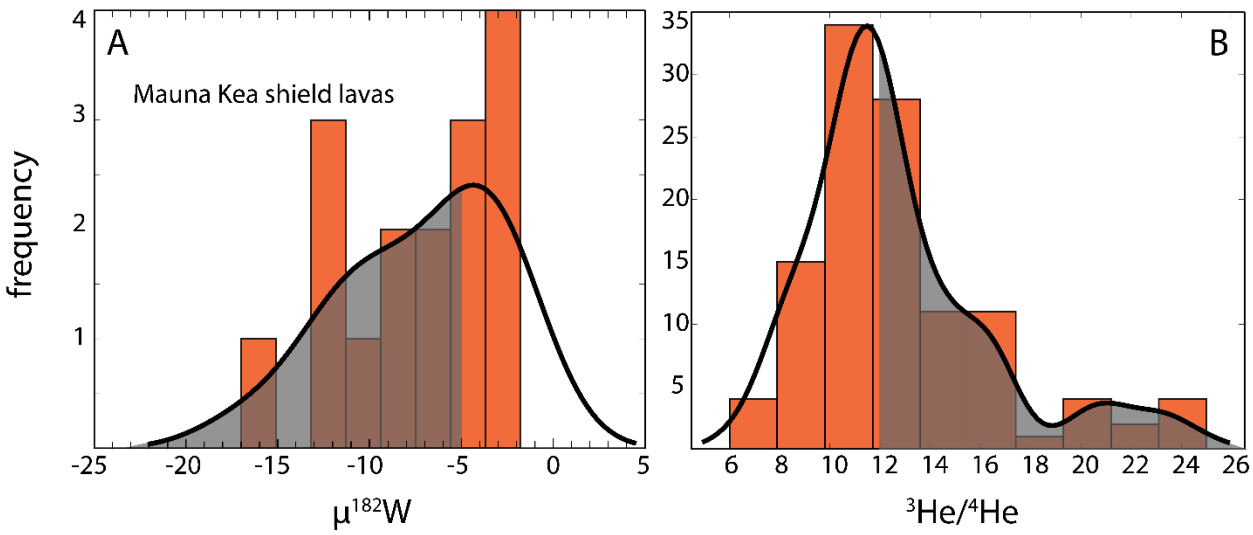

Figure 4.4. (**A**) Kernel probability density function (pdf, black line) superimposed on a histogram of the $\mu^{182}W$ of Mauna Kea shield stage lavas. The grey shaded region represents the integral of the pdf from -5 to -25, yielding a 62% probability of a new value falling within that range of $\mu^{182}W$. Data are from Mundl et al. (2017), Mundl-Petermeier et al. (2020), and Willhite et al. (2024). (**B**) Kernel pdf superimposed on a histogram of the $^{3}He/^{4}He$ of shield stage Mauna Kea shield stage lavas. The grey shaded region represents the integral of the pdf from 12 to 25, yielding a 48% probability of a new value falling within that range. Data from Kurz et al. (2004).

The $\mu^{182}W$ and $^{3}He/^{4}He$ distributions for Mauna Kea indicate that the anomalous component is sampled by approximately half of shield stage lavas. If the thermal structure of the plume is comparable across time and space, then other Hawaiian shield volcanoes may also sample the anomalous component in ~50% of erupted products. Several factors could alter the probability density function of a given volcano, including a cooler mantle potential temperature during the shield building stage of a volcano. For example, fluctuations in the mantle potential temperature and melt flux of the plume would reduce the probability of melt sampling a refractory, anomalous

component. Similarly, variations in the physical distribution, such as absence of a smaller volume of the anomalous component in the melting region, would reduce the probability of the shield stage sampling $\mu^{182}W$ deficits. The volume of the anomalous component in different portions of the plume may in fact be related to the mantle potential temperature and buoyancy flux (e.g., Jackson et al., 2017), which in turn may influence the melt flux (Wessel, 2016).

The Mauna Kea volcano is among the least geochemically enriched (e.g., least radiogenic $^{87}Sr/^{86}Sr$, $^{187}Os/^{188}Os$) and is the most radiogenic endmember of Pb isotopic compositions in Hawaii. It is not clear if the anomalous $\mu^{182}W$ component is always present in the plume and will exhibit similar characteristics (e.g., high Ti/Ti*, Nb/Nb*, and $^{208}Pb/^{206}Pb$) in other volcanic centers. When all Hawaiian volcanic centers are considered, there are statistically significant correlations between $\mu^{182}W$ and $^{208}Pb/^{204}Pb$ ($R^2 = 0.2$, p value = 0.003), Ti/Ti* ($R^2 = 0.2$, p value = 0.02), and Nb/Nb* ($R^2 = 0.3$, p value = 0.0003) (Figure 4.5). There are no correlations between $\mu^{182}W$ and Sr-Nd-Hf-Os isotopic ratios, chemical indicators of melt composition, or melt degree and differentiation, such as Mg#, SiO_2, La/Sm, Sm/Yb, CaO/Al_2O_3, etc. Given that the geochemical variability at the inter-island scale is much greater than within the Mauna Kea volcano, different components are likely present in the mantle sources of volcanic centers throughout Hawaii. These components may influence the expression of $\mu^{182}W$ within and among volcanic centers.

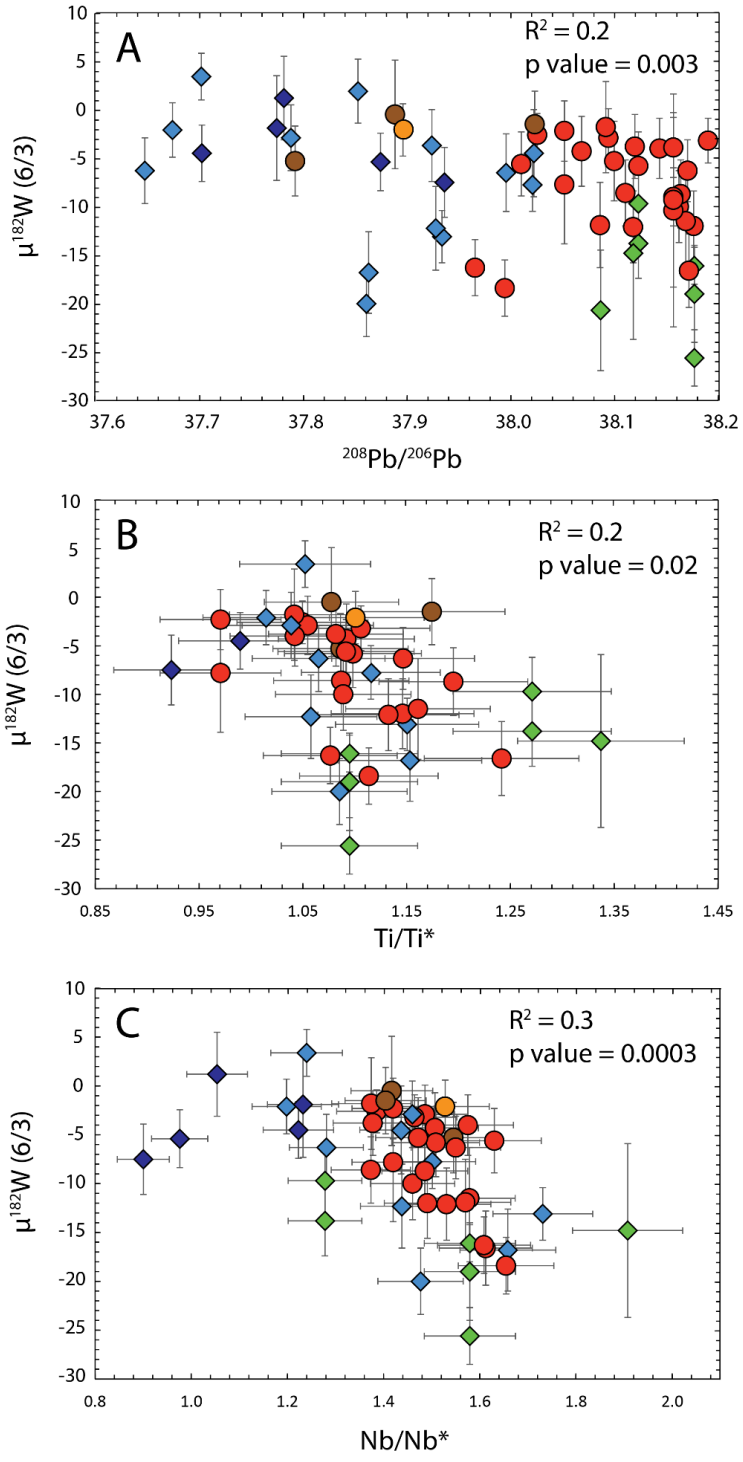

Figure 4.5. (A) $\mu^{182}W$ isotopic compositions versus $^{208}Pb/^{204}Pb$, **(B)** Ti/Ti* ($Ti/Ti^*=Ti_N/(Sm_N*Tb_N)^{0.5}$), and **(C)** Nb/Nb* ($Nb/Nb^*=Nb_N/(La_N*Th_N)^{0.5}$).

Although it is not clear why the anomalous component has negative $\mu^{182}W$ values, radiogenic $^{208}Pb/^{204}Pb$, and elevated Ti and Nb relative to similarly incompatible elements, this relationship could be explained by a process that increased the W/Hf and Th/Pb, with the caveat that it must have occurred while ^{182}Hf was extant (i.e., within the first ~60 Myr of Solar System history). One example of how this could occur is crystal-liquid fractionation in a basal magma ocean. As bridgmanite and Ca-perovskite crystallize, the residual liquid may inherit low Hf/W and high Th/Pb (Corgne et al., 2005; Brown et al., 2014).

Grainy late accretion, or some mechanisms of core-mantle interaction (e.g., Humayun, 2011), would not be expected to produce correlations between $\mu^{182}W$ and high Ti/Ti* and $^{208}Pb/^{206}Pb$. These processes could result in elevated HSE in addition to negative $\mu^{182}W$. A particularly useful HSE to assess their abundances in the mantle source is Pt because it is not substantially fractionated between most solids and melts through either partial melting or crystal-liquid fractionation (Pitcher et al., 2009). In the Mauna Kea volcano, there is no relationship between $\mu^{182}W$ and Pt concentration, leading to the conclusion that the anomalous component was not enriched in HSE relative to the ambient plume mantle (Chapter 2 of this dissertation). In the entire Hawaiian suite, however, there is a modest correlation between $\mu^{182}W$ and Pt, leaving open the possibility that grainy late accretion, or some mechanism of core-mantle interaction, generated $\mu^{182}W$ and HSE signatures in the plume (Figure 4.6). The linear correlation is statistically significant (p value < 0.05), but the correlation coefficient is low ($R^2 = 0.3$), likely as a result of non-linear mixing and the presence of more than two components.

An additional correlation between $\mu^{182}W$ and Cu abundance is apparent in Hawaiian lavas (Figure 4.6). This relationship is unlikely to result from sulfides as a carrier of the anomalous $\mu^{182}W$ signature, because W, unlike Cu, is not strongly chalcophile (Lodders and Palme, 1991;

Mengason et al., 2011) and there are no relationships between $\mu^{182}W$ (or Cu or Pt) and other chalcophile elements such as Mo, Ga, Bi, Pb, in the Hawaiian lavas. Only a portion of Hawaiian lavas have been analyzed for high quality Cu data, however, thus the relationship between $\mu^{182}W$ and Cu is based on a limited subset of samples. Elevated Cu may be a source characteristic of the anomalous component, though additional analyses are warranted.

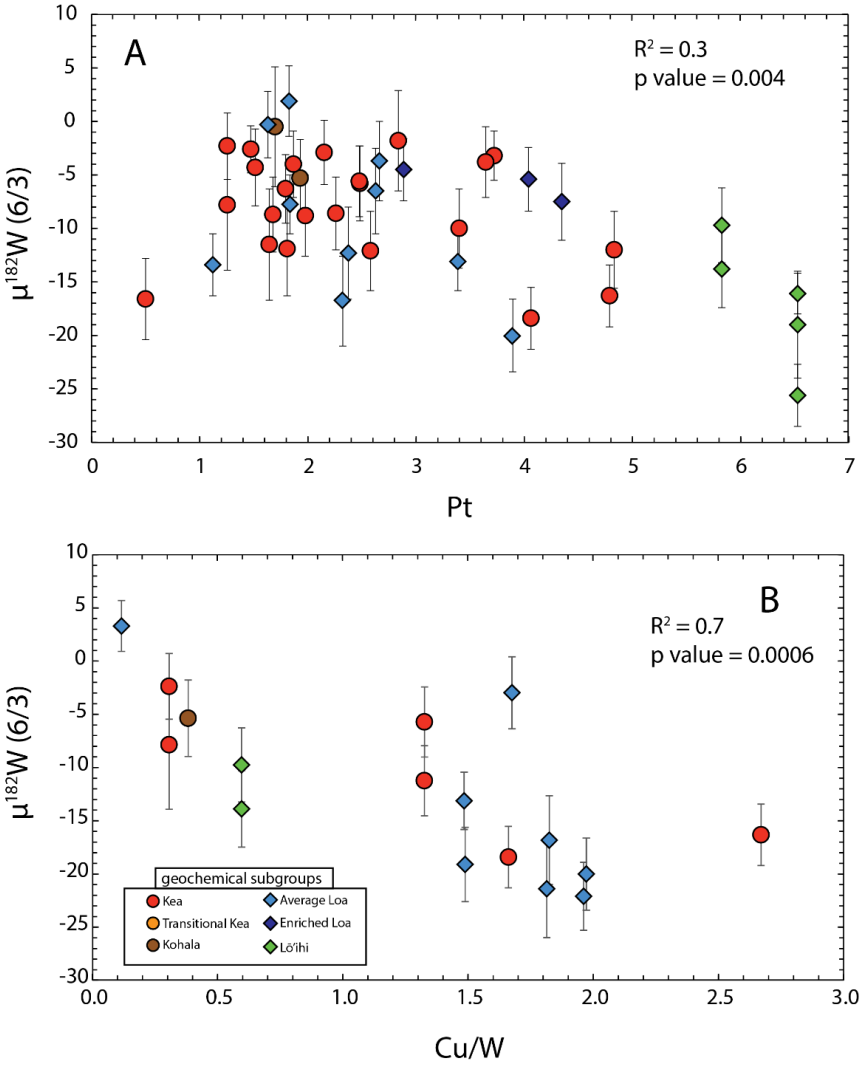

Figure 4.6. $\mu^{182}W$ isotopic compositions versus (**A**) Pt abundances and (**B**) Cu/W of Hawaiian lavas. There are statistically significant linear correlations at the 95% confidence interval (p value < 0.05) between $\mu^{182}W$ and Pt and Cu/W.

In the Hawaiian plume, $\mu^{182}W$ anomalies appear in Kaua‘i in rocks that are ~5 Ma. Then for a ~3.5 Myr period spanning 300 km, there is only one observed $\mu^{182}W$ anomaly, at Ko’olau (-7.5 ± 3.6). Anomalous $\mu^{182}W$ reappears at <1 Ma to present in volcanoes spanning ~100 km (Hualālai, Mauna Loa, Mauna Kea, Kīlauea, and Kama‘ehuakanaloa). One interpretation of the current dataset is that the anomalous material is irregularly distributed in the rising plume. Alternatively, anomalous material may be uniformly present in the plume, but is either not sampled by partial melting or is diluted by W with normal $\mu^{182}W$ in other plume components.

The two geochemically distinct volcanic chains, the Loa and Kea trends, have distinct geographic distributions and isotopic compositions over the ~500 km spatial scale of the Hawaiian archipelago. Loa trend compositions include relatively radiogenic $^{87}Sr/^{86}Sr$, and unradiogenic $^{143}Nd/^{144}Nd$, $^{176}Hf/^{177}Hf$, and $^{206,207,208}Pb/^{204}Pb$, relative to Kea trend volcanoes (e.g., Figure 4.7). Loa characteristics also include radiogenic $^{187}Os/^{188}Os$, as well as higher $^{208}Pb/^{204}Pb$ at a given $^{206}Pb/^{204}Pb$ (i.e., a high time-integrated Th/U), compared to the Kea trend. The characteristics of the Loa trend can be explained by the incorporation of geochemically enriched, recycled materials that experienced U loss either prior to, or as a result of subduction and recycling (e.g., pelagic or terrigenous sediment and basalt, Lassiter and Hauri, 1998). Kea trend compositions are typically less geochemically enriched than Loa trend, but do not overlap with the compositions of spatially associated MORB, and have been interpreted to reflect the signature of the deep mantle possibly containing recycled ultramafic material (Lassiter and Hauri, 1998; Weis et al., 2020). The two trends have also been interpreted to reflect physically distinct deep mantle sources (Weis et al., 2011, 2020; Harrison et al., 2017). If the Loa and Kea trends are produced by physically (and

compositionally) distinct mantle domains, then $\mu^{182}W$ systematics of Loa and Kea trends would likely be distinct.

Along the archipelago, the Loa and Kea trends host both normal $\mu^{182}W$ and anomalous $\mu^{182}W$ (Figure 4.2). The greatest magnitude $\mu^{182}W$ deficits in the Loa and Kea trends, -25.6 ± 2.9 and -19.1 ± 3.5, respectively, and are within uncertainty of each other. Furthermore, volcanic centers from both the Loa and Kea trends exhibit $\mu^{182}W$ deficits at the same time intervals along the ~5 Myr record of the archipelago. Thus, it does not appear the anomalous component is unique to either trend, but instead varies spatially and temporally along the archipelago in both trends. If these trends are sampling physically and chemically distinct deep mantle reservoirs, then both deep reservoirs contain $\mu^{182}W$ anomalies. This would diverge from current models, in which anomalous $\mu^{182}W$ is "contained" in a physically distinct mantle region (e.g., Weis et al., 2020). It is unlikely that $\mu^{182}W$ anomalies are redistributed during entrainment and ascent of the plume material, as heterogeneities at the thermal boundary layer where the plume originates have been interpreted to be elongated and stretched, but not mixed or sheared laterally (Farnetani et al., 2002).

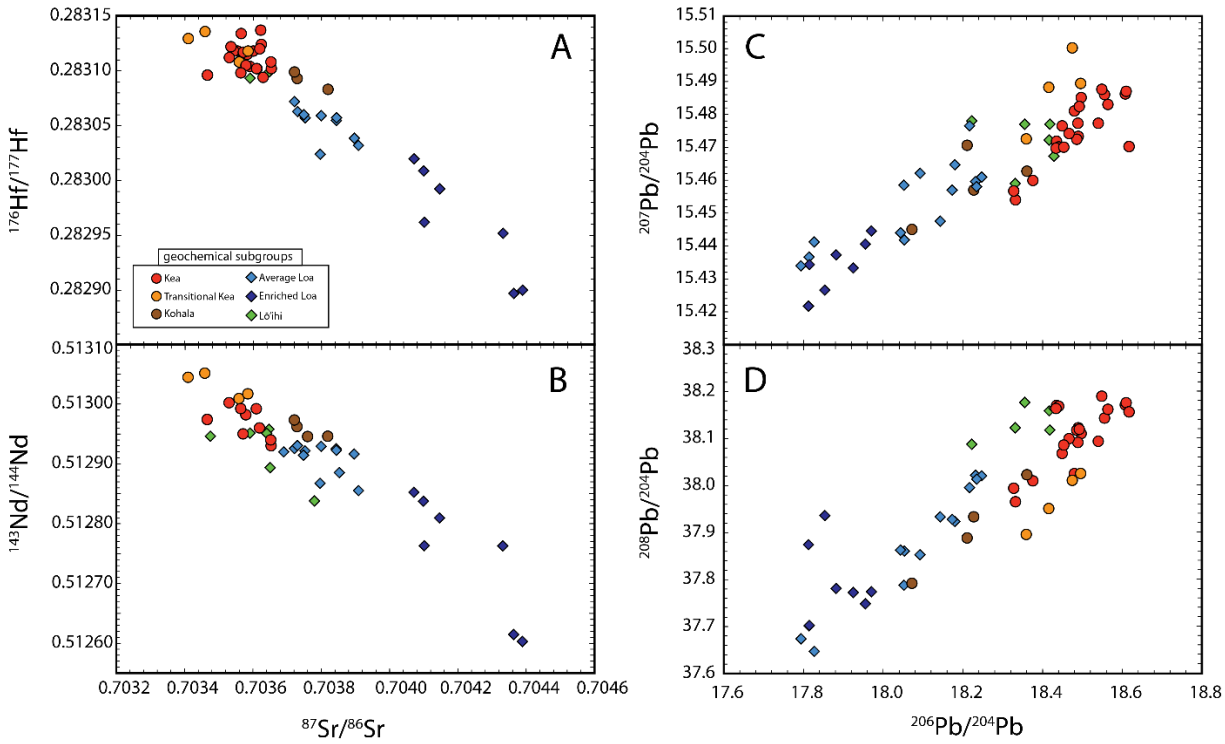

Figure 4.7. Sr, Nd, Hf, and Pb isotopic compositions of Hawaiian lavas examined here. Loa trend subgroups are represented by diamonds and Kea trend subgroups are represented by circles.

There is a ~3.5 Myr period, between Kaua‘i and Hawai‘i, during which only one resolved $\mu^{182}W$ anomaly was present in either the Loa or Kea trend (Figure 4.2). We consider three hypotheses for the absence of $\mu^{182}W$ variability in this time interval. The first is that anomalous $\mu^{182}W$ has been attenuated by the contribution of recycled W with normal $\mu^{182}W$. A second hypothesis is that the anomalous component is present but is not sampled by partial melting, perhaps because it is more refractory. Finally, it is possible that the anomalous component is not present in the portion of the plume that is contributing melt during the time interval where no resolved $\mu^{182}W$ anomalies are observed. These processes are not mutually exclusive, and all three

may have occurred at different time intervals in the Hawaiian plume. To investigate the processes and materials that control $\mu^{182}W$ in Hawaiian volcanoes, the Loa and Kea trends are separately examined first, as well as the geochemically defined subgroups of each trend.

The isotopic and chemical differences among these subgroups likely arise from the incorporation of heterogenous primitive, depleted, and recycled materials, including those with a crustal and/or metasomatized history. For example, the extreme isotopic signatures of the Enriched Loa subgroup (e.g., radiogenic $^{87}Sr/^{86}Sr$ ~0.7040-0.7045, and $^{187}Os/^{188}Os$ ~0.1415) can be explained by the addition of recycled, continental-derived materials, such as terrigenous sediments, into the Hawaiian mantle plume (e.g., Lassiter and Hauri, 1998). The Lō‘ihi subgroup has radiogenic Pb isotopic compositions compared to Average and Enriched Loa. The Lō‘ihi subgroup is also characterized by high $^{3}He/^{4}He$ and negative $\mu^{182}W$ anomalies that are among the greatest magnitude observed in global OIB (Kurz et al., 1983; Mundl-Petermeier et al., 2020). These characteristics may relate to a higher proportion of the component bearing the anomalous $\mu^{182}W$ in the mantle source. Despite a larger signal from the anomalous component in the Lō‘ihi subgroup, there is also an enriched recycled component(s) present in the Lō‘ihi mantle source that is unrelated to anomalous W and He. This is evident from the moderately radiogenic $^{187}Os/^{188}Os$ (0.1337-0.1352), $^{87}Sr/^{86}Sr$ (0.7035-0.7038), and unradiogenic $^{143}Nd/^{144}Nd$ (0.5128-0.5129) compared to Kea trend subgroups. Submarine West Ka‘ena Ridge lavas, which are part of the Average Loa subgroup, erupted during a duration of relatively low magma production along the Hawaiian archipelago (Greene et al., 2010; Wessel, 2016). West Ka‘ena lavas have moderate $^{87}Sr/^{86}Sr$ (~0.7038-0.7039) for Hawaiian tholeiites and have extremely unradiogenic $^{208}Pb/^{204}Pb$ (~37.65) and $^{206}Pb/^{204}Pb$ (17.8) compared to most Hawaiian tholeiites, except for overlapping Ko’olau (Makapu’u) lavas.

The Kea trend has less overall variance in Sr-Nd-Hf-Pb isotopic ratios—both within and among volcanic centers. The isotopic characteristics of $^{87}Sr/^{86}Sr$ (~0.7034-0.7038) and $^{143}Nd/^{144}Nd$ (~0.5129-0.5131) indicate a slightly depleted to relatively less enriched mantle source, compared to Loa. Lead isotopic compositions of Kea trend volcanoes are consistently radiogenic compared to the Loa trend, but generally have a lower $^{208}Pb^*/^{206}Pb^*$ (~0.939) compared to Loa (~0.960), indicating a lower time-integrated Th/U. The isotopic compositions of Kea trend volcanoes do not overlap Pacific MORB, and have been interpreted to result from a deeper mantle source. There is a spatially coherent trend from lower $^{208}Pb^*/^{206}Pb^*$ West Maui to higher $^{208}Pb^*/^{206}Pb^*$ from Haleakalā to Kohala and to Mauna Kea and Kīlauea. The gradation in isotopic composition may reflect either a variable proportion of one endmember or a change in the Th/U of the source over time.

4.5.2 Tungsten isotope systematics of the Kea trend: Kea, Kohala, and Transitional Kea

The Kea subgroup of the larger scale Kea trend includes West Nāpali (~5 Ma), Mauna Kea, and Kīlauea (both <1 Ma) volcanic centers. All three are characterized by a range of $\mu^{182}W$ values from BSE-like to negative values. The $^{87}Sr/^{88}Sr$, $^{143}Nd/^{144}Nd$, and $^{176}Hf/^{177}Hf$ values of West Nāpali overlap Kea subgroup volcanoes, Mauna Kea and Kīlauea, but are distinctly less radiogenic in $^{208}Pb/^{204}Pb$, $^{207}Pb/^{204}Pb$, and $^{206}Pb/^{204}Pb$. The two additional Kea subgroups include Transitional Kea and Kohala. The volcanic centers that comprise Transitional Kea and Kohala subgroups do not exhibit any $\mu^{182}W$ deficits. Additionally, these volcanic centers have less radiogenic Pb than Mauna Kea and Kīlauea, and therefore $\mu^{182}W$ deficits may be attenuated by recycling of a component with unradiogenic Pb and normal $\mu^{182}W$ (e.g., altered terrigenous or pelagic

sediments). Alternatively, $\mu^{182}W$ anomalies may be absent in the mantle sources of these volcanoes or are not sampled by partial melting of the plume source.

Unlike the individual Mauna Kea volcano, there is no statistically significant correlation between $\mu^{182}W$ and $^{208}Pb/^{204}Pb$ within the larger Kea trend. A two-component mixing line cannot account for the W-Pb, W-Os, or W-Sr relationships in the Kea trend. There is, however, a modest correlation between estimated magmatic flux and $^{208}Pb/^{204}Pb$ along the Hawaiian archipelago, indicating a relationship between plume dynamics and mantle source (Harrison et al., 2017). Local maxima in magmatic flux (Wessel, 2016) also correspond to periods of $\mu^{182}W$ anomalies in the archipelago (Figure 4.8). An increase in the magnitude of $\mu^{182}W$ anomalies in the volcanic centers on the big island of Hawai‘i into the Kama‘ehuakanaloa seamount parallels the increasing magmatic flux to an absolute maximum for the Hawai‘i-Emperor chain (Wessel, 2016).

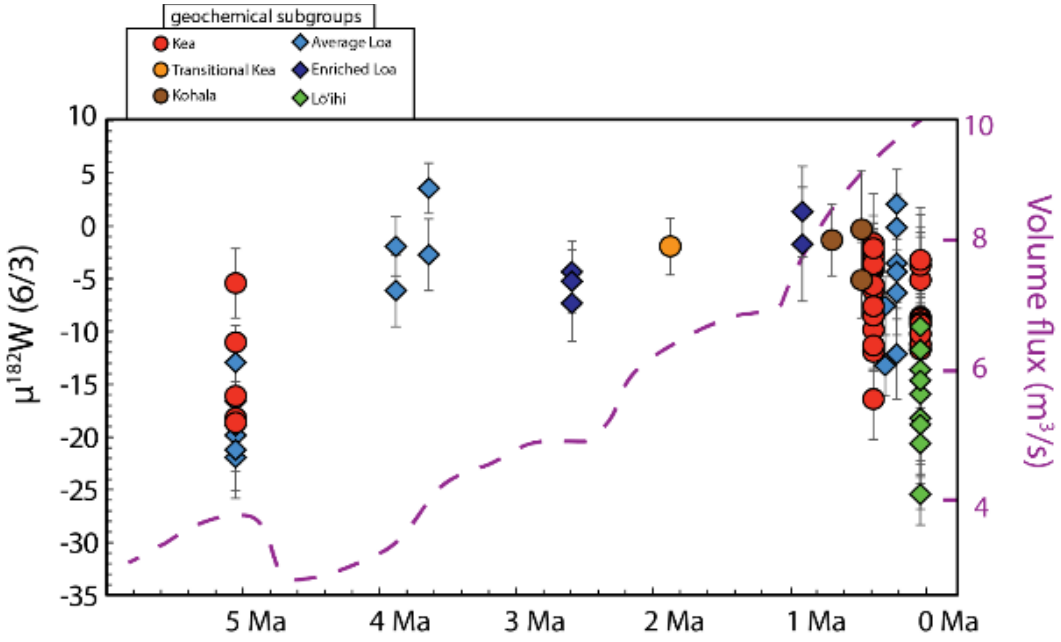

Figure 4.8. $\mu^{182}W$ plotted as a function of age of the shield stage of each respective volcano. Measured ages are not available for every sample, so each volcano is plotted at an approximate age during the shield stage. The right, purple axis corresponds to the purple dashed line, which is the estimated volume flux over the ~5 Myr interval sampled for $\mu^{182}W$ (Wessel, 2016).

A relationship between magmatic flux and $\mu^{182}W$ provides corroborative evidence for a "pulsing" of anomalous material in the plume. During periods of higher mantle potential temperature and magma flux, the probability of the plume containing and melting the anomalous component increases, especially if the component is refractory relative to the ambient plume material. A subset of Kea trend lavas (from West Maui, Haleakalā, and Kohala) do not contain any of the anomalous $\mu^{182}W$ component, and thus, do not fall on the possible mixing line, which may explain the W-Sr-Os-Pb compositions. It is difficult to discern whether the anomalous $\mu^{182}W$

component is not absent in the portion of the plume that is contributing melt during this time interval, or if it is present but is not melted. Using the Mauna Kea shield stage model, there is a 47 to 62% (using $^{3}He/^{4}He$ or $\mu^{182}W$ as a model, respectively) chance of sampling the anomalous component in the shield stage of a Hawaiian volcano if the thermal and compositional structure of the plume remains constant over time and space. Therefore, there is only a 2 to 8% chance of the four random shield stage lavas across West Maui, Haleakalā, and Kohala to be characterized by normal $\mu^{182}W$ if the anomalous component is present in a similar proportion as the Mauna Kea mantle source. The probability may be lower due to the decrease in local magmatic flux, and therefore, lesser proportion of the anomalous component in the melting region, when West Maui, Haleakalā, and Kohala were in their shield stage. Regardless of the cause of normal $\mu^{182}W$ in these volcanoes, the expression of $\mu^{182}W$ in erupted products appears to be related to plume dynamics: lower magmatic flux decreases the probability of negative $\mu^{182}W$.

An alternative to plume structure variation, three (or more) component mixing can capture the Kea trend, but requires that the anomalous $\mu^{182}W$ component has the same Sr-Os-Pb isotopic composition as one of the "normal" $\mu^{182}W$ endmembers. This is possible if negative $\mu^{182}W$ material is introduced to the mantle via isotopic equilibration with Earth's core. The same mantle composition (Sr-Os-Pb) would experience different degrees of isotopic equilibration with distance from the core-mantle boundary (Ferrick and Korenaga, 2023). The core is not a significant reservoir of Sr, though may house 55-60% of Earth's Pb inventory and >98% of Earth's Os (McDonough, 2003). The mechanism through which proposed isotopic equilibration occurs at the core-mantle boundary is unknown, but it would be unlikely to affect the Sr isotopic composition of the BSE. It is not clear if additional elements, like Pb and Os, experience isotopic equilibration between the core and mantle. Further, the core would likely introduce very unradiogenic Pb

isotopic compositions, based on best estimates of the Pb isotopic composition of the early Solar System (Blichert-Toft et al., 2010). The anomalous $\mu^{182}W$ is associated with relatively radiogenic Pb across Hawaii, which is the opposite relationship anticipated from isotopic exchange of both elements between core and mantle. The $^{187}Os/^{188}Os$ of the core is likely to be similar to the mantle, as early (>3.5 Ga) inner core crystallization is required to fractionate Re/Os and allow sufficient time for radiogenic ingrowth of ^{187}Os in the outer core (e.g., Brandon and Walker, 2005). The inner core is likely only 1 to 2.5 Ga, which is not sufficiently old to produce the required Re/Os fractionation to generate distinct $^{187}Os/^{188}Os$ between the core and mantle (Labrosse et al., 2001; Lassiter, 2006). Therefore, $^{187}Os/^{188}Os$ is not likely an effective tracer of core-mantle interactions.

4.5.3 Tungsten isotope systematics of the Loa trend: Average Loa, Enriched Loa, and Lō‘ihi

The Loa trend comprises three subgroups: Average Loa, Enriched Loa, and Lō‘ihi. Average Loa subgroup is present at 5 Ma in the East Nāpali formation of Kaua‘i . At ~5 Ma, $\mu^{182}W$ deficits are present in the Average Loa, and extend to approximately -25, which is comparable to the largest $\mu^{182}W$ deficits observed in global OIB (Mundl-Petermeier et al., 2020). Average Loa continues into the submarine volcanoes of West Ka‘ena Ridge and the western volcano of O‘ahu, Wai‘anae. There are no resolvable $\mu^{182}W$ deficits in West Ka‘ena or Wai‘anae. East Nāpali has distinct $\mu^{182}W$ from West Ka‘ena and Wai‘anae, despite composing the same subgroup with indistinguishable $^{87}Sr/^{88}Sr$, $^{143}Nd/^{144}Nd$, and $^{176}Hf/^{177}Hf$. This demonstrates that a geochemical subgroup can have variable $\mu^{182}W$ over time both within and among volcanic centers, and that $\mu^{182}W$ does not change with Sr-Nd-Hf isotopic compositions. As with the Kea trend, this may reflect a change in plume structure and dynamics: the anomalous component is present in East Nāpali’s mantle source where there is a local maxima in magmatic flux (Figure 4.8), but is not present in West Ka‘ena (where

magmatic flux is so low that there are no subaerial volcanoes) or Wai‘anae. Average Loa is also present at <1 Ma in Hualālai and Mauna Loa, where $\mu^{182}W$ anomalies return and magmatic flux is at its absolute maximum within the Hawaiian-Emperor chain (Wessel, 2016).

Within the Loa trend, extreme geochemical enrichment appears in the Makapu’u section of Ko’olau and in Lāna‘i. These volcanic centers make up the Enriched Loa subgroup. Surface-derived materials, such as terrigenous or pelagic sediments, can explain the radiogenic $^{87}Sr/^{86}Sr$ and unradiogenic $^{143}Nd/^{144}Nd$ and $^{176}Hf/^{177}Hf$ in Ko’olau – Makapu’u and Lāna‘i. The Enriched Loa lavas generally lack resolved $\mu^{182}W$ anomalies, though one sample from Ko’olau – Makapu’u has a small $\mu^{182}W$ deficit (-7.5 ± 3.6). Recycling of W-rich materials could lead to attenuation of $\mu^{182}W$ anomalies, as has been hypothesized to explain $\mu^{182}W$ variability in global OIB (e.g., Jackson et al., 2020). In this case, recycling of a small fraction of continentally-derived sediment characterized by high W concentration could introduce material with normal $\mu^{182}W$ into the Hawaiian plume, along with radiogenic $^{87}Sr/^{86}Sr$ and unradiogenic $^{143}Nd/^{144}Nd$ and $^{176}Hf/^{177}Hf$. For example, upper continental crust is estimated to have a W concentration of 1.9 ppm (Rudnick and Gao, 2003), whereas the upper mantle (DMM) and BSE are estimated to have only ~0.003 and 0.013 ppm W, respectively (Arevalo and McDonough, 2008). Using the concentration of W in upper continental crust (Rudnick and Gao, 2003), as well the Sr concentration and isotopic composition of globally subducted sediment (GLOSS; Plank and Langmuir, 1998), a 0.6% addition of subducted, continentally-derived sediment could explain some, but not all, of the Ko’olau – Makapu’u and Lāna‘i lavas (Figure 4.9). In this mixing scenario, the anomalous component is defined as $\mu^{182}W$ of -53 (the greatest observed $\mu^{182}W$ anomaly in plume-derived material; Walker et al., 2023) and a W concentration similar to the depleted mantle, 3 ppb (Arevalo and McDonough, 2008). To define the Sr composition of the anomalous component, the Sr

concentration is based on primitive mantle (20 ppm; McDonough and Sun, 1995) and the $^{87}Sr/^{86}Sr$ is based on the unradiogenic endmember observed in Hawai‘i (~0.7035).

This mixing scenario does not work for Pb isotopes, as GLOSS is expected to have radiogenic Pb (e.g., $^{208}Pb/^{204}Pb$ ~38.9; Plank and Langmuir, 1998) compared to Hawaiian lavas that would result in a positive correlation between $\mu^{182}W$ and Pb isotopic compositions that does not overlap the Hawaiian field in W-Pb isotopic space. Instead, there is a statistically significant *negative* correlation between $\mu^{182}W$ and Pb in the Loa trend. The recycled material in Enriched Loa must have lost a significant portion of U and Th prior to or during subduction (McCulloch and Gamble, 1991) in order to explain the unradiogenic Pb compositions in Ko’olau – Makapu’u and Lāna‘i. A mixing model could plausibly capture the Ko’olau – Makapu’u and Lāna‘i data, however, the Pb concentration and isotopic composition are unconstrained at this point. It is not clear whether W, which can also exhibit fluid-mobility in subduction zones (e.g., König et al., 2008), would likely be similarly affected. If W is removed from the slab prior to or during subduction, then it is unlikely that recycled material would strongly attenuate $\mu^{182}W$ anomalies in the Hawaiian plume. If normal $\mu^{182}W$ is retained in the slab during subduction, then mixing between a low Th/Pb, W-rich sediment component and the anomalous component may explain W-Sr-Pb. Lavas with high W/Th and W/U have high W concentrations but not lower U and Th relative to the entire Hawaiian suite.

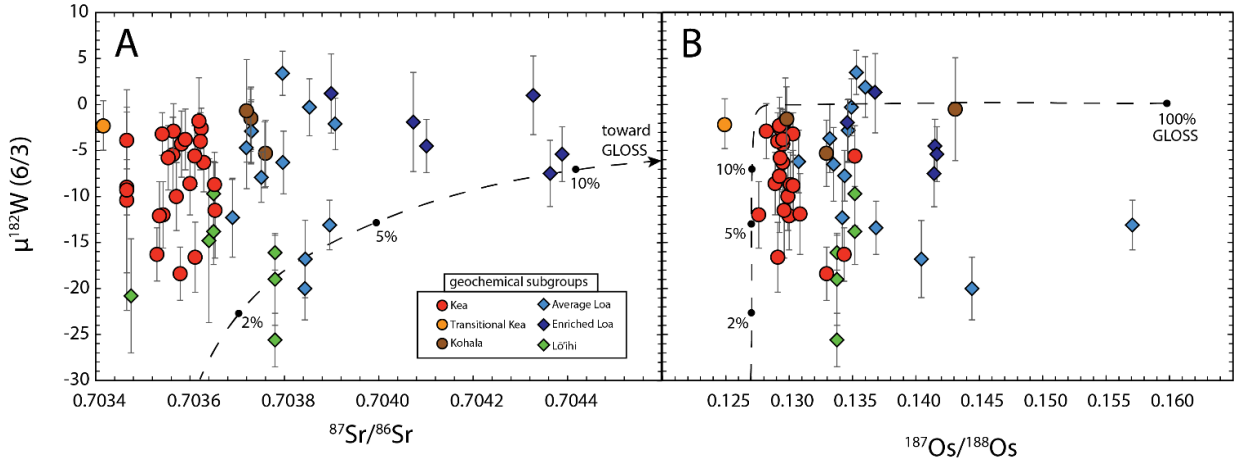

Figure 4.9. Mixing model between globally subducted sediment (GLOSS) and an anomalous $\mu^{182}W$ component in the Hawaiian mantle plume. The model fails to explain the W-Sr-Os compositions of the Enriched Loa subgroup (Ko'olau – Makapu'u and Lāna'i).

Mixing between an anomalous component and surface-derived sediment also does not fit Os isotopic data in the Loa trend. Though the $^{187}Os/^{188}Os$ and Os concentration of GLOSS is poorly constrained, based on low Os concentrations in upper continental crust (~0.03 ppb; Rudnick and Gao, 2003) and the most extreme $^{187}Os/^{188}Os$ observed in Hawai'i (~0.16), a strongly hyperbolic mixing curve would result when mixing continentally-derived sediments with the unradiogenic $^{187}Os/^{188}Os$ endmember in Hawai'i (~0.127), using the average Os concentration observed in Hawai'i (Figure 4.9). Recycled sediment may be present in Enriched Loa mantle sources, but it cannot account for the observed $^{187}Os/^{188}Os$ and $\mu^{182}W$ values, requiring at least one additional component. Furthermore, Hawaiian lavas with the greatest magnitude $\mu^{182}W$ anomalies have a wide range of $^{187}Os/^{188}Os$ that extends from BSE-like values, ~0.1291, to radiogenic values of

>0.14 (Figure 4.9). Radiogenic Os of >0.14, as observed at East Nāpali, likely indicates that recycled materials are present in the mantle source, and yet $\mu^{182}W$ deficits are also present. Therefore, the rare $\mu^{182}W$ anomalies observed in Enriched Loa may result from dilution of $\mu^{182}W$ anomalies by recycled material only if: (a) the recycled material has very low U and Th abundances, generating low time-integrated U/Pb and Th/Pb, or (B) a different recycled material dominates the Os isotopic composition of Average Loa, despite overlapping $^{187}Os/^{188}Os$ Enriched Loa. Alternatively, the Enriched Loa subgroup may not sample the anomalous $\mu^{182}W$ component as effectively due to lower degrees of partial melting, and/or the absence of the anomalous component due to plume structure and dynamics. Lower degree partial melting would decrease the probability of sampling the anomalous component, especially one that is relatively refractory. Lavas produced by lower degree partial melting would also preferentially sample a more fusible, incompatible element enriched component, like recycled sediments, explaining the extreme isotopic signatures in Enriched Loa. However, there is no relationship between lesser degrees of partial melt (e.g., higher La/Sm) and $\mu^{182}W$ apparent across the Loa subgroup or the Hawaiian suite as a whole.

The Lō‘ihi subgroup includes only one volcanic center, the Kama‘ehuakanaloa seamount, which is the youngest among all Hawaiian volcanoes, and typifies the pre-shield stage (e.g., Garcia et al., 1995). Lavas from the seamount have negative $\mu^{182}W$ as low as -25, a return to, and possible extension of, the largest $\mu^{182}W$ deficit along the archipelago since ~5 Ma. Although the $\mu^{182}W$ values of the Kama‘ehuakanaloa seamount overlap with values from East Nāpali (~5 Ma), the two volcanic centers are otherwise geochemically distinct. Compared to East Nāpali, the Kama‘ehuakanaloa seamount has less radiogenic $^{87}Sr/^{86}Sr$ and $^{187}Os/^{188}Os$, but significantly more radiogenic $^{208}Pb/^{204}Pb$, $^{207}Pb/^{204}Pb$, and $^{206}Pb/^{204}Pb$ (e.g., Figures 4.5 and 4.7). In the Lō‘ihi

subgroup, the $^{87}Sr/^{86}Sr$ of 0.7035 to 0.7038, $^{143}Nd/^{144}Nd$ of 0.5128 to 0.5130, and $^{187}Os/^{188}Os$ of 0.1338 to 0.1352 indicate moderate geochemical enrichment compared to all other Hawaiian volcanic centers. The Rb/Sr, Sm/Nd, and Re/Os of the mantle source are apparently separate from the Th/Pb history of the mantle source. The Sr, Nd, and Os isotopic compositions are intermediate to the entire range for the Hawaii suite, yet the Kama‘ehuakanaloa seamount is on the extreme end of radiogenic $^{208}Pb/^{204}Pb$, overlapping with Mauna Kea.

Unlike the Kea trend, the Loa trend exhibits a statistically significant correlation between $^{208}Pb/^{204}Pb$ and $\mu^{182}W$ ($R^2 = 0.5$, p value = 0.0002). The relationship between Pb and W may result from mixing between the anomalous component and a recycled component with unradiogenic Pb and normal $\mu^{182}W$. In this case, some of the $\mu^{182}W$ variability may have been attenuated by recycling of W-rich sediments with normal $\mu^{182}W$. Given that the Kea trend does not exhibit the same relationship between $^{208}Pb/^{204}Pb$ and $\mu^{182}W$, one or more components in Loa is likely not present in Kea. This is most likely the recycled sediment component with radiogenic Sr-Os and unradiogenic Pb (e.g., Lassiter and Hauri, 1998). Recycling does not always attenuate $\mu^{182}W$ anomalies, as there are geochemical signatures of recycled material in both East Nāpali and Kama‘ehuakanaloa, both of which have larger magnitude $\mu^{182}W$ deficits than most other volcanic centers. This indicates that the anomalous component can coexist with and be melted in the presence of recycled materials. The absence of $\mu^{182}W$ deficits indicates that some volcanic shields do not sample the anomalous $\mu^{182}W$ component due to vertical or lateral heterogeneity in the plume (plume structure) or smaller degree partial melting of the mantle source such that a refractory component is not melted.

4.6 Conclusions

The presence of $\mu^{182}W$ anomalies in the Hawaiian mantle is most likely related to an anomalous component entrained in the deep mantle that experienced core-mantle isotopic equilibration, early silicate differentiation, or grainy late accretion. The Hawaiian archipelago samples this anomalous component in similar proportions at ~5 Ma in Kauaʻi (Nāpali) and <1 Ma at Kamaʻehuakanaloa, but contributes little to volcanic centers in between Kauaʻi and Hawaii. Variability in $\mu^{182}W$ is correlated with $^{208}Pb/^{204}Pb$, Ti/Ti*, and Nb/Nb*, indicating that the anomalous component is likely enriched in high field strength elements, like W, Th, Ti, and Nb. The anomalous component may also be enriched in Pt, and other HSE, and possibly Cu, though additional analyses are warranted. The anomalous component is likely relatively less fusible than ambient mantle and recycled materials, as $\mu^{182}W$ deficits appear when there are local and absolute maxima in the magmatic flux of the Hawaiian plume. This may indicate that the anomalous component is only entrained, and/or partially melted, when the plume experiences pulses of larger buoyancy flux and higher mantle potential temperatures. The thermal structure of the plume, therefore, affects the expression of $\mu^{182}W$ both within and among Hawaiian volcanoes.

4.7 Acknowledgements

This work was supported by NSF-EAR #2121979 to R. J. W. and V. A. F. Samples were prepared for Sr-Nd-Hf-Pb isotopic analyses by D. Daquioag BSc. and analysed by K. Gordon MSc. by MC-ICP-MS at the PCIGR labs at UBC.

4.8 Author credit statement

Lori Willhite: Conceptualization, Methodology, Investigation, Formal analysis, Data curation, Visualization, Writing – original draft, Writing – review & editing. **Nicole Williamson:** Investigation, Data curation, Resources. **Valerie A Finlayson:** Conceptualization, Methodology, Investigation, Resources, Funding acquisition. **Dominique Weis:** Conceptualization, Investigation, Resources, Supervision. **Richard J Walker:** Conceptualization, Supervision, Investigation, Resources, Writing – review & editing, Funding acquisition.

4.9 Appendix

4.9.1 Supplementary Table A.4.1 Tungsten isotope data for Alfa Aesar W standard

Standard	Alfa Aesar W	Alfa Aesar W	Alfa Aesar W	Alfa Aesar W	Alfa Aesar W	Alfa Aesar W	Alfa Aesar W	Alfa Aesar W	Alfa Aesar W	Alfa Aesar W	Alfa Aesar W	Alfa Aesar W	Alfa Aesar W	Alfa Aesar W	Alfa Aesar W	Alfa Aesar W	Alfa Aesar W	Alfa Aesar W
$^{182}W/^{184}W$ (6/3)	0.864861	0.864864	0.864860	0.864862	0.864859	0.864863	0.864862	0.864863	0.864861	0.864860	0.864861	0.864862	0.864861	0.864861	0.864860	0.864861	0.864862	0.864860
2StdDev (%)	0.006	0.007	0.007	0.008	0.007	0.008	0.007	0.007	0.007	0.007	0.006	0.007	0.009	0.008	0.009	0.016	0.008	0.006
2StdDev (abs)	0.00006	0.00006	0.00006	0.00007	0.00006	0.00007	0.00006	0.00006	0.00006	0.00006	0.00006	0.00006	0.00007	0.00007	0.00008	0.00013	0.00007	0.00005
2SE (ppm)	2.8	3.2	2.9	3.3	2.9	3.8	3.2	3.0	3.2	3.1	2.8	3.2	3.7	3.4	4.1	6.7	3.4	2.6
2SE (abs)	0.000002	0.000003	0.000002	0.000003	0.000003	0.000003	0.000003	0.000003	0.000003	0.000003	0.000002	0.000003	0.000003	0.000003	0.000004	0.000006	0.000003	0.000002
N of ratios	540	505	537	530	535	481	524	530	477	535	535	535	538	536	530	531	535	541
$\mu^{182}W$ (6/3)	-0.9	3.1	-1.9	0.4	-2.7	1.6	1.2	2.2	-0.1	-1.2	-0.8	1.2	-0.4	-0.2	-1.5	-0.5	0.5	-1.6
$^{182}W/^{184}W$ (6/4)	0.864888	0.864891	0.864888	0.864889	0.864888	0.864892	0.864892	0.864891	0.864889	0.864891	0.864889	0.864892	0.864891	0.864888	0.864887	0.864893	0.864888	0.864890
2StdDev (%)	0.009	0.009	0.009	0.010	0.009	0.011	0.010	0.009	0.009	0.010	0.009	0.010	0.011	0.010	0.012	0.019	0.010	0.008
2StdDev (abs)	0.00008	0.00008	0.00008	0.00009	0.00008	0.00010	0.00008	0.00008	0.00008	0.00008	0.00008	0.00008	0.00010	0.00008	0.00010	0.00017	0.00009	0.00007
2SE (ppm)	3.7	4.2	3.9	4.3	3.9	5.1	4.2	4.0	4.3	4.1	3.8	4.3	4.9	4.2	5.0	8.4	4.5	3.3
2SE (abs)	0.000003	0.000004	0.000003	0.000004	0.000003	0.000004	0.000004	0.000003	0.000004	0.000004	0.000003	0.000004	0.000004	0.000004	0.000004	0.000007	0.000004	0.000003
N of ratios	540	508	538	533	535	480	526	531	475	541	541	529	537	536	526	529	533	536
$\mu^{182}W$ (6/4)	-2.8	0.1	-2.8	-1.9	-3.2	2.0	1.0	0.6	-2.3	1.0	-2.3	1.6	0.3	-3.5	-4.0	2.2	-3.4	-1.2
$^{183}W/^{184}W$ (6/4)	0.467151	0.467150	0.467151	0.467150	0.467150	0.467150	0.467152	0.467152	0.467152	0.467152	0.467151	0.467151	0.467151	0.467150	0.467152	0.467155	0.467150	0.467153
2StdDev (%)	0.008	0.008	0.008	0.009	0.008	0.009	0.008	0.008	0.008	0.008	0.008	0.009	0.010	0.009	0.011	0.018	0.010	0.007
2StdDev (abs)	0.00004	0.00004	0.00004	0.00004	0.00004	0.00004	0.00004	0.00004	0.00004	0.00004	0.00004	0.00004	0.00005	0.00004	0.00005	0.00008	0.00005	0.00003
2SE (ppm)	3.4	3.6	3.4	3.8	3.3	4.1	3.7	3.5	3.8	3.6	3.6	3.7	4.4	3.9	4.6	7.8	4.4	3.0
2SE (abs)	0.000002	0.000002	0.000002	0.000002	0.000002	0.000002	0.000002	0.000002	0.000002	0.000002	0.000002	0.000002	0.000002	0.000002	0.000002	0.000004	0.000002	0.000001
N of ratios	537	506	539	536	531	475	532	534	476	531	541	536	530	539	533	529	527	538
$\mu^{183}W$	-2.4	-4.1	-2.0	-4.2	-3.3	-3.3	0.0	-0.8	-0.6	0.0	-2.5	-2.3	-2.5	-3.4	0.1	7.1	-4.6	1.4

4.9.1 Supplementary Table A.4.1 continued

Alfa Aesar W	Alfa Aesar W	Alfa Aesar W	Alfa Aesar W	Alfa Aesar W	Alfa Aesar W	Alfa Aesar W	Alfa Aesar W	Alfa Aesar W	Alfa Aesar W	Alfa Aesar W	Alfa Aesar W	Alfa Aesar W	Alfa Aesar W	Alfa Aesar W	Alfa Aesar W	Alfa Aesar W	Alfa Aesar W	Alfa Aesar W	Alfa Aesar W
0.864862	0.864861	0.864860	0.864864	0.864862	0.864863	0.864860	0.864861	0.864861	0.864863	0.864860	0.864862	0.864862	0.864857	0.864862	0.864866	0.864862	0.864862	0.864859	0.864860
0.008	0.007	0.018	0.008	0.007	0.007	0.007	0.009	0.008	0.011	0.007	0.008	0.008	0.006	0.008	0.008	0.006	0.008	0.008	0.008
0.00007	0.00006	0.00015	0.00007	0.00006	0.00006	0.00006	0.00008	0.00007	0.00009	0.00006	0.00007	0.00007	0.00005	0.00007	0.00007	0.00005	0.00007	0.00007	0.00007
3.5	2.9	7.7	3.4	2.9	3.0	3.1	3.8	3.5	4.6	3.0	3.3	3.5	2.7	3.3	3.5	2.5	3.5	3.4	3.7
0.000003	0.000003	0.000007	0.000003	0.000002	0.000003	0.000003	0.000003	0.000003	0.000004	0.000003	0.000003	0.000003	0.000002	0.000003	0.000003	0.000002	0.000003	0.000003	0.000003
532	538	524	535	532	544	535	537	532	533	535	534	534	533	536	534	535	534	538	535
0.4	-0.7	-1.9	3.1	0.3	2.1	-0.9	-0.9	-0.5	2.1	-1.7	1.3	1.3	-5.2	1.1	4.9	0.3	0.3	-2.5	-1.5
0.864892	0.864890	0.864893	0.864893	0.864892	0.864894	0.864889	0.864891	0.864893	0.864891	0.864892	0.864891	0.864893	0.864888	0.864890	0.864895	0.864892	0.864892	0.864890	0.864886
0.011	0.009	0.025	0.010	0.009	0.008	0.009	0.011	0.011	0.014	0.009	0.010	0.010	0.008	0.010	0.011	0.008	0.011	0.010	0.011
0.00009	0.00008	0.00021	0.00009	0.00007	0.00007	0.00008	0.00010	0.00010	0.00012	0.00008	0.00009	0.00009	0.00007	0.00008	0.00009	0.00007	0.00009	0.00009	0.00009
4.7	3.8	10.7	4.4	3.8	3.6	4.0	4.9	4.8	6.1	3.9	4.3	4.4	3.6	4.2	4.6	3.3	4.6	4.3	4.7
0.000004	0.000003	0.000009	0.000004	0.000003	0.000003	0.000003	0.000004	0.000004	0.000005	0.000003	0.000004	0.000004	0.000003	0.000004	0.000004	0.000003	0.000004	0.000004	0.000004
537	534	525	541	530	536	538	535	536	534	536	535	534	529	536	535	536	535	535	530
1.8	-0.5	2.7	3.1	1.8	3.4	-1.6	-0.1	3.2	0.4	1.2	0.7	2.4	-3.0	-0.7	4.5	2.1	2.1	-0.6	-5.6
0.467152	0.467151	0.467154	0.467151	0.467152	0.467153	0.467152	0.467153	0.467155	0.467153	0.467153	0.467151	0.467154	0.467153	0.467151	0.467153	0.467153	0.467153	0.467152	0.467151
0.010	0.008	0.022	0.009	0.008	0.007	0.008	0.010	0.009	0.012	0.008	0.009	0.009	0.008	0.008	0.009	0.007	0.010	0.009	0.010
0.00004	0.00004	0.00010	0.00004	0.00004	0.00003	0.00004	0.00004	0.00004	0.00006	0.00004	0.00004	0.00004	0.00004	0.00004	0.00004	0.00003	0.00005	0.00004	0.00005
4.2	3.4	9.4	3.9	3.4	3.2	3.4	4.2	3.9	5.2	3.5	3.8	3.9	3.4	3.6	4.0	2.9	4.2	3.8	4.3
0.000002	0.000002	0.000004	0.000002	0.000002	0.000001	0.000002	0.000002	0.000002	0.000002	0.000002	0.000002	0.000002	0.000002	0.000002	0.000002	0.000001	0.000002	0.000002	0.000002
532	537	524	535	537	528	532	526	528	533	536	534	533	533	531	536	534	538	531	536
0.5	-2.3	5.1	-1.2	-0.3	3.2	-0.7	2.2	5.6	2.8	2.2	-1.1	3.9	3.2	-2.2	2.5	1.9	1.7	0.6	-2.1

4.9.1 Supplementary Table A.4.2 New Sr-Nd-Hf-Pb isotopic compositions

Supplementary Table A.4.1 New Sr, Nd, Hf, Pb isotopic measurements

Sample	$^{87}Sr/^{86}Sr$	2SE	$^{143}Nd/^{144}Nd$	2SE	$^{176}Hf/^{177}Hf$	2SE	$^{208}Pb/^{204}Pb$	2SE	$^{207}Pb/^{204}Pb$	2SE	$^{206}Pb/^{204}Pb$	2SE	$^{208}Pb/^{206}Pb$	2SE	$^{207}Pb/^{206}Pb$	2SE	$^{204}Pb/^{206}Pb$	2SE
H27	0.703754	0.000007	0.512927	0.000005	0.283056	0.000004	38.0242	0.0022	15.4625	0.0009	18.2514	0.0009	2.08335	0.00004	0.84718	0.00002	0.054790	0.000003
H27 replicate	0.703755	0.000008					38.0210	0.0017	15.4609	0.0006	18.2500	0.0008	2.08335	0.00004	0.84717	0.00001	0.054794	0.000002
H27 duplicate	0.703751	0.000008	0.512917	0.000005	0.283058	0.000004	38.0172	0.0019	15.4595	0.0007	18.2390	0.0008	2.08436	0.00004	0.84760	0.00001	0.054828	0.000002
H9	0.703748	0.000008	0.512912	0.000004	0.283057	0.000004	38.0143	0.0019	15.4584	0.0007	18.2347	0.0008	2.08473	0.00004	0.84775	0.00001	0.054840	0.000002
H9 replicate			0.512916	0.000004	0.283063	0.000004	38.0129	0.0023	15.4577	0.0008	18.2342	0.0009	2.08475	0.00004	0.84774	0.00001	0.054842	0.000003
MIR2338-5	0.703591	0.000007	0.512951	0.000005	0.283093	0.000004	38.1696	0.0019	15.4685	0.0006	18.4303	0.0007	2.07103	0.00005	0.83930	0.00001	0.054258	0.000002
MIR2338-5 replicate							38.1591	0.0031	15.4660	0.0011	18.4261	0.0013	2.07093	0.00005	0.83935	0.00001	0.054271	0.000004
KIL-1-17	0.703564	0.000009	0.512992	0.000006	0.283098	0.000004	38.0996	0.0022	15.4742	0.0008	18.4663	0.0009	2.06319	0.00004	0.83797	0.00001	0.054153	0.000003
KO-1-20	0.703721	0.000006	0.512973	0.000005	0.283099	0.000003	37.8884	0.0019	15.4706	0.0007	18.2106	0.0008	2.08059	0.00004	0.84954	0.00001	0.054913	0.000002
85-LAN-4	0.704071	0.000007	0.512852	0.000006	0.283020	0.000004	37.7718	0.0019	15.4435	0.0007	17.9690	0.0008	2.10206	0.00004	0.85946	0.00001	0.055651	0.000003
85-LAN-4 replicate							37.7766	0.0018	15.4456	0.0007	17.9712	0.0008	2.10209	0.00003	0.85947	0.00001	0.055644	0.000002
85-LAN-7	0.704331	0.000007	0.512763	0.000006	0.282952	0.000004	37.7813	0.0013	15.4367	0.0005	17.8815	0.0005	2.11285	0.00003	0.86328	0.00001	0.055923	0.000002
85-LAN-7 replicate							37.7810	0.0049	15.4379	0.0017	17.8816	0.0021	2.11284	0.00006	0.86333	0.00003	0.055923	0.000007
LWAW-4	0.704146	0.000007	0.512809	0.000006	0.282992	0.000004	37.7724	0.0039	15.4333	0.0015	17.9248	0.0019	2.10725	0.00005	0.86100	0.00003	0.055788	0.000006
LWAW-7	0.704099	0.000008	0.512838	0.000006	0.283009	0.000003	37.7485	0.0020	15.4405	0.0008	17.9550	0.0008	2.10237	0.00003	0.85994	0.00001	0.055695	0.000002
ML-2-12	0.703721	0.000007	0.512922	0.000006	0.283074	0.000003	38.0203	0.0019	15.4589	0.0007	18.2311	0.0007	2.08551	0.00004	0.84795	0.00001	0.054851	0.000002
ML-2-12 replicate			0.512929	0.000006	0.283070	0.000004	38.0239	0.0020	15.4602	0.0007	18.2318	0.0009	2.08556	0.00004	0.84796	0.00001	0.054849	0.000003
02-WA-10	0.703410	0.000006	0.513045	0.000005	0.283129	0.000004	37.8959	0.0018	15.4725	0.0007	18.3589	0.0008	2.06416	0.00004	0.84277	0.00001	0.054469	0.000002
00-OL-33a	0.703459	0.000006	0.513052	0.000004	0.283136	0.000004	38.0258	0.0020	15.4894	0.0007	18.4956	0.0008	2.05596	0.00004	0.83747	0.00001	0.054067	0.000002
In house reference materials																		
Kil93	0.703594	0.000007	0.512989	0.000005	0.283096	0.000004	38.0670	0.0015	15.4735	0.0005	18.4085	0.0007	2.06789	0.00004	0.84056	0.00001	0.054323	0.000002
Kil 93 replicate							38.0678	0.0022	15.4735	0.0008	18.4091	0.0009	2.06789	0.00003	0.84053	0.00001	0.054321	0.000003
Kil 93 replicate 2							38.0681	0.0019	15.4741	0.0007	18.4100	0.0007	2.06782	0.00004	0.84053	0.00001	0.054318	0.000002
Ko'olau	0.704093	0.000007	0.512773	0.000006	0.282955	0.000004	37.7455	0.0022	15.4366	0.0008	17.8392	0.0008	2.11588	0.00004	0.86531	0.00001	0.056056	0.000003

4.9.3 Supplementary Table A.4.2 New trace element compositions

Sample	Volcanic center	Cs	Rb	Ba	Th	U	Ta	Nb	La	Ce	Pb	Pr	Nd
H27	Hualalai	0.05	4.4	58	0.44	0.15	0.47	7.7	7.1	18.2	0.7	2.6	13.1
H27-duplicat	Hualalai	0.05	4.3	60	0.44	0.15	0.47	7.8	7.2	18.5	0.7	2.6	13.0
H27-replicate	Hualalai	0.04	4.4	59	0.44	0.15	0.47	7.7	7.0	18.2	0.7	2.6	12.8
H9	Hualalai	0.05	4.7	61	0.48	0.16	0.52	8.4	7.9	19.9	0.7	2.9	14.6
KIL-1-17	Kilauea	0.10	6.1	80	0.68	0.29	0.65	10.8	9.4	22.9	0.8	3.4	16.1
KO-1-20	Kohala	0.07	6.4	92	0.68	0.25	0.67	11.3	11.0	28.6	2.1	4.0	19.8
LWAW-4	Lanai	0.00	0.1	40	0.47	0.09	0.42	6.7	7.9	17.9	0.9	2.7	13.7
LWAW-7	Lanai	0.01	0.3	74	0.48	0.10	0.46	7.6	10.0	21.8	0.9	4.0	20.6
85-LAN-4	Lanai	0.06	4.8	62	0.48	0.17	0.43	6.9	7.8	20.5	0.9	3.1	15.6
85-LAN-7	Lanai	0.05	4.8	76	0.41	0.14	0.37	6.1	9.7	27.0	0.8	4.2	24.0
MIR 2338-5	Loihi	0.07	5.6	77	0.60	0.20	0.66	11.0	8.3	20.0	0.8	2.7	12.6
ML-2-12	Mauna Loa	0.05	5.7	76	0.66	0.22	0.61	10.5	9.6	24.0	0.8	3.4	16.4
02-WA-10	West Maui	0.05	5.3	139	1.11	0.32	1.08	18.7	16.1	38.4	1.1	5.7	26.9
00-OL-33a	West Maui	0.02	2.6	54	0.65	0.21	0.66	11.1	10.6	26.1	0.8	4.2	20.7
In house reference materials													
Kil93-1	Kilauea	0.07	7.0	100	0.80	0.28	0.78	12.8	11.5	28.4	0.9	4.1	19.8
Kil-93-2	Kilauea	0.07	7.0	100	0.80	0.28	0.78	12.9	11.4	28.4	0.9	4.1	20.1
Kil-93-3	Kilauea	0.07	7.0	99	0.79	0.27	0.78	13.0	11.2	27.9	0.9	4.1	19.8
Koolau	Koolau	0.06	6.4	86	0.58	0.18	0.50	8.3	11.3	28.1	1.3	4.2	20.6

4.9.2 Supplementary Table A.4.3 continued

Sample	Volcanic center	Sr	Sm	Zr	Hf	Eu	Gd	Tb	Dy	Ho	Y	Er	Tm	Yb	Lu
H27	Hualalai	236	3.6	94	2.5	1.4	4.3	0.7	4.0	0.8	23	2.0	0.3	1.7	0.2
H27-duplicat	Hualalai	238	3.5	95	2.5	1.3	4.2	0.7	4.1	0.8	23	2.0	0.3	1.6	0.2
H27-replicate	Hualalai	238	3.4	96	2.5	1.3	3.9	0.6	4.0	0.7	23	2.0	0.3	1.5	0.2
H9	Hualalai	256	3.8	102	2.8	1.5	4.6	0.7	4.4	0.8	24	2.1	0.3	1.7	0.2
KIL-1-17	Kilauea	260	4.1	113	3.0	1.5	4.6	0.7	4.0	0.8	23	2.0	0.2	1.6	0.2
KO-1-20	Kohala	342	5.2	144	3.8	1.8	5.6	0.9	5.0	0.9	27	2.4	0.3	1.9	0.3
LWAW-4	Lanai	260	3.6	93	2.5	1.3	4.5	0.7	3.9	0.8	26	2.0	0.3	1.5	0.2
LWAW-7	Lanai	314	5.7	117	3.0	2.2	6.5	1.1	5.9	1.1	30	2.9	0.4	2.5	0.3
85-LAN-4	Lanai	314	4.4	117	3.2	1.5	5.2	0.8	4.7	0.9	27	2.3	0.3	1.9	0.3
85-LAN-7	Lanai	263	6.6	103	2.7	2.3	8.6	1.3	7.8	1.6	60	4.5	0.6	3.6	0.5
MIR 2338-5	Loihi	229	3.0	84	2.2	1.1	3.4	0.5	2.8	0.5	16	1.3	0.2	1.1	0.1
ML-2-12	Mauna Loa	251	4.3	120	3.2	1.4	4.6	0.8	4.5	0.8	26	2.2	0.3	1.8	0.2
02-WA-10	West Maui	420	6.9	194	5.0	2.3	6.8	1.1	6.0	1.1	32	2.8	0.4	2.2	0.3
00-OL-33a	West Maui	324	5.5	150	3.9	1.9	6.2	1.0	5.8	1.0	30	2.8	0.4	2.1	0.3
In house reference materials															
Kil93-1	Kilauea	327	5.2	139	3.7	1.8	5.7	0.9	5.1	1.0	27	2.6	0.3	2.0	0.3
Kil-93-2	Kilauea	327	5.2	140	3.7	1.8	5.7	0.9	5.3	1.0	27	2.6	0.4	2.0	0.3
Kil-93-3	Kilauea	325	5.0	141	3.7	1.8	5.5	0.9	5.2	0.9	27	2.5	0.3	2.0	0.3
Koolau	Koolau	429	5.1	142	3.6	1.8	5.3	0.8	4.3	0.8	24	2.1	0.3	1.6	0.2

Chapter 5: Conclusions

The short-lived radioactive isotope system $^{182}Hf \rightarrow ^{182}W$ has provided a tool to investigate processes that occurred during the first ~60 Myr of the Solar System, including the early stages of Earth's accretion and differentiation. In bulk, undifferentiated Solar System materials, the average $\mu^{182}W$ (parts-per-million deviation of the $^{182}W/^{184}W$ relative to the bulk silicate Earth) is approximately -200 (e.g.; Hellmann et al., 2024). During Earth's core formation, more than 90% of the moderately siderophile element W was partitioned into metal, while Hf remained in the silicate Earth (McDonough, 2003). As a result, the Hf/W of the bulk silicate Earth (BSE) was much greater than chondritic materials and Earth's core while ^{182}Hf was extant. Following the extinction of ^{182}Hf, large impacts and mantle convective mixing may have completely melted and stirred the BSE, leading to homogenization of isotopic compositions. Globally, ocean island basalts (OIB) ranging from 0 to ~15 Ma exhibit negative $\mu^{182}W$ signatures that must have been preserved in the Earth's interior for over 4.5 Gyr (e.g., Mundl et al., 2017; Mundl-Petermeier et al., 2020, Rizo et al., 2019). Three hypotheses are considered to explain negative $\mu^{182}W$ in the mantle sources of OIB. The first hypothesis is isotopic equilibration between the mantle and the core. The details of this mechanism are not well understood, but it is a process that does not require preservation of *mantle* heterogeneity generated prior to the Moon forming impact and billions of years of mantle mixing. The second hypothesis is that an early formed (i.e., >4.51 Ga) silicate reservoir, with an initial Hf/W lower than BSE, has been stored in the mantle for nearly all of Earth's history. This is plausible given that crystallization of high pressure phases, such as bridgmanite and Ca-pervoskite, may leave behind a residual liquid, such as a basal magma ocean, with lower Hf/W than the

crystallizing solid (Corgne et al., 2005; Brown et al., 2014). Finally, "grainy" late accretion could lead to domains in the mantle with negative $\mu^{182}W$ due to the contrast of $\mu^{182}W$ between the BSE and broadly chondritic materials. The two latter hypotheses require preservation of a mantle domain(s) with negative $\mu^{182}W$ for billions of years.

The mode of origin of $\mu^{182}W$ anomalies in OIB remains unclear; however, this dissertation provides new constraints concerning the physical and chemical properties of the anomalous component, which hopefully provide the next stepping stone to solve the mystery surrounding these isotopic signatures. Here, new insights on the characteristics of the anomalous $\mu^{182}W$ component, and the structure and dynamics of the Hawaiian mantle plume from the perspective of $\mu^{182}W$, are outlined.

5.1 Refractory nature of the anomalous $\mu^{182}W$ component

In global OIB, complex componentry and diverse petrogenetic processes can overprint mantle source characteristics associated with negative $\mu^{182}W$, so that very few geochemical parameters are associated with the appearance of anomalous $\mu^{182}W$ in global mantle plumes (e.g., Jackson et al., 2020). To overcome the complexity of analyzing global OIB collectively, investigating the $\mu^{182}W$ variations in the Mauna Kea volcano provides the benefit of a petrogenetically-related suite of rocks with limited chemical and isotopic heterogeneity compared to the global scale. Additionally, the well-characterized stratigraphic section of Mauna Kea produced by the Hawaiian Scientific Drilling Project phase-2 (HSDP-2) provides a time series for exploration of the $\mu^{182}W$ evolution of a volcano over time. The HSDP-2 core samples over 300 Kyr of Mauna Kea shield-stage volcanism (Rhodes and Vollinger, 2004; Sharp and Renne, 2005).

The HSDP-2 core has revealed three major new insights into the nature of $\mu^{182}W$ anomalies in OIB. First, contrary to global OIB, the $\mu^{182}W$ and $^{3}He/^{4}He$ systematics can be explained solely by two-component mixing in Mauna Kea. Second, the anomalous $\mu^{182}W$ component is enriched in some high field strength elements (HFSE), which may provide evidence for early silicate differentiation as the mode of origin for these coupled signatures. And third, the Mauna Kea volcano most efficiently sampled the anomalous $\mu^{182}W$ component when the volcano was closest to the plume axis, where the mantle potential temperature was greatest.

The $\mu^{182}W$ of the shield stage lavas in the lower section of the stratigraphy host larger $\mu^{182}W$ deficits than the upper half of the stratigraphic column. The magnitude of the $\mu^{182}W$ anomalies decreases stratigraphically upward. Normal $\mu^{182}W$ is interspersed throughout the entire stratigraphic section, which likely implies that even when anomalous $\mu^{182}W$ is present in the mantle source, the volume is small enough that the anomalous signature is not always sampled. The thermal structure of the plume best explains the $\mu^{182}W$ evolution throughout the Mauna Kea stratigraphic section. For example, greater magnitude $\mu^{182}W$ deficits are present when the relative distance between the volcano and the plume axis, where mantle potential temperatures are greatest, is at a minimum during the period of time captured by the drill core (DePaolo et al., 2001; Chapter 2 of this dissertation). This is consistent with previous work that interpreted the lower stratigraphic section of the HSDP-2 core as lavas that formed by higher magma production rate and higher degree of partial melting compared to the later shield stage in the upper stratigraphic section (Feigenson et al., 2003; Sharp and Renne, 2005). As the Pacific plate moved Mauna Kea distally from the plume axis, the magnitude and rate of $\mu^{182}W$ anomalies decreased in erupted lavas (Chapter 2 of this dissertation). The Mauna Kea study produced the first observed correlation between $\mu^{182}W$ and trace element signatures, as well as a lithophile isotopic composition

($^{208}Pb/^{204}Pb$). The trace element signatures associated with $\mu^{182}W$ deficits include elevated Ti and Nb, relative to similarly incompatible elements during mantle partial melting. These signatures, denoted as Ti/Ti* ($Ti/Ti^*=Ti_N/(Sm_N*Tb_N)^{0.5}$), and Nb/Nb* ($Nb/Nb^*=Nb_N/(La_N*Th_N)^{0.5}$), reflect the mantle source characteristics of the anomalous $\mu^{182}W$ component, and are associated with refractory lithologies, which would be most efficiently melted where the mantle potential temperature is greatest.

5.2 The $\mu^{182}W$ of minimally altered OIB is a reliable mantle source signature

The radiogenic isotopic compositions of mantle-derived rocks have been used to interpret the physical and chemical structure of Earth's interior (e.g., Zindler and Hart, 1986). To accurately identify the components, and interpret their histories (e.g., enrichment by recycling, depletion by partial melting, etc.), precise and accurate isotopic compositions are required. In order for the interpretation of $\mu^{182}W$ to be useful for understanding the mantle, the $\mu^{182}W$ of the melt must reflect that of its mantle source. Ocean island basalts are subject to physical and chemical weathering. These processes can affect the radiogenic isotopic compositions, such as Sr and Pb isotopic ratios (Nobre Silva et al., 2009, 2010). Progressive acid leaching experiments have demonstrated that alteration of Hawaiian rocks can lead to radiogenic Pb and Sr compositions in altered rocks relative to their mantle source (Nobre Silva et al., 2009, 2010). The effect of alteration of the isotopic compositions of HFSE, like Hf and W, have not been conclusively determined. Given the variability of $\mu^{182}W$ in OIB is limited (range of ~25 ppm total), especially relative to analytical uncertainties (~3-5 ppm), accurate and reproducible $\mu^{182}W$ measurements are critical to the application of this isotope system to mantle tracing studies.

Using minimally altered rocks (e.g., loss on ignition <2.5 wt. %), because minimally altered rocks are most likely to be selected for, or already be characterized by, high precision isotopic studies, a two-step acid leaching protocol was performed on powdered Hawaiian lavas to determine whether $\mu^{182}W$ is affected by alteration. Subaerial lavas (~5 Ma) from Kauai have consistently reproducible $\mu^{182}W$ within analytical uncertainty, between aliquots with and without acid leaching (Chapter 3 of this dissertation). All leached powders produce a small offset (2-4 ppm) towards more negative $\mu^{182}W$ values, which may hint that alteration adds a minor amount of normal $\mu^{182}W$ to OIB, but that this process is essentially negligible for minimally altered rocks.

One submarine lava from the HSDP-2 drill core shows a potentially resolvable difference in $\mu^{182}W$ between the unleached and leached powders. This result is enigmatic because the unleached powder resulted in a $\mu^{182}W$ that is more negative, indicating alteration could have introduced negative $\mu^{182}W$ to the rock. The origin of exogenous, negative $\mu^{182}W$ that could be introduced in the submarine environment is unclear. Seawater has a very low concentration of W (Fujiwara et al., 2020), which would require a large mass of water to interact with the submarine basalt for any resolvable effect to occur. There is no evidence for significant seawater interaction in the minimally altered HSDP-2 lavas (Rhodes and Vollinger, 2004). Furthermore, seawater is not likely to have a distinctly negative $\mu^{182}W$.

Additional sources of W that could affect the submarine Mauna Kea lavas include Fe- and Mn-oxides, which have a W concentration ~1000x that of the Mauna Kea lavas (Kashiwabara et al., 2013; Chapter 2 of this dissertation), or drilling mud, introduced during HSDP-2, which has an unknown W concentration but has been shown to have affected other isotopic systems, like Sr and Pb, in the drill core samples (Nobre Silva et al., 2009, 2010). Future work should explore additional acid leaching of drill core samples from a $\mu^{182}W$ perspective, as well as submarine

samples that are not associated with drilling. Available W isotopic and abundance data suggest there is limited possibility for contamination of $\mu^{182}W$ by natural materials, and $\mu^{182}W$ in minimally altered basalts is a reliable signature of the mantle source.

5.3 The Hawaiian plume experiences pulses of anomalous $\mu^{182}W$

Initial studies of $\mu^{182}W$ in Hawaii found $\mu^{182}W$ deficits in nearly every volcanic center on the island of Hawaii and in the Kama'ehuakanaloa seamount (Mundl et al., 2017; Mundl-Petermeier et al., 2020). The spatial extent of the anomalous $\mu^{182}W$ component beyond the island of Hawaii was unconstrained. The appearance or absence of $\mu^{182}W$ anomalies along the Hawaiian archipelago has implications for the extent of entrainment and the amount of total anomalous material hosted in the plume.

Starting at ~5 Ma in Kauai, negative $\mu^{182}W$ is present in the plume and is sampled by shield stage, tholeiitic lavas from the Napali member (Chapter 4 of this dissertation). The magnitude of $\mu^{182}W$ anomalies at 5 Ma in Hawaii is approximately -20 to -25, which is within analytical uncertainty of the largest magnitude $\mu^{182}W$ compositions measured among global OIB, overlapping Kama'ehuakanaloa and Galapagos (Mundl-Petermeier et al., 2020). Between 5 Ma and <1 Ma, only one lava from Ko'olau (~2.6 Ma) exhibits a resolvable $\mu^{182}W$ deficit of -7.5 ± 3.6. There is no distinction in major element compositions or trace element proxies for degree of partial melting, such as La/Sm, among volcanic centers and individual lavas that have $\mu^{182}W$ deficits or not. There is no clear evidence for the attenuation of $\mu^{182}W$ variability by the introduction of recycled W. The interpretation is that the absence of $\mu^{182}W$ anomalies in the volcanic centers between Kauai and Hawaii reflects plume structure, where the anomalous component is not present in the melting region. There is evidence for pulsing in the plume, such as inflections in the magmatic flux produced by the plume over time (Wessel, 2016). Time periods

associated with a greater slope in the magmatic flux versus time are generally correlated with anomalous $\mu^{182}W$ in volcanic centers along the archipelago. Thus, larger buoyancy flux and higher mantle potential temperature may be required to entrain the anomalous component, and lead to a higher probability of the anomalous component being sampled by partial melting near Earth's surface.

5.4 The mode of origin of $\mu^{182}W$ heterogeneity in modern ocean island basalts

The mechanism(s) that generated $\mu^{182}W$ anomalies in the mantle source of ocean island basalts have yet to be unambiguously determined. Here, the potential lines of corroborative evidence for three proposed modes of origins are outlined.

5.4.1 Core-mantle interactions

The metal core is thought to have ~90% of Earth's W budget, and as a result of its low Hf/W, a very negative $\mu^{182}W$ (-220) relative to the silicate Earth (McDonough, 2003; Kleine and Walker, 2017). As a result of the siderophile nature of W, in addition to its incompatibility during mantle partial melting, the mantle is largely depleted in W relative to chondritic compositions. Thus, $\mu^{182}W$ should be an effective test for core contribution to the mantle (e.g., Scherstén et al., 2004). Indeed, observed $\mu^{182}W$ deficits in modern rocks have been interpreted as signals from Earth's core (e.g., Rizo et al., 2019; Mundl-Petermeier et al., 2020).

Osmium isotopic compositions, especially correlated $^{187}Os/^{188}Os$ and $^{186}Os/^{188}Os$, have also been attributed to core-mantle interaction (e.g., Walker et al., 1995; Brandon et al., 1999). Originally, it was thought that crystallization of the inner core would fractionate Re/Os and Pt/Os, leading elevated ^{187}Re and ^{190}Pt in the outer liquid core, which both decay to produce radiogenic Os isotopes, ^{187}Os and ^{186}Os, respectively (Brandon and Walker, 2005). The Os isotopic

composition of the outer core is affected by both the age and degree of inner core crystallization, as well as the partition coefficients of Re-Pt-Os between liquid and solid core material. In order to produce the $^{187}Os/^{188}Os$ and $^{186}Os/^{188}Os$ correlations observed in Hawaiian lavas, the required age of the inner core is ~3.5 Ga (Brandon and Walker, 2005). Updated models for the thermal evolution of the core predict the inner core is less than 2.5 Ga, and likely closer to ~1 Ga (Labrosse et al., 2001; Labrosse, 2003). The younger age of the inner core decreases the probability that Re/Os and Pt/Os fractionation was significant in the core system to produce observed radiogenic $^{187}Os/^{188}Os$ and $^{186}Os/^{188}Os$ in Hawaii (Lassiter, 2006). At this stage, it is unclear whether the isotopic composition of the outer core is distinct from the BSE, and Os isotope systematics are likely tracing recycled components that have radiogenic Os due to silicate fractionation events.

Bulk entrainment of core material into the mantle has largely been ruled out using highly siderophile element (HSE) abundances, which should be elevated in core-contaminated mantle sources, but are not elevated or correlated with $\mu^{182}W$ in modern OIB (Rizo et al., 2019; Mundl-Petermeier et al., 2020). Though, as pointed by Rizo et al. (2019), it can be difficult to constrain the HSE abundance of the mantle source of erupted lavas, especially when residual sulfides retain HSE in the solid mantle during partial melting. Platinum may be the most reliable HSE for mantle source abundance estimates, as it is not significantly fractionated during partial melting or crystallization of olivine, or, more importantly, is not fractionated by sulfide precipitation (Pitcher et al., 2009). A detailed study of the Mauna Kea volcano in Hawaii provides the most paired HSE and $\mu^{182}W$ data for a single volcano (Chapter 2 of this dissertation). This study, found that the petrogenetically related rocks at Mauna Kea do not have correlated Pt and $\mu^{182}W$. However, Chapter 4 of this dissertation documents a modest correlation between Pt and $\mu^{182}W$ when considering all Hawaiian volcanic centers together, indicating that the enhanced scale (both

spatially and in the total variability of Pt abundances) may be required to resolve elevated Pt abundances in portions of the Hawaiian mantle plume. The Hawaiian data do not provide conclusive evidence that elevated Pt is associated with $\mu^{182}W$ deficits in meaningful way, but the potential correlation does mean that some mechanisms of core-mantle exchange remain a viable mode of origin for $\mu^{182}W$ deficits. For example, an alternative to bulk entrainment of liquid outer core in the mantle is trapping of crystallized liquid metal in the mantle, either during core formation or by interaction of liquid outer core with Fe-rich cumulate piles at the core-mantle boundary (CMB) (Rushmer et al., 2005; Humayun, 2011). The metallic solids host a lower concentration of HSE, relative to the bulk outer core or the residual liquid, and therefore, produce a smaller increase in the HSE abundance of the mantle source (Humayun, 2011). This mechanism would also produce smaller $\mu^{182}W$ deficits, and may or may not produce radiogenic and correlated $^{187}Os/^{188}Os$ and $^{186}Os/^{188}Os$, depending on the age and degree of entrapment and crystallization (Humayun, 2011).

An additional mechanism of core-mantle exchange is isotopic equilibration (Puchtel and Humayan, 2000; Mundl-Petermeier et al., 2020; Ferrick and Korenaga, 2023). The geochemical effects of equilibration at the CMB depend on the chemical compositions, especially relative concentrations of a specific element between the core and mantle, and oxygen fugacity fO_2 of the lower most mantle region that is interacting with the core, because of the effect of fO_2 on the partition coefficients and diffusivity of W at the CMB (Mundl-Petermeier et al., 2020). Several iterations of these parameters resulted in a core-mantle equilibrated reservoir (CMER) that has the same $\mu^{182}W$ as the core, but variable HSE abundances that may or may not result in detectable HSE- $\mu^{182}W$ correlation in OIB, depending on the conditions of the model (Mundl-Petermeier et al., 2020). There is an anticorrelation between $\mu^{182}W$ and $^{3}He/^{4}He$ both within and among OIB localities (Rizo et al., 2019; Mundl-Petermeier et al., 2020; Chapter 2 of this dissertation). Whether

or not high $^{3}He/^{4}He$ is a signature of Earth's core is a matter of debate, which depends on the total amount of He in the core, especially in relation to radioactive nuclides that produce alpha particles (i.e., ^{4}He), such as Th, U, Pt (Ozgurel and Caracas, 2023). The amount of He estimated for Earth's core ranges from negligible (Matsuda et al., 1993) to all of the initial budget of He (Horton et al., 2023). Despite the uncertainties pertaining to the abundance and isotopic composition of He in the core, it remains a viable reservoir for high $^{3}He/^{4}He$, in part because the core provides a solution to the problem of storing primordial He in the mantle, which has a higher abundance of alpha producers than the core, and experienced large impacts, magma oceans, and billions of years of degassing and convective mixing.

5.4.2 Early silicate differentiation

Earth's accretion and early stages included a period of large impacts and multiple magma oceans (e.g., Canup, 2008; Elkins-Tanton, 2012). Chemical differentiation in the silicate Earth while ^{182}Hf was extant (i.e., within ~60 Myr of Solar System start), would have occurred as a result of magma ocean crystallization. High pressure experiments have attempted to constrain the partitioning behavior of elements in the deep mantle, relevant to the crystallization of a basal magma ocean. Uncertainties remain surrounding the partitioning behavior of Hf and W at high pressure and temperature. For example, experiments predict a range of Hf/W in bridgmanite and Ca-perovskite from ~0.5 to ~100, though most studies predict a higher Hf/W in the two solid phases relative to the residual liquid (Brown et al., 2014). Therefore, the residual liquid formed from basal magma ocean crystallization during the lifetime of ^{182}Hf would likely be a low Hf/W reservoir, which would evolve negative $\mu^{182}W$.

The low Hf/W liquid would also be predicted to have Sm/Nd < 1 (Brown et al., 2014). The short-lived $^{146}Sm \rightarrow {}^{142}Nd$, with a half-life of either 103 Myr (e.g., Meissner et al., 1987), or, recently remeasured to be 92 Myr (e.g., Chiera et al., 2024), could provide correlative evidence for an early silicate differentiation event like the crystallization of a basal magma ocean. There is limited evidence for $\mu^{142}Nd$ variability in modern OIB (Caro et al., 2006; Jackson and Carlson, 2012; Horan et al., 2018; Peters et al., 2018). Samples from the Réunion hotspot show small deviations (<10 ppm) in $\mu^{142}Nd$ from the terrestrial standard presumed to represent the composition of the BSE (Peters et al., 2018). A complication in the interpretation of the $\mu^{142}Nd$ anomalies in the Réunion mantle source is that both positive and negative $\mu^{142}Nd$ anomalies are observed. Combined $\mu^{142}Nd$ and $\mu^{182}W$ data from Réunion do not have a positive correlation, which would be expected if the anomalies in both systems were formed by early silicate fractionation (Peters et al., 2018, 2021). Samples from Samoa and Hawaii have also been characterized for both $\mu^{142}Nd$ and $\mu^{182}W$ (Horan et al., 2018). The localities have smaller $\mu^{142}Nd$ values compared to Réunion, only debatably resolved from the BSE value, and $\mu^{142}Nd$ and $\mu^{182}W$ are not correlated within or among Samoa and Hawaii (Horan et al., 2018). Thus far, $\mu^{142}Nd$ in OIB does not provide support for early silicate differentiation as the mode of origin for $\mu^{182}W$ deficits in OIB mantle sources. There are multiple mechanisms that could explain a lack of correlation between $\mu^{142}Nd$ and $\mu^{182}W$ even if early silicate differentiation produced $\mu^{182}W$ deficits in the mantle (e.g., Chapter 2 of this dissertation). The first is that the experimentally-derived partition coefficients for Sm and Nd during crystallization of a basal magma ocean allow for an insufficient degree of fractionation between the two elements to resolve $\mu^{142}Nd$ variations (Brown et al., 2014). Additionally, ancient $\mu^{142}Nd$ variability in the mantle may be attenuated more readily than $\mu^{182}W$ heterogeneity during recycling and mantle mixing, due to a high Nd/W in mantle- and

continental-derived lithologies (Rudnick and Gao, 2003; Arevalo and McDonough, 2010). Further, the effect of recycling on $\mu^{142}Nd$ relative to $\mu^{182}W$ may be compounded by the fluid-mobility of W during subduction, which may remove W from a subducting slab and reduce the efficiency of $\mu^{182}W$ homogenization in the mantle (Bali et al., 2012).

The remnant basal magma ocean after bridgmanite and Ca-perovskite crystallization would be enriched in high field strength elements (HFSE), like W, Ti, Nb, and Th, relative to similarly incompatible elements, such as rare earth elements (REE). In the Mauna Kea volcano of Hawaii there is a negative correlation between $\mu^{182}W$ and Ti/Ti* ($Ti/Ti^*=Ti_N/(Sm_N*Tb_N)^{0.5}$), and Nb/Nb* ($Nb/Nb^*=Nb_N/(La_N*Th_N)^{0.5}$), as well as $^{208}Pb/^{204}Pb$ (which reflect the time-integrated Th/U) (Chapter 2 of this dissertation). These correlations remain when the dataset is expanded to include all Hawaiian volcanic centers together (Chapter 4 of this dissertation). The relationship between $\mu^{182}W$ and Ti/Ti*, Nb/Nb*, and $^{208}Pb/^{204}Pb$ provides one of the first lines of corroborative evidence for silicate differentiation as the mode of origin for $\mu^{182}W$ deficits in mantle plume sources. If elevated Ti/Ti*, Nb/Nb*, and $^{208}Pb/^{204}Pb$ are source characteristics of the anomalous $\mu^{182}W$ component, then the correlation between $\mu^{182}W$ and these parameters may be present in other plume localities where $\mu^{182}W$ deficits have been observed (e.g., Iceland, Galapagos, Samoa, etc.). In Icelandic lavas, there is correlation between $\mu^{182}W$ and $^{208}Pb/^{204}Pb$, but not Ti/Ti* or Nb/Nb*. The absence of correlations between $\mu^{182}W$ and Ti/Ti* and Nb/Nb* does not preclude the possibility that these parameters are characteristics of the mantle source with negative $\mu^{182}W$. For example, Ti/Ti* and Nb/Nb* of the mantle source could be overprinted and modified by fractional crystallization of oxide phases (e.g., Peters and Day, 2014). In Samoa, there is a relationship between $\mu^{182}W$ and Ti/Ti* and Nb/Nb*. In Samoa there is a *positive* correlation between $\mu^{182}W$ and $^{208}Pb/^{204}Pb$, which is the opposite of the trend observed in Hawaii and Iceland. The $^{208}Pb/^{204}Pb$

of Samoan lavas with normal $\mu^{182}W$ is more radiogenic than any lavas from Hawaii or Iceland, leaving open the possibility that a more radiogenic mantle or recycled component is creating the opposite W-Pb systematics in Samoa. Isotopic and trace element data for the Galapagos samples that have been characterized for $\mu^{182}W$ are limited such that it is not yet possible to discern whether relationships between $\mu^{182}W$ and Ti/Ti*, Nb/Nb*, and $^{208}Pb/^{204}Pb$ are present in the Galapagos plume. The observed relationships between $\mu^{182}W$ and HFSE in Hawaii are not a "smoking gun" for an early silicate differentiation event as the mode of origin for $\mu^{182}W$ deficits.

Problems with the early silicate differentiation model for the origin of $\mu^{182}W$ include preservation of high $^{3}He/^{4}He$ in the same reservoir as negative $\mu^{182}W$ to produce the anticorrelation between $\mu^{182}W$ and $^{3}He/^{4}He$ in OIB (Mundl et al., 2017; Mundl-Petermeier et al., 2020). The low Hf/W residual liquid of a crystallizing basal magma ocean would also be enriched in alpha producers, namely Th and U, compared to the BSE (Corgne et al., 2005). Production of ^{4}He by decay of Th and U would lower the $^{3}He/^{4}He$ over time. In order for this reservoir to have both negative $\mu^{182}W$ and high $^{3}He/^{4}He$, it must have had a high concentration of He. Contradictory to this requirement, OIB with high $^{3}He/^{4}He$ tend to have lower He concentrations and lower He/Ne and He/Ar than mid-ocean ridge basalts (MORB) with "normal" (i.e., $^{3}He/^{4}He$ of ~8, relative to Earth's atmosphere; Graham, 2002). This apparent problem has been coined "the helium paradox" (Anderson, 1998). The helium paradox may be explained as a result of non-equilibrium degassing, allowing the mantle source to have elevated He concentrations but preferentially lose He relative to Ne and Ar during degassing (Gonnermann and Mukhopadhyay, 2007). Furthermore, heavy noble gas isotopic compositions (e.g., low $^{129}Xe/^{130}Xe$ and high $^{20}Ne/^{22}Ne$ at a given $^{21}Ne/^{22}Ne$) in plume-derived systems relative to MORB, provide corroborative evidence for one or more less

degassed deep mantle reservoirs (Mukhopadhyay, 2012; Parai et al., 2019). It cannot be ruled out that a less degassed plume source was able to retain high $^{3}He/^{4}He$ and negative $\mu^{182}W$.

One additional complication for the formation and retention of $\mu^{182}W$ deficits in the silicate portion of the Earth is that this reservoir must have formed within the first ~60 Myr of Earth's history, and avoided homogenization throughout giant impacts that partially or completely melted the Earth (e.g., Elkins-Tanton, 2012). Furthermore, this reservoir must have also resisted homogenization, despite evidence for whole-mantle convection (van der Hilst et al., 1997). If silicate processes formed the anomalous $\mu^{182}W$ reservoir, then combined negative $\mu^{182}W$ and noble gas isotopic systematics imply that Earth's mantle was likely never homogenized, which may have implications for formation and evolution of Earth's interior, such as the extent of melting caused by giant impacts, such as the Moon-forming event.

5.4.3 Grainy late accretion

The $^{182}Hf \rightarrow ^{182}W$ system has been applied to the study of late accretion, in which a fraction of Earth's mass (~0.5%) was delivered after core and Moon formation (e.g., Bottke et al., 2010). Early examples of the application of $\mu^{182}W$ to the study of late accretion include the interpretation that positive $\mu^{182}W$ values in Archean rocks represent the mantle composition before late accretion (Willbold et al., 2011; Puchtel et al., 2016; Rizo et al., 2016). The $\mu^{182}W$ of the Earth-Moon system has also been used as supporting evidence for late accretion to the Earth, especially relative to the Moon (Touboul et al., 2015). The hypotheses discussed in these works explain that a change in the Earth's mantle $\mu^{182}W$ from positive to "normal" or negative values, as well as addition of HSE to the mantle, occurred as a result of late accreting material. In the event that some pockets of the mantle experienced a larger degree of late accretion, or remained isolated so that the chemical and isotopic signatures of late accretion have been homogenized, then those mantle domains would be

expected to have negative $\mu^{182}W$ and elevated HSE abundances (e.g., Rizo et al., 2016). The compatible nature of some HSE during partial melting and olivine crystallization, in addition to the possibility of HSE retention in residual sulfides, makes it difficult to constrain the absolute and relative HSE abundances in the mantle source of mantle-derived rocks (e.g., Ireland et al., 2009; Pitcher et al., 2009; Archer et al., 2023). In modern OIB, evidence for a correlation between $\mu^{182}W$ and HSE abundances, using Pt as a proxy for the HSE content of the mantle source, is limited to Hawaiian volcanic centers considered together (Chapter 4 of this dissertation). A relationship between $\mu^{182}W$ and HSE was not observed in a series of lavas from a single Hawaiian volcano (Chapter 2 of this dissertation), or in other OIB systems (Rizo et al., 2019; Mundl-Petermeier et al., 2020). At this stage, whether or not mantle plumes entrain domains of the mantle characterized by negative $\mu^{182}W$ and elevated HSE is inconclusive.

The hypothesis that grainy late accretion generated $\mu^{182}W$ heterogeneity in the mantle is unique among the three hypotheses discussed in this dissertation, in that unlike core-mantle exchange and early silicate differentiation, $\mu^{182}W$ variability is related to radiogenic ingrowth of ^{182}W *and* nucleosynthetic variability. (Budde et al., 2022; Archer et al., 2023). Nucleosynthetic effects on $\mu^{182}W$ would likely produce correlated effects on $\mu^{183}W$, as the two isotopes are similarly effected by s- and r-processes (Archer et al., 2023). Correlation between $\mu^{182}W$ and $\mu^{183}W$ has not consistently identified in OIB (Archer et al., 2023; Chapter 2 of this dissertation). A potential area of future work would be to continue investigate other nucleosynthetic signatures that could identify whether late accretion affected the $\mu^{182}W$ of isolated mantle domains. Though grainy late accretion remains a viable mechanism for producing $\mu^{182}W$ heterogeneity in the mantle, there is little evidence to support this hypothesis at this time.

Bibliography

Abouchami W., Galer S. J. G. and Hofmann A. W. (2000) High precision lead isotope systematics of lavas from the Hawaiian Scientific Drilling Project. *Chemical Geology* **169**, 187–209.

Abouchami W., Hofmann A. W., Galer S. J. G., Frey F. A., Eisele J. and Feigenson M. (2005) Lead isotopes reveal bilateral asymmetry and vertical continuity in the Hawaiian mantle plume. *Nature* **434**, 851–856.

Allègre C. J. (1982) Chemical geodynamics. *Tectonophysics* **81**, 109–132.

Anderson D. L. (1998) The helium paradoxes. *Proceedings of the National Academy of Sciences* **95**, 4822–4827.

Archer G. J., Budde G., Worsham E. A., Stracke A., Jackson M. G. and Kleine T. (2023) Origin of ^{182}W anomalies in ocean island basalts. *Geochemistry, Geophysics, Geosystems* **24**, e2022GC010688.

Archer G. J., Mundl A., Walker R. J., Worsham E. A. and Bermingham K. R. (2017) High-precision analysis of ^{182}W/^{184}W and ^{183}W/^{184}W by negative thermal ionization mass spectrometry: Per-integration oxide corrections using measured ^{18}O/^{16}O. *Int J Mass Spectrom* **414**, 80–86.

Arevalo R. and McDonough W. F. (2010) Chemical variations and regional diversity observed in MORB. *Chemical Geology* **271**, 70–85.

Arevalo R. and McDonough W. F. (2008) Tungsten geochemistry and implications for understanding the Earth's interior. *Earth and Planetary Science Letters* **272**, 656–665.

Bali E., Keppler H. and Audetat A. (2012) The mobility of W and Mo in subduction zone fluids and the Mo–W–Th–U systematics of island arc magmas. *Earth and Planetary Science Letters* **351–352**, 195–207.

Ballentine C. J., van Keken P. E., Porcelli D. and Hauri E. H. (2002) Numerical models, geochemistry and the zero–paradox noble–gas mantle. *Philosophical Transactions of the Royal Society of London. Series A: Mathematical, Physical and Engineering Sciences* **360**, 2611–2631.

Becker H., Horan M. F., Walker R. J., Gao S., Lorand J.-P. and Rudnick R. L. (2006) Highly siderophile element composition of the Earth's primitive upper mantle: Constraints from new data on peridotite massifs and xenoliths. *Geochimica et Cosmochimica Acta* **70**, 4528–4550.

Bermingham K. R., Worsham E. A. and Walker R. J. (2018) New insights into Mo and Ru isotope variation in the nebula and terrestrial planet accretionary genetics. *Earth and Planetary Science Letters* **487**, 221–229.

Blichert-Toft J., Chauvel C. and Albarède F. (1997) Separation of Hf and Lu for high-precision isotope analysis of rock samples by magnetic sector-multiple collector ICP-MS. *Contrib Mineral Petrol* **127**, 248–260.

Blichert-Toft J., Weis D., Maerschalk C., Agranier A. and Albarède F. (2003) Hawaiian hot spot dynamics as inferred from the Hf and Pb isotope evolution of Mauna Kea volcano. *Geochemistry, Geophysics, Geosystems* **4**.

Blichert-Toft J., Zanda B., Ebel D. S. and Albarède F. (2010) The Solar System primordial lead. *Earth and Planetary Science Letters* **300**, 152–163.

Bottke W. F., Walker R. J., Day J. M. D., Nesvorny D. and Elkins-Tanton L. (2010) Stochastic Late Accretion to Earth, the Moon, and Mars. *Science* **330**, 1527–1530.

Bouhifd M. A., Jephcoat A. P., Heber V. S. and Kelley S. P. (2013) Helium in Earth's early core. *Nature Geoscience* **6**, 982–986.

Brandon A. D., Norman M. D., Walker R. J. and Morgan J. W. (1999) ^{186}Os–^{187}Os systematics of Hawaiian picrites. *Earth and Planetary Science Letters* **174**, 25–42.

Brandon A. D. and Walker R. J. (2005) The debate over core–mantle interaction. *Earth and Planetary Science Letters* **232**, 211–225.

Brown S. M., Elkins-Tanton L. T. and Walker R. J. (2014) Effects of magma ocean crystallization and overturn on the development of ^{142}Nd and ^{182}W isotopic heterogeneities in the primordial mantle. *Earth and Planetary Science Letters* **408**, 319–330.

Bryce J., Depaolo D. and Lassiter J. (2005) Geochemical structure of the Hawaiian plume: Sr, Nd, and Os isotopes in the 2.8 km HSDP-2 section of Mauna Kea Volcano. *Geochemistry Geophysics Geosystems, v.6 (2005)* **6**.

Budde G., Archer G. J., Tissot F. L. H., Tappe S. and Kleine T. (2022) Origin of the analytical ^{183}W effect and its implications for tungsten isotope analyses. *J. Anal. At. Spectrom.* **37**, 2005–2021.

Burkhardt C., Kleine T., Dauphas N. and Wieler R. (2012) Nucleosynthetic tungsten isotope anomalies in acid leachates of the murchison chondrite: Implications for hafnium–tungsten chronometry. *Astrophysical Journal Letters* **753**, L6.

Campbell I. H. and Griffiths R. W. (1990) Implications of mantle plume structure for the evolution of flood basalts. *Earth and Planetary Science Letters* **99**, 79–93.

Canup R. M. (2008) Accretion of the Earth. *Philosophical Transactions of the Royal Society A: Mathematical, Physical and Engineering Sciences* **366**, 4061–4075.

Caro G., Bourdon B., Birck J.-L. and Moorbath S. (2006) High-precision $^{142}Nd/^{144}Nd$ measurements in terrestrial rocks: Constraints on the early differentiation of the Earth's mantle. *Geochimica et Cosmochimica Acta* **70**, 164–191.

Chauvel C., Hofmann A. W. and Vidal P. (1992) himu-em: The French Polynesian connection. *Earth and Planetary Science Letters* **110**, 99–119.

Chen C. Y. and Frey F. A. (1985) Trace element and isotopic geochemistry of lavas from Haleakala Volcano, east Maui, Hawaii: Implications for the origin of Hawaiian basalts. *Journal of Geophysical Research: Solid Earth* **90**, 8743–8768.

Chiera N. M., Sprung P., Amelin Y., Dressler R., Schumann D. and Talip Z. (2024) The ^{146}Sm half-life re-measured: consolidating the chronometer for events in the early Solar System. *Sci Rep* **14**, 17436.

Corgne A., Liebske C., Wood B. J., Rubie D. C. and Frost D. J. (2005) Silicate perovskite-melt partitioning of trace elements and geochemical signature of a deep perovskitic reservoir. *Geochimica et Cosmochimica Acta* **69**, 485–496.

Cottaar S. and Romanowicz B. (2012) An unsually large ULVZ at the base of the mantle near Hawaii. *Earth and Planetary Science Letters* **355–356**, 213–222.

Dana J. D. (1849) Geology United States Exploring Expedition Philadelphia. C. Sherman, 10 (1849), p. 756.

Dasgupta R. and Hirschmann M. M. (2010) The deep carbon cycle and melting in Earth's interior. *Earth and Planetary Science Letters* **298**, 1–13.

DePaolo D. J., Bryce J. G., Dodson A., Shuster D. L. and Kennedy B. M. (2001) Isotopic evolution of Mauna Loa and the chemical structure of the Hawaiian plume. *Geochemistry, Geophysics, Geosystems* **2**.

Eisele J., Abouchami W., Galer S. J. G. and Hofmann A. W. (2003) The 320 kyr Pb isotope evolution of Mauna Kea lavas recorded in the HSDP-2 drill core. *Geochemistry, Geophysics, Geosystems* **4**.

Elkins-Tanton L. T. (2012) Magma oceans in the inner Solar System. *Annual Review of Earth and Planetary Sciences* **40**, 113–139.

Engel A. E. J., Engel C. G. and Havens R. G. (1965) Chemical characteristics of oceanic basalts and the upper mantle. *GSA Bulletin* **76**, 719–734.

Farley K. A., Natland J. H. and Craig H. (1992) Binary mixing of enriched and undegassed (primitive?) mantle components (He, Sr, Nd, Pb) in Samoan lavas. *Earth and Planetary Science Letters* **111**, 183–199.

Farnetani C. G. and Hofmann A. W. (2009) Dynamics and internal structure of a lower mantle plume conduit. *Earth and Planetary Science Letters* **282**, 314–322.

Farnetani C. G. and Hofmann A. W. (2010) Dynamics and internal structure of the Hawaiian plume. *Earth and Planetary Science Letters* **295**, 231–240.

Farnetani C. G., Hofmann A. W., Duvernay T. and Limare A. (2018) Dynamics of rheological heterogeneities in mantle plumes. *Earth and Planetary Science Letters* **499**, 74–82.

Farnetani C. G., Legras B. and Tackley P. J. (2002) Mixing and deformations in mantle plumes. *Earth and Planetary Science Letters* **196**, 1–15.

Feigenson M. D., Bolge L. L., Carr M. J. and Herzberg C. T. (2003) REE inverse modeling of HSDP2 basalts: Evidence for multiple sources in the Hawaiian plume. *Geochemistry, Geophysics, Geosystems* **4**.

Ferrick A. L. and Korenaga J. (2023) Long-term core–mantle interaction explains W-He isotope heterogeneities. *Proceedings of the National Academy of Sciences* **120**, e2215903120.

Foley B. J. (2015) The role of plate tectonic–climate coupling and exposed land area in the development of habitable climates on rocky planets. *Astrophysical Joural* **812**, 36.

Fourny A., Weis D. and Scoates J. S. (2016) Comprehensive Pb-Sr-Nd-Hf isotopic, trace element, and mineralogical characterization of mafic to ultramafic rock reference materials. *Geochemistry, Geophysics, Geosystems* **17**, 739–773.

French S. W. and Romanowicz B. (2015) Broad plumes rooted at the base of the Earth's mantle beneath major hotspots. *Nature* **525**, 95–99.

Frey F. A., Garcia M. O. and Roden M. F. (1994) Geochemical characteristics of Koolau Volcano: Implications of intershield geochemical differences among Hawaiian volcanoes. *Geochimica et Cosmochimica Acta* **58**, 1441–1462.

Fujiwara Y., Tsujisaka M., Takano S. and Sohrin Y. (2020) Determination of the tungsten isotope composition in seawater: The first vertical profile from the western North Pacific Ocean. *Chemical Geology* **555**, 119835.

Garcia M. O., Foss D. J. P., West H. B. and Mahoney J. J. (1995) Geochemical and Isotopic Evolution of Loihi Volcano, Hawaii. *Journal of Petrology* **36**, 1647–1674.

Garcia M. O., Swinnard L., Weis D., Greene A. R., Tagami T., Sano H. and Gandy C. E. (2010) Petrology, Geochemistry and Geochronology of Kaua'i Lavas over 4·5 Myr: Implications for the Origin of Rejuvenated Volcanism and the Evolution of the Hawaiian Plume. *Journal of Petrology* **51**, 1507–1540.

Gast P. W. (1968) Trace element fractionation and the origin of tholeiitic and alkaline magma types. *Geochimica et Cosmochimica Acta* **32**, 1057–1086.

Gast P. W., Tilton G. R. and Hedge C. (1964) Isotopic composition of lead and strontium from Ascension and Gough Islands. *Science*.

Gonnermann H. M. and Mukhopadhyay S. (2007) Non-equilibrium degassing and a primordial source for helium in ocean-island volcanism. *Nature* **449**, 1037–1040.

Graham D. W. (2002) Noble gas isotope geochemistry of mid-ocean ridge and ocean island basalts: Characterization of mantle source reservoirs. *Reviews in Mineralogy and Geochemistry* **47**, 247–317.

Greaney A. T., Rudnick R. L., Helz R. T., Gaschnig R. M., Piccoli P. M. and Ash R. D. (2017) The behavior of chalcophile elements during magmatic differentiation as observed in Kilauea Iki lava lake, Hawaii. *Geochimica et Cosmochimica Acta* **210**, 71–96.

Greene A. R., Garcia M. O., Weis D., Ito G., Kuga M., Robinson J. and Yamasaki S. (2010) Low-productivity Hawaiian volcanism between Kaua‘i and O‘ahu. *Geochemistry, Geophysics, Geosystems* **11**.

Hanan B. B. and Graham D. W. (1996) Lead and helium isotope evidence from oceanic basalts for a common deep source of mantle plumes. *Science* **272**, 991–995.

Hanano D., Scoates J. S. and Weis D. (2015) Alteration mineralogy and the effect of acid-leaching on the Pb-isotope systematics of ocean-island basalts. *American Mineralogist* **94**.

Hanyu T. and Kaneoka I. (1997) The uniform and low $^{3}He/^{4}He$ ratios of HIMU basalts as evidence for their origin as recycled materials. *Nature* **390**, 273–276.

Hanyu T., Kawabata H., Tatsumi Y., Kimura J.-I., Hyodo H., Sato K., Miyazaki T., Chang Q., Hirahara Y., Takahashi T., Senda R. and Nakai S. (2014) Isotope evolution in the HIMU reservoir beneath St. Helena: Implications for the mantle recycling of U and Th. *Geochimica et Cosmochimica Acta* **143**, 232–252.

Harðardóttir S. and Jackson M. G. (2024) A new geochemical database for ocean island basalts: Inferring an OIB mantle source from unevenly sampled oceanic hotspots. *Chemical Geology*, 122505.

Harrison L. N., Weis D. and Garcia M. O. (2017) The link between Hawaiian mantle plume composition, magmatic flux, and deep mantle geodynamics. *Earth and Planetary Science Letters* **463**, 298–309.

Hart S. R., Erlank A. J. and Kable E. J. D. (1974) Sea floor basalt alteration: Some chemical and Sr isotopic effects. *Contr. Mineral. and Petrol.* **44**, 219–230.

Hart S. R. and Gaetani G. A. (2006) Mantle Pb paradoxes: the sulfide solution. *Contrib Mineral Petrol* **152**, 295–308.

Hart S. R., Hauri E. H., Oschmann L. A. and Whitehead J. A. (1992) Mantle Plumes and Entrainment: Isotopic Evidence. *Science* **256**, 517–520.

Hellmann J. L., Budde G., Willhite L. N. and Walker R. J. (2024) Hf–W isotope systematics of bulk chondrites: Implications for early Solar System evolution. *Geochimica et Cosmochimica Acta* **387**, 38–52.

van der Hilst R. D., Widiyantoro S. and Engdahl E. R. (1997) Evidence for deep mantle circulation from global tomography. *Nature* **386**, 578–584.

Hirose K., Shimizu N., van Westrenen W. and Fei Y. (2004) Trace element partitioning in Earth's lower mantle and implications for geochemical consequences of partial melting at the core–mantle boundary. *Physics of the Earth and Planetary Interiors* **146**, 249–260.

Hirschmann M. M. (2012) Magma ocean influence on early atmosphere mass and composition. *Earth and Planetary Science Letters* **341–344**, 48–57.

Hirschmann M. M. (2006) Water, melting, and the deep earth H_2O cycle. *Annual Review of Earth and Planetary Sciences* **34**, 629–653.

Hofmann A. W. (1997) Mantle geochemistry: the message from oceanic volcanism. *Nature* **385**, 219–229.

Hofmann A. W., Farnetani C. G., Spiegelman M. and Class C. (2011) Displaced helium and carbon in the Hawaiian plume. *Earth and Planetary Science Letters* **312**, 226–236.

Hofmann A. W., Jochum K. P., Seufert M. and White W. M. (1986) Nb and Pb in oceanic basalts: new constraints on mantle evolution. *Earth and Planetary Science Letters* **79**, 33–45.

Hofmann A. W. and White W. M. (1982) Mantle plumes from ancient oceanic crust. *Earth and Planetary Science Letters* **57**, 421–436.

Horan M. F., Carlson R. W., Walker R. J., Jackson M., Garçon M. and Norman M. (2018) Tracking Hadean processes in modern basalts with 142-Neodymium. *Earth and Planetary Science Letters* **484**, 184–191.

Horan M. F., Walker R. J., Morgan J. W., Grossman J. N. and Rubin A. E. (2003) Highly siderophile elements in chondrites. *Chemical Geology* **196**, 27–42.

Horton F., Asimow P. D., Farley K. A., Curtice J., Kurz M. D., Blusztajn J., Biasi J. A. and Boyes X. M. (2023) Highest terrestrial $^{3}He/^{4}He$ credibly from the core. *Nature* **623**, 90–94.

Huang S. and Frey F. A. (2003) Trace element abundances of Mauna Kea basalt from phase 2 of the Hawaii Scientific Drilling Project: Petrogenetic implications of correlations with major element content and isotopic ratios. *Geochemistry, Geophysics, Geosystems* **4**.

Humayun M. (2011) A model for osmium isotopic evolution of metallic solids at the core-mantle boundary. *Geochemistry, Geophysics, Geosystems* **12**.

Ireland T. J., Arevalo R., Walker R. J. and McDonough W. F. (2009a) Tungsten in Hawaiian picrites: A compositional model for the sources of Hawaiian lavas. *Geochimica et Cosmochimica Acta* **73**, 4517–4530.

Ireland T. J., Walker R. J. and Garcia M. O. (2009b) Highly siderophile element and ^{187}Os isotope systematics of Hawaiian picrites: Implications for parental melt composition and source heterogeneity. *Chemical Geology* **260**, 112–128.

Jackson M. G., Blichert-Toft J., Halldórsson S. A., Mundl-Petermeier A., Bizimis M., Kurz M. D., Price A. A., Harðardóttir S., Willhite L. N., Breddam K., Becker T. W. and Fischer R. A. (2020) Ancient helium and tungsten isotopic signatures preserved in mantle domains least modified by crustal recycling. *Proceedings of the National Academy of Sciences* **117**, 30993–31001.

Jackson M. G. and Carlson R. W. (2012) Homogeneous superchondritic $^{142}Nd/^{144}Nd$ in the mid-ocean ridge basalt and ocean island basalt mantle. *Geochemistry, Geophysics, Geosystems* **13**.

Jackson M. G., Hart S. R., Koppers A. A. P., Staudigel H., Konter J., Blusztajn J., Kurz M. and Russell J. A. (2007) The return of subducted continental crust in Samoan lavas. *Nature* **448**, 684–687.

Jackson M. G., Hart S. R., Saal A. E., Shimizu N., Kurz M. D., Blusztajn J. S. and Skovgaard A. C. (2008) Globally elevated titanium, tantalum, and niobium (TITAN) in ocean island basalts with high $^{3}He/^{4}He$. *Geochemistry, Geophysics, Geosystems* **9**.

Jackson M. G., Konter J. G. and Becker T. W. (2017) Primordial helium entrained by the hottest mantle plumes. *Nature* **542**, 340–343.

Javoy M. (1998) The birth of the Earth's atmosphere: the behaviour and fate of its major elements. *Chemical Geology* **147**, 11–25.

Jochum K. P., Weis U., Schwager B., Stoll B., Wilson S. A., Haug G. H., Andreae M. O. and Enzweiler J. (2016) Reference Values Following ISO Guidelines for Frequently Requested Rock Reference Materials. *Geostand Geoanal Res* **40**, 333–350.

Kashiwabara T., Takahashi Y., Marcus M. A., Uruga T., Tanida H., Terada Y. and Usui A. (2013) Tungsten species in natural ferromanganese oxides related to its different behavior from molybdenum in oxic ocean. *Geochimica et Cosmochimica Acta* **106**, 364–378.

Kent A. J. R., Clague D. A., Honda M., Stolper E. M., Hutcheon I. D. and Norman M. D. (1999) Widespread assimilation of a seawater-derived component at Loihi Seamount, Hawaii. *Geochimica et Cosmochimica Acta* **63**, 2749–2761.

Kim D., Lekić V., Ménard B., Baron D. and Taghizadeh-Popp M. (2020) Sequencing seismograms: A panoptic view of scattering in the core-mantle boundary region. *Science* **368**, 1223–1228.

Kleine T., Hans U., Irving A. J. and Bourdon B. (2012) Chronology of the angrite parent body and implications for core formation in protoplanets. *Geochimica et Cosmochimica Acta* **84**, 186–203.

Kleine T., Mezger K., Münker C., Palme H. and Bischoff A. (2004a) ^{182}Hf-^{182}W isotope systematics of chondrites, eucrites, and martian meteorites: Chronology of core formation and early mantle differentiation in Vesta and Mars. *Geochimica et Cosmochimica Acta* **68**, 2935–2946.

Kleine T., Mezger K., Palme H. and Münker C. (2004b) The W isotope evolution of the bulk silicate Earth: constraints on the timing and mechanisms of core formation and accretion. *Earth and Planetary Science Letters* **228**, 109–123.

Kleine T., Münker C., Mezger K. and Palme H. (2002) Rapid accretion and early core formation on asteroids and the terrestrial planets from Hf-W chronometry. *Nature* **418**, 952–955.

Kleine T. and Walker R. J. (2017) Tungsten isotopes in planets. *Annual Review of Earth and Planetary Sciences* **45**, 389–417.

König S., Münker C., Schuth S. and Garbe-Schönberg D. (2008) Mobility of tungsten in subduction zones. *Earth and Planetary Science Letters* **274**, 82–92.

Kurz M. D., Curtice J., Lott III D. E. and Solow A. (2004) Rapid helium isotopic variability in Mauna Kea shield lavas from the Hawaiian Scientific Drilling Project. *Geochemistry, Geophysics, Geosystems* **5**.

Kurz M. D., Jenkins W. J., Hart S. R. and Clague D. (1983) Helium isotopic variations in volcanic rocks from Loihi Seamount and the Island of Hawaii. *Earth and Planetary Science Letters* **66**, 388–406.

Labrosse S. (2003) Thermal and magnetic evolution of the Earth's core. *Physics of the Earth and Planetary Interiors* **140**, 127–143.

Labrosse S., Hernlund J. W. and Coltice N. (2007) A crystallizing dense magma ocean at the base of the Earth's mantle. *Nature* **450**, 866–869.

Labrosse S., Poirier J.-P. and Le Mouël J.-L. (2001) The age of the inner core. *Earth and Planetary Science Letters* **190**, 111–123.

Lassiter J. C. (2006) Constraints on the coupled thermal evolution of the Earth's core and mantle, the age of the inner core, and the origin of the ^{186}Os/^{188}Os "core signal" in plume-derived lavas. *Earth and Planetary Science Letters* **250**, 306–317.

Lassiter J. C. and Hauri E. H. (1998) Osmium-isotope variations in Hawaiian lavas: evidence for recycled oceanic lithosphere in the Hawaiian plume. *Earth and Planetary Science Letters* **164**, 483–496.

Le Bas M. J., Maitre R. W. L., Streckeisen A., Zanettin B., and IUGS Subcommission on the Systematics of Igneous Rocks (1986) A Chemical Classification of Volcanic Rocks Based on the Total Alkali-Silica Diagram. *Journal of Petrology* **27**, 745–750.

Lin Y.-Z., Day J. M. D., Brown D. B., Harvey J. and Liu C.-Z. (2024) Evidence for large-scale, long-term highly siderophile element heterogeneities in the Atlantic mantle from Leg 153 and 209 peridotites. *Geochimica et Cosmochimica Acta* **378**, 300–314.

Lodders K. and Palme H. (1991) On the chalcophile character of molybdenum: determination of sulfide/silicate partition coefficients of Mo and W. *Earth and Planetary Science Letters* **103**, 311–324.

Lupton J. E. and Craig H. (1975) Excess ^{3}He in oceanic basalts: Evidence for terrestrial primordial helium. *Earth and Planetary Science Letters* **26**, 133–139.

Macdonald G. A. and Katsura T. (1964) Chemical composition of Hawaiian lavas. *Journal of Petrology* **5**, 82–133.

Mahaffy P. R., Donahue T. M., Atreya S. K., Owen T. C. and Niemann H. B. (1998) Galileo probe measurements of D/H and ^{3}He/^{4}He in Jupiter's atmosphere. *Space Science Reviews* **84**, 251–263.

Matsuda, Sudo M., Ozima M., Ito K., Ohtaka O. and Ito E. (1993) Noble gas partitioning between metal and silicate under high pressures. *Science* **259**, 788–790.

McCulloch M. T. and Gamble J. A. (1991) Geochemical and geodynamical constraints on subduction zone magmatism. *Earth and Planetary Science Letters* **102**, 358–374.

McDonough W. F. (2003) 2.15 - Compositional Model for the Earth's Core. In *Treatise on Geochemistry*. pp. 547–568.

McDonough W. F. (1991) Partial melting of subducted oceanic crust and isolation of its residual eclogitic lithology. *Philosophical Transactions: Physical Sciences and Engineering* **335**, 407–418.

McDonough W. F. and Chauvel C. (1991) Sample contamination explains the Pb isotopic composition of some Rurutu island and Sasha seamount basalts. *Earth and Planetary Science Letters* **105**, 397–404.

McDonough W. F. and Sun S. -s. (1995) The composition of the Earth. *Chemical Geology* **120**, 223–253.

McDougall I. (1979) Age of shield-building volcanism of Kauai and linear migration of volcanism in the Hawaiian island chain. *Earth and Planetary Science Letters* **46**, 31–42.

McNamara A. K., Garnero E. J. and Rost S. (2010) Tracking deep mantle reservoirs with ultra-low velocity zones. *Earth and Planetary Science Letters* **299**, 1–9.

Meissner F., Schmidt-Ott W.-D. and Ziegeler L. (1987) Half-life and α-ray energy of ^{146}Sm. *Z. Physik A - Atomic Nuclei* **327**, 171–174.

Mengason M. J., Candela P. A. and Piccoli P. M. (2011) Molybdenum, tungsten and manganese partitioning in the system pyrrhotite–Fe–S–O melt–rhyolite melt: Impact of sulfide segregation on arc magma evolution. *Geochimica et Cosmochimica Acta* **75**, 7018–7030.

Moreira M., Blusztajn J., Curtice J., Hart S., Dick H. and Kurz M. D. (2003) He and Ne isotopes in oceanic crust: implications for noble gas recycling in the mantle. *Earth and Planetary Science Letters* **216**, 635–643.

Moreira M. and Kurz M. D. (2001) Subducted oceanic lithosphere and the origin of the 'high μ' basalt helium isotopic signature. *Earth and Planetary Science Letters* **189**, 49–57.

Morgan W. J. (1971) Convection plumes in the lower mantle. *Nature* **230**, 42–43.

Mukhopadhyay S. (2012) Early differentiation and volatile accretion recorded in deep-mantle neon and xenon | Nature. *Nature* **486**.

Mundl A., Touboul M., Jackson M. G., Day J. M. D., Kurz M. D., Lekic V., Helz R. T. and Walker R. J. (2017) Tungsten-182 heterogeneity in modern ocean island basalts. *Science* **356**, 66–69.

Mundl-Petermeier A., Walker R. J., Fischer R. A., Lekic V., Jackson M. G. and Kurz M. D. (2020) Anomalous ^{182}W in high ^{3}He/^{4}He ocean island basalts: Fingerprints of Earth's core? *Geochimica et Cosmochimica Acta* **271**, 194–211.

Mundl-Petermeier A., Walker R. J., Jackson M. G., Blichert-Toft J., Kurz M. D. and Halldórsson S. A. (2019) Temporal evolution of primordial tungsten-182 and ^{3}He/^{4}He signatures in the Iceland mantle plume. *Chemical Geology* **525**, 245–259.

Nagai Y. and Yokoyama T. (2014) Chemical Separation of Mo and W from Terrestrial and Extraterrestrial Samples via Anion Exchange Chromatography. *Anal. Chem.* **86**, 4856–4863.

Nakajima M. and Stevenson D. J. (2015) Melting and mixing states of the Earth's mantle after the Moon-forming impact. *Earth and Planetary Science Letters* **427**, 286–295.

Nakanishi N., Giuliani A., Carlson R. W., Horan M. F., Woodhead J., Pearson D. G. and Walker R. J. (2021) Tungsten-182 evidence for an ancient kimberlite source. *Proceedings of the National Academy of Sciences* **118**, e2020680118.

Nobre Silva I. G., Weis D., Barling J. and Scoates J. S. (2009) Leaching systematics and matrix elimination for the determination of high-precision Pb isotope compositions of ocean island basalts. *Geochemistry, Geophysics, Geosystems* **10**.

Nobre Silva I. G., Weis D. and Scoates J. S. (2010) Effects of acid leaching on the Sr-Nd-Hf isotopic compositions of ocean island basalts. *Geochemistry, Geophysics, Geosystems* **11**.

Nobre Silva I. G., Weis D. and Scoates J. S. (2013) Isotopic systematics of the early Mauna Kea shield phase and insight into the deep mantle beneath the Pacific Ocean. *Geochemistry, Geophysics, Geosystems* **14**, 659–676.

Ohtani E. (2015) Hydrous minerals and the storage of water in the deep mantle. *Chemical Geology* **418**, 6–15.

O'Nions R. K. and Oxburgh E. R. (1988) Helium, volatile fluxes and the development of continental crust. *Earth and Planetary Science Letters* **90**, 331–347.

Ozgurel O. and Caracas R. (2023) The magma ocean was a huge helium reservoir in the early Earth. *Geochem. Persp. Let.* **25**, 46–50.

Palacz Z. A. and Saunder A. D. (1986) Coupled trace element and isotope enrichment in the Cook-Austral-Samoa Islands, Southwest Pacific. *Earth and Planetary Science Letters* **79**, 270–280.

Parai R. (2022) A dry ancient plume mantle from noble gas isotopes. *Proceedings of the National Academy of Sciences* **119**, e2201815119.

Parai R., Mukhopadhyay S., Tucker J. M. and Pető M. K. (2019) The emerging portrait of an ancient, heterogeneous and continuously evolving mantle plume source. *Lithos* **346–347**, 105153.

Peters B. J., Carlson R. W., Day J. M. D. and Horan M. F. (2018) Hadean silicate differentiation preserved by anomalous $^{142}Nd/^{144}Nd$ ratios in the Réunion hotspot source. *Nature* **555**, 89–93.

Peters B. J. and Day J. M. D. (2014) Assessment of relative Ti, Ta, and Nb (TITAN) enrichments in ocean island basalts. *Geochemistry, Geophysics, Geosystems* **15**, 4424–4444.

Peters B. J., Mundl-Petermeier A., Carlson R. W., Walker R. J. and Day J. M. D. (2021) Combined lithophile-siderophile isotopic constraints on hadean processes preserved in ocean island basalt sources. *Geochemistry, Geophysics, Geosystems* **22**, e2020GC009479.

Peters B. J., Mundl-Petermeier A. and Finlayson V. A. (2023) A multi-siderophile element connection between volcanic hotspots and Earth's core. *Earth and Planetary Science Letters* **618**, 118285.

Peters D., Rizo H., O'Neil J., Hamelin C. and Shirey S. B. (2024) Comparative ^{142}Nd and ^{182}W study of MORBs and the 4.5 Gyr evolution of the upper mantle. *Geochemical Perspective Letters* **29**, 51–56.

Pitcher L., Helz R. T., Walker R. J. and Piccoli P. (2009) Fractionation of the platinum-group elments and Re during crystallization of basalt in Kilauea Iki Lava Lake, Hawaii. *Chemical Geology* **260**, 196–210.

Plank T. and Langmuir C. H. (1998) The chemical composition of subducting sediment and its consequences for the crust and mantle. *Chemical Geology* **145**, 325–394.

Porcelli D. and Halliday A. N. (2001) The core as a possible source of mantle helium. *Earth and Planetary Science Letters* **192**, 45–56.

Prytulak J. and Elliott T. (2007) TiO_2 enrichment in ocean island basalts. *Earth and Planetary Science Letters* **263**, 388–403.

Puchtel I. S., Blichert-Toft J., Touboul M., Horan M. F. and Walker R. J. (2016) The coupled ^{182}W-^{142}Nd record of early terrestrial mantle differentiation. *Geochemistry, Geophysics, Geosystems* **17**, 2168–2193.

Puchtel I. S., Blichert-Toft J., Touboul M. and Walker R. J. (2018) ^{182}W and HSE constraints from 2.7 Ga komatiites on the heterogeneous nature of the Archean mantle. *Geochimica et Cosmochimica Acta* **228**, 1–26.

Puchtel I. S., Humayan M. (2000) Platinum group elements in Kostomuksha komatiites and basalts: implications for oceanic crust recycling and core-mantle interaction. *Geochimica et Cosmochimica Acta* **64**, 4227-4242,

Raczek I., Stoll B., Hofmann A. W. and Peter Jochum K. (2001) High-Precision Trace Element Data for the USGS Reference Materials BCR-1, BCR-2, BHVO-1, BHVO-2, AGV-1, AGV-2, DTS-1, DTS-2, GSP-1 and GSP-2 by ID-TIMS and MIC-SSMS. *Geostandards Newsletter* **25**, 77–86.

Reifenröther R., Münker C., Scheibner B. (2021) Evidence for tungsten mobility during oceanic crust alteration. *Chemical Geology* **584**, 120504

Reimink J. R., Chacko T., Carlson R. W., Shirey S. B., Liu J., Stern R. A., Bauer A. M., Pearson D. G. and Heaman L. M. (2018) Petrogenesis and tectonics of the Acasta Gneiss Complex derived from integrated petrology and ^{142}Nd and ^{182}W extinct nuclide-geochemistry. *Earth and Planetary Science Letters* **494**, 12–22.

Rhodes J. M. and Vollinger M. J. (2004) Composition of basaltic lavas sampled by phase-2 of the Hawaii Scientific Drilling Project: Geochemical stratigraphy and magma types. *Geochemistry, Geophysics, Geosystems* **5**.

Rizo H., Andrault D., Bennett N. R., Humayun M., Brandon A., Vlastelic I., Moine B., Poirier A., Bouhifd M. A. and Murphy D. T. (2019) ^{182}W evidence for core-mantle interaction in the source of mantle plumes. *Geochemical Perspective Letters*, 6–11.

Rizo H., Walker R. J., Carlson R. W., Touboul M., Horan M. F., Puchtel I. S., Boyet M. and Rosing M. T. (2016) Early Earth differentiation investigated through ^{142}Nd, ^{182}W, and highly siderophile element abundances in samples from Isua, Greenland. *Geochimica et Cosmochimica Acta* **175**, 319–336.

Roth A. S. G., Liebske C., Maden C., Burton K. W., Schönbächler M. and Busemann H. (2019) The primordial He budget of the Earth set by percolative core formation in planetesimals. *Geochem. Persp. Let.*, 26–31.

Rudnick R. L. and Gao S. (2003) 3.01 - Composition of the Continental Crust. In *Treatise on Geochemistry* pp. 1–64.

Rushmer T., Petford N., Humayun M. and Campbell A. J. (2005) Fe-liquid segregation in deforming planetesimals: Coupling Core-Forming compositions with transport phenomena. *Earth and Planetary Science Letters* **239**, 185–202.

Russell S., Irving J. C. E., Jagt L. and Cottaar S. (2023) Evidence for a kilometer-scale seismically slow layer atop the core-mantle boundary from normal modes. *Geophysical Research Letters* **50**, e2023GL105684.

Scherstén A., Elliott T., Hawkesworth C. and Norman M. (2004) Tungsten isotope evidence that mantle plumes contain no contribution from the Earth's core. *Nature* **427**, 234–237.

Sharp W. D. and Renne P. R. (2005) The 40Ar/39Ar dating of core recovered by the Hawaii Scientific Drilling Project (phase 2), Hilo, Hawaii. *Geochemistry, Geophysics, Geosystems* **6**.

Shirey S. B. and Walker R. J. (1995) Carius Tube Digestion for Low-Blank Rhenium-Osmium Analysis. *Anal. Chem.* **67**, 2136–2141.

Sleep N. H., Zahnle K. J. and Lupu R. E. (2014) Terrestrial aftermath of the Moon-forming impact. *Philosophical Transactions of the Royal Society A: Mathematical, Physical and Engineering Sciences* **372**, 20130172.

Sohrin Y., Isshiki K., Kuwamoto T. and Nakayama E. (1987) Tungsten in north pacific waters. *Marine Chemistry* **22**, 95–103.

Stracke A. (2021) A process-oriented approach to mantle geochemistry. *Chemical Geology* **579**, 120350.

Stracke A., Willig M., Genske F., Béguelin P. and Todd E. (2022) Chemical Geodynamics Insights From a Machine Learning Approach. *Geochemistry, Geophysics, Geosystems* **23**, e2022GC010606.

Thorne M. S., Garnero E. J. and Grand S. P. (2004) Geographic correlation between hot spots and deep mantle lateral shear-wave velocity gradients. *Physics of the Earth and Planetary Interiors* **146**, 47–63.

Tornabene H. A., Hilton C. D., Bermingham K. R., Ash R. D. and Walker R. J. (2020) Genetics, age and crystallization history of group IIC iron meteorites. *Geochimica et Cosmochimica Acta* **288**, 36–50.

Touboul M., Liu J., O'Neil J., Puchtel I. S. and Walker R. J. (2014) New insights into the Hadean mantle revealed by ^{182}W and highly siderophile element abundances of supracrustal rocks from the Nuvvuagittuq Greenstone Belt, Quebec, Canada. *Chemical Geology* **383**, 63–75.

Touboul M., Puchtel I. S. and Walker R. J. (2012) ^{182}W evidence for long-term preservation of early mantle differentiation products. *Science*.

Touboul M., Puchtel I. S. and Walker R. J. (2015) Tungsten isotopic evidence for disproportional late accretion to the Earth and Moon. *Nature* **520**, 530–533.

Valbracht P. J., Staudigel H., Honda M., McDougall I. and Davies G. R. (1996) Isotopic tracing of volcanic source regions from Hawaii: decoupling of gaseous from lithophile magma components. *Earth and Planetary Science Letters* **144**, 185–198.

Vockenhuber C., Oberli F., Bichler M., Ahmad I., Quitté G., Meier M., Halliday A. N., Lee D.-C., Kutschera W., Steier P., Gehrke R. J. and Helmer R. G. (2004) New half-life measurement of ^{182}Hf: Improved chronometer for the early Solar System. *Phys. Rev. Lett.* **93**, 172501.

Walker R. J., Morgan J. W. and Horan M. F. (1995) Osmium-187 enrichment in some plumes: evidence for core-mantle interaction? *Science* **269**, 819–822.

Walker R. J., Mundl-Petermeier A., Puchtel I. S., Nicklas R. W., Hellmann J. L., Echeverría L. M., Ludwig K. D., Bermingham K. R., Gazel E., Devitre C. L., Jackson M. G. and Chauvel C. (2023) ^{182}W and ^{187}Os constraints on the origin of siderophile isotopic heterogeneity in the mantle. *Geochimica et Cosmochimica Acta* **363**, 15–39.

Warren P. H. (2011) Stable-isotopic anomalies and the accretionary assemblage of the Earth and Mars: A subordinate role for carbonaceous chondrites. *Earth and Planetary Science Letters* **311**, 93–100.

Watson S. and McKenzie D. (1991) Melt generation by plumes: A study of Hawaiian volcanism. *Journal of Petrology* **32**, 501–537.

Weis D., Garcia M. O., Rhodes J. M., Jellinek M. and Scoates J. S. (2011) Role of the deep mantle in generating the compositional asymmetry of the Hawaiian mantle plume. *Nature Geosci* **4**, 831–838.

Weis D., Harrison L. N., McMillan R. and Williamson N. M. B. (2020) Fine-scale structure of Earth's deep mantle resolved through statistical analysis of Hawaiian basalt geochemistry. *Geochemistry, Geophysics, Geosystems* **21**, e2020GC009292.

Weis D., Kieffer B., Maerschalk C., Barling J., de Jong J., Williams G. A., Hanano D., Pretorius W., Mattielli N., Scoates J. S., Goolaerts A., Friedman R. M. and Mahoney J. B. (2006) High-precision isotopic characterization of USGS reference materials by TIMS and MC-ICP-MS. *Geochemistry, Geophysics, Geosystems* **7**.

Wessel P. (2016) Regional–residual separation of bathymetry and revised estimates of Hawaii plume flux. *Geophysical Journal International* **204**, 932–947.

White W. M. and Hofmann A. W. (1982) Sr and Nd isotope geochemistry of oceanic basalts and mantle evolution. *Nature* **296**, 821–825.

Willbold M., Elliott T. and Moorbath S. (2011) The tungsten isotopic composition of the Earth's mantle before the terminal bombardment. *Nature* **477**, 195–198.

Willbold M., Mojzsis S. J., Chen H.-W. and Elliott T. (2015) Tungsten isotope composition of the Acasta Gneiss Complex. *Earth and Planetary Science Letters* **419**, 168–177.

Willhite L. N., Finlayson V. A. and Walker R. J. (2024) Evolution of tungsten isotope systematics in the Mauna Kea volcano provides new constraints on anomalous $\mu^{182}W$ and high $^{3}He/^{4He}$ in the mantle. *Earth and Planetary Science Letters* **640**, 118795.

Willhite L. N., Jackson M. G., Blichert-Toft J., Bindeman I., Kurz M. D., Halldórsson S. A., Harðardóttir S., Gazel E., Price A. A. and Byerly B. L. (2019) Hot and Heterogenous High-$^{3}He/^{4}He$ Components: New Constraints From Proto-Iceland Plume Lavas From Baffin Island. *Geochemistry, Geophysics, Geosystems* **20**, 5939–5967.

Williams Q. and Garnero E. J. (1996) Seismic evidence for partial melt at the base of Earth's mantle. *Science* **273**, 1528–1530.

Williamson N. M. B., Weis D. and Prytulak J. (2021) Thallium Isotopic Compositions in Hawaiian Lavas: Evidence for Recycled Materials on the Kea Side of the Hawaiian Mantle Plume. *Geochemistry, Geophysics, Geosystems* **22**, e2021GC009765.

Williamson N. M. B., Weis D., Scoates J. S. and Garcia M. O. (2023) Emergence of the Loa Mantle Component in the Hawaiian Islands Based on the Geochemistry of Kaua'i Shield-Stage Basalts. *Geochemistry, Geophysics, Geosystems* **24**, e2023GC010980.

Williamson N. M. B., Weis D., Scoates J. S., Pelletier H. and Garcia M. O. (2019) Tracking the Geochemical Transition Between the Kea-Dominated Northwest Hawaiian Ridge and the Bilateral Loa-Kea Trends of the Hawaiian Islands. *Geochemistry, Geophysics, Geosystems* **20**, 4354–4369.

Worsham E. A., Burkhardt C., Budde G., Fischer-Gödde M., Kruijer T. S. and Kleine T. (2019) Distinct evolution of the carbonaceous and non-carbonaceous reservoirs: Insights from Ru, Mo, and W isotopes. *Earth and Planetary Science Letters* **521**, 103–112.

Yoshino T., Makino Y., Suzuki T. and Hirata T. (2020) Grain boundary diffusion of W in lower mantle phase with implications for isotopic heterogeneity in oceanic island basalts by core-mantle interactions. *Earth and Planetary Science Letters* **530**, 115887.

Zhao C., Garnero E. J., McNamara A. K., Schmerr N. and Carlson R. W. (2015) Seismic evidence for a chemically distinct thermochemical reservoir in Earth's deep mantle beneath Hawaii. *Earth and Planetary Science Letters* **426**, 143–153.

Zindler A. and Hart S. (1986) Chemical Geodynamics. *Annual Review of Earth and Planetary Sciences* **14**, 493–571.